"Markers of response to the targeting of the cholinic phenotype in experimental tumor xenografts : magnetic resonance studies"

Mignion, Lionel

Abstract

The aim of the thesis is to assess response to modulations of the choline pathway in the context of the cholinic tumor phenotype. Conventional measurements like anatomically based endpoints may be inadequate to monitor the tumor response to targeted agents that usually do not result in tumor shrinkage while used in monotherapy. Therefore, the identification of more sensitively, non-invasive biomarkers are needed to optimize the schedule and dosage of novels therapeutics. The results illustrate that the assessment of total choline with 1H-MRS is able to confirm the inhibition of the target but is not sufficient to predict tumor response to the targeted treatment. Adding DW-MRI as a marker of tumor response to choline inhibition improves specificity of the monitoring. In addition, 13C-magnetic resonance spectroscopy and the detection of hyperpolarized 13C-fumarate to 13C-malate conversion has been suggested as a marker of cell death and treatment response in tumors. We showed here that...

Document type : *Thèse (Dissertation)*

Université Catholique de Louvain
Sector of Health Sciences
Thematic Doctoral School in Pharmaceutical Sciences
Louvain Drug Research Institute
Biomedical Magnetic Resonance Unit

Markers of response to the targeting of the cholinic phenotype in experimental tumor xenografts: Magnetic Resonance studies.

Lionel MIGNION

2015

Thesis presented in fullfillment of the requirements for the degree of
'Docteur en Sciences Biomédicales et Pharmaceutiques'

Supervisor : Bénédicte JORDAN

Co-supervisor : Vincent GREGOIRE

«Pour réussir, retenez bien ces trois maximes:

voir c’est savoir, vouloir c’est pouvoir, oser c’est avoir»

Alfred de Musset

En préambule à ce manuscrit, je voudrais effectuer quelques remerciements aux personnes ayant contribué à l'aboutissement de cette thèse.

Mes premiers remerciements vont à ma promotrice, le Professeur Bénédicte Jordan, qui a accepté de me donner la chance d'explorer toutes les possibilités de l'imagerie par résonance magnétique. J'ai beaucoup appris grâce à elle et j'ai toujours trouvé en elle un soutien tant dans l'écriture parfois fastidieuse de nos papiers que dans ses bons conseils pour mener à bien cette aventure mouvementée. Je la remercie également pour sa disponibilité, pour son oreille attentive et pour le temps consacré à l'avancement de ce travail.

Je remercie également mon co-promoteur, le professeur Vincent Grégoire, pour son aide, son point de vue plus clinique du travail ainsi que pour son soutien franc et indéfectible afin que cette thèse se passe au mieux.

Comment ne pas remercier le professeur Gallez qui a suivi l'évolution de mes recherches, semaines après semaines, très attentivement. Il m'a apporté de nombreux conseils lors de nos échanges et son expérience m'a bien souvent aidé à trouver une solution dans les situations difficiles.

Merci au professeur Sonveaux pour ses conseils, pour sa prise de recul indispensable à la mise en perspective du travail et pour l'aide que lui et son équipe ont pu m'apporter dans certains aspects plus biomoléculaires de mon travail.

Merci au professeur Machiels d'avoir accepté de participer au jury de cette thèse. Après un mémoire réalisé dans son laboratoire, j'ai eu la chance de continuer à recevoir ses conseils bienveillants et ses encouragements lors de ma

thèse. Merci également à lui de m'avoir aidé à comprendre l'apport pratique concret en clinique de certaines techniques et résultats.

Merci au Professeur Feron pour ses conseils avisés lors du comité de confirmation.

Merci au Professeur Delzenne d'avoir accepté la présidence de mon jury de thèse ainsi que pour ses conseils avisés et constructifs.

Merci aux professeurs Himmelreich et Heerschap pour le temps qu'ils ont consacré à l'analyse de ma thèse et pour leurs remarques pertinentes.

Je remercie tous les doctorants et post doctorants du laboratoire de résonance magnétique avec lesquels j'ai eu l'occasion de travailler et/ ou de passer de bons moments.

Je commencerai par remercier mes co-locataires de bureau qui ont défilé au cours des années : Florence, ton dynamisme et ta bonne humeur ont mis beaucoup de vie dans le labo et dans notre bureau. Merci pour les conversations scientifiques ou non et pour les bons moments passés. Pierre, tes connaissances en biomoléculaire m'ont souvent aidé à voir clair sur la marche à suivre pour certaines expériences. Merci également pour tes conseils et tes anecdotes de jeune parent. An, nous avons débuté notre thèse ensemble et ce fut un grand plaisir de collaborer avec toi dès le début de la thèse.

Marie-Aline, merci pour les bons moments partagés et pour les conversations enjouées. Merci d'avoir accéléré les trains de la SNCB par des discussions animées. Géraldine, merci pour ta gentillesse et ta bonne humeur. Céline, merci pour ton courage et pour le cœur que tu mets à l'ouvrage. Marta, merci de nous

apporter un apport clinique qui nous manquait. Nicolas, merci pour ton apport et pour ton plaisir à partager tes connaissances du monde fascinant de l'IRM. Merci également pour ton entrain à collaborer dans la résolution des problèmes made in Bruker. Julie, merci pour ta bonne humeur. Valérie, merci pour les moments de convivialité et pour les attentions que tu portes à chaque membre du labo. Trang, merci pour ton humilité et ta bonne humeur. Linda, merci pour ton dynamisme et pour le partage de tes connaissances. Philippe, merci pour tes conseils, ton attention lors de mes présentations m'a permis d'éviter certains pièges et de prendre le recul bien nécessaire à la clarification des résultats bruts.

Je tiens également à remercier les anciennes et nouvelles recrues du laboratoire pour les bons moments passés et à venir.

Je remercie également toutes les personnes avec lesquelles j'ai eu le plaisir de collaborer et dont j'ai eu le plaisir de partager l'expérience toujours enrichissante: Daniel Labar, Anne Bol, Paolo Porporato, Julien Masquelier, Roxana Albu, Xavier Caignet, Olivier Schakman, Etienne Marbais.

Je remercie également Robert Gillies pour m'avoir ouvert les portes de son laboratoire en Floride et pour m'avoir initié aux plaisirs de l'hyperpolarisation. Merci à toutes les personnes avec lesquelles j'ai pu collaborer sur place : Prasanta Dutta pour ses explications hyperpolarisées, Gary Martinez et Parastou Foroustan pour leur aide dans le maniement d'un aimant Varian.

Je terminerai en remerciant ma famille, tout d'abord mes parents pour m'avoir toujours soutenu au cours de mes études et pour m'avoir si bien accompagné puis aidé à diriger ma barque seul mais en étant toujours présents à mes côtés. Merci à ma sœur pour son soutien et pour tous les bons moments m'aidant à déconnecter ; ce qui est toujours primordial pour avancer. Un grand merci

également à mon épouse Anne pour sa présence à mes côtés ; elle m'aide à avancer et à voir le positif dans chaque chose. Merci à elle pour sa relecture très attentive de cette thèse et pour ses critiques constructives qui ont grandement contribués à la finalisation de ce manuscrit.

Markers of response to the targeting of the cholinic phenotype in experimental tumor xenografts: Magnetic Resonance studies.

Abbreviation list

Abbreviation list

5-FU:	5-fluorouracil
AA:	arachidonic acid
ADCw:	apparent diffusion coefficient of water
Ago:	argonaute 2
ATP:	adenosine triphosphate
CA:	contrast agent
CDP-Cho:	cytosine diphosphate-choline
Cho:	choline
ChoK:	choline kinase
CHT:	high affinity choline transporter
CT:	computed tomography
CTL:	choline transporter like protein
CTP:	phosphocholine cytidylyltransferase
DAG:	diacylglycerol
DCE-MRI:	dynamic contrast enhanced magnetic resonance imaging
DNP:	dynamic nuclear polarization
dUMP:	deoxyuridine monophosphate
DW-MRI:	diffusion weighted magnetic resonance imaging
EPR:	electron paramagnetic resonance
FDG:	fluorodeoxyglucose
FID:	free induction decay
FLT DP:	fluorothymidine diphosphate
FLT MP:	fluorothymidine monophosphate
FLT TP:	fluorothymidine triphosphate
FLT:	fluorothymidine
GPC:	glycerophosphocholine
GPE:	glycero-phospho-ethanolamine
Gro3P:	glycerol-3-phosphate
HC-3:	hemicholinium-3
HFB:	hexafluorobenzene

HIF-1:	hypoxia inducible factor-1
Lac/Pyr:	lactate/pyruvate
LDH:	lactate deshydrogenase
LPA:	lyso-phosphatidic acid
LPtdCho:	lyso-phosphatidylcholine
mRNA:	messenger ribonucleic acid
MRS:	magnetic resonance spectroscopy
NMR:	nuclear magnetic resonance
NTP:	nucleotide triphosphate
OCT:	organic cation transporter
OCTN:	organic cation/carnitine transporter novel
PA:	phosphatidic acid
PCho:	phosphocholine
PC-PLC:	phosphatidylcholine specific phospholipase C
PCr:	phosphocreatine
PD:	phosphodiesterase
PDE:	phosphodiester
PDGF:	platelet derived growth factor
PE:	phospho-ethanolamine
PET:	positron emission tomography
PFC:	perfluorocarbon
Pi:	inorganic phosphate
PI3K:	phosphoinositide-3-kinase
PIP2:	phosphatidyl inositol biphosphate
PIP3:	phosphatidyl inositol triphosphate
PKA:	protein kinase A
PL:	phospholipase
PLA2:	phospholipase A2
PLC:	phospholipase C
PLD:	phospholipase D
PME:	phosphomonoester
ppm:	parts per million

PRESS: point resolved spectroscopy

PS: phosphatidylserine

PtdCho: phosphatidylcholine

PtdE: phosphatidyl-ethanolamine

PTEN: phosphatase and tensin homolog

RAF: rapidily accelerated fibrosarcoma

Ral-GDS: ral guanine nucleotide dissociation stimulator

RECIST: response evaluation criteria in solid tumors

rf: radio frequency

RISC: ribonucleic acid interference specificity complex

ROI: region of interest

ROS: reactive oxygen species

scr: scrambled

shRNA: small hairpin ribonucleic acid

siRNA: small interfering ribonucleic acid

SPECT: single photon emission computerized tomography

TDP: thymidine diphosphate

TEA: tetraethylammonium

TK: thymidine kinase

TMP: thymidine monophosphate

TS: thymidilate synthase

TTP: thymidine triphosphate

Chapter I : Introduction

1. Introduction

1.1 Background

Choline (2-hydroxy-N,N,N-trimethylethanaminium) is a water soluble, essential, quaternary amine (Blusztajn, 1998). This molecule is a critical part of acetylcholine, which acts as a neurotransmitter in many organisms. Activated choline metabolism is characterized by increased phosphatidylcholine, one of the most common phospholipids used in membrane formation (Zeisel, 2012). Choline's main uses are for acetylcholine and phospholipid biosynthesis, but it is also oxidized to betaine, a methyl donor and osmolyte in the body. Choline can also be used as methyl donor in the synthesis of methionine, an essential amino acid (Vigneaud, 1940). Choline has multiple functions in the body and is involved in many physiological processes. It is an essential nutrient involved in the structure of cell membranes, primarily as a structural component of phospholipids. Choline is also involved in other process as cholinergic neurotransmission, lipid transport and methyl metabolism. Choline plays important roles in brain and memory development in the fetus and appears to decrease the risk of the development of neural tube defects (Shaw, 2004). Many aliments are source of this essential choline, including eggs, meat, and fish.

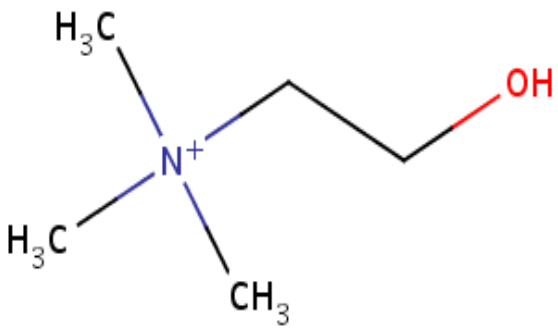

Fig.1. Chemical structure of choline

1.2 Choline metabolism

Choline is an essential nutrient for a normal function of all cells and is a major substrate of cell membranes phospholipids. The transformation of choline in phosphatidylcholine is a major step to form phospholipids of the cell membrane and phosphatidylcholine constitutes around the half of the membrane phospholipids (Zeisel, 1994). The intracellular enzymatic cycle of choline is called the “Kennedy pathway”. Activated choline metabolism is characterized by increased phosphocholine and total choline. The major molecular causes for this increase are a higher expression and activity of choline kinase alpha (Glunde, 2005), a higher rate of choline transport (Katz-brull, 1996) and increased activities of phosphatidylcholine specific phospholipase C and D (Iorio, 2005). All these enzymes participate in the synthesis of the major membrane phospholipid phosphatidylcholine (Glunde, 2004). The “cholinic phenotype” is being explored for radiological diagnosis, prognosis, monitoring treatment response and the development of novel therapies (Glunde, 2011).

The first step in the choline pathway (fig.2) is the uptake of choline into cells by choline transporters. The first reaction phosphorylates choline to form phosphocholine; catalyzed by choline kinase (ChoK). Phosphocholine is then converted by phosphocholine cytidylyltransferase (CTP) to form CDP-choline (cytosine diphosphate-choline). CDP-choline is then metabolized into phosphatidylcholine by addition onto a diacylglycerol. Phosphatidylcholine can be degraded by different phospholipases (PL) as PLA, PLC and PLD and increased levels of choline and phosphocholine (Georges, 1989). Intracellular accumulation of choline is a necessary step to increase tumor cells number and proliferation. (Michel, 2006).

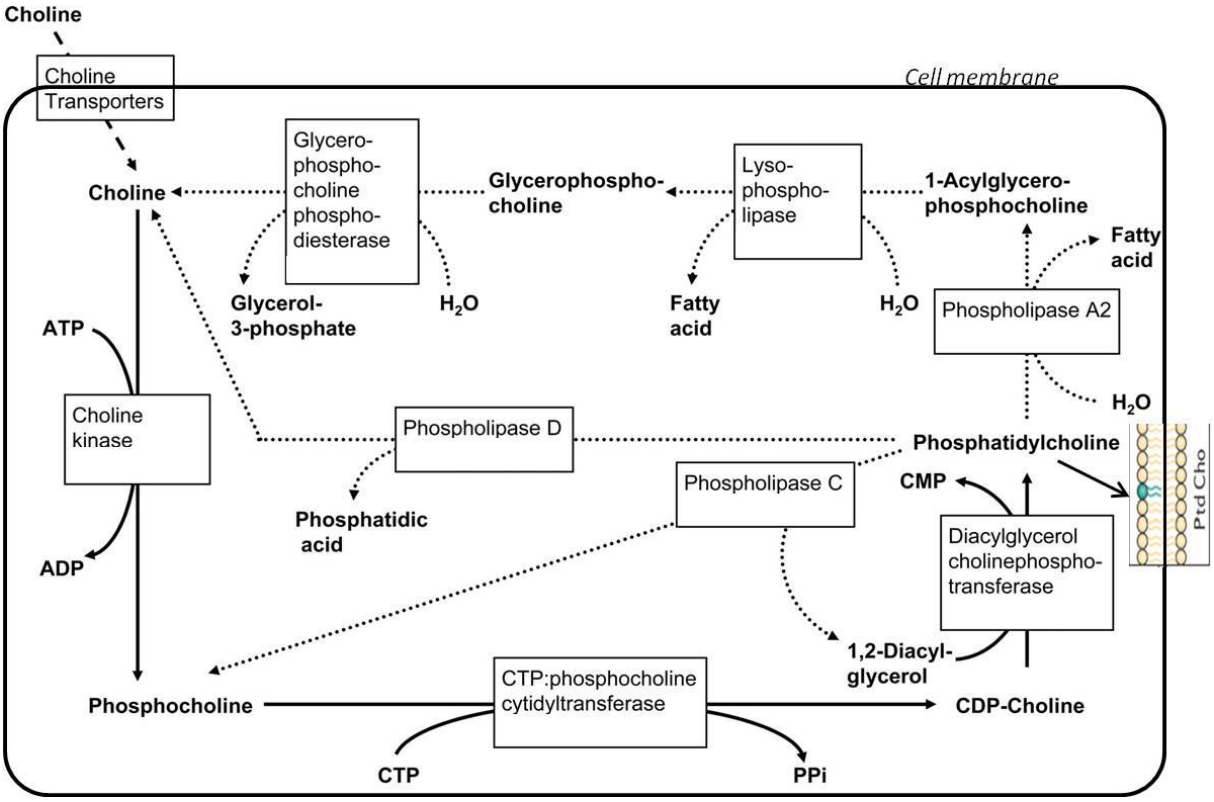

Fig.2. Choline pathway or Kennedy pathway: from choline uptake by transporters to phosphatidylcholine formation in the cell membrane. Adapted from Glunde, 2004.

1.21 Choline transporters

Choline is a charged hydrophilic cation and cannot pass into the cell by simple diffusion, which means that transport must be facilitated by some type of transporter. The transport of free extracellular choline into cancer cell can be a rate limiting step in phosphocholine formation (katz-bull, 1996). Choline is taken up into cell by four major classes of transporters; a high affinity choline transporter (CHT); a choline transporter like proteins (CTL), an organic cation transporters (OCT) and an organic cation/ carnitine transporter novel (OCTN) (Michel et al, 2006).

High affinity choline specific transporters (CHT) have CHT1 as major representative transporter. Those transporters are very active in the nervous system in cholinergic neurons. Those transporters are sodium dependent and this system is coupled to the biosynthesis of acetylcholine specific to neuronal tissue (Simon, 1976).

Choline specific transporters like proteins are represented by CTL1 who is expressed in cancers of various origins: central nervous system, breast, colon, ovary or prostate (Yuan, 2006) The CTL family is composed of at least six genes. This choline transporters family is sodium–independent and has an intermediate affinity for choline and hemicholinium-3 (HC-3) as compared to CHT1 (O'Regan, 2000).

OCT and OCTN are low affinity transporters for choline. Three OCT members (OCT1–3) and two OCTN members (OCTN1 and OCTN2) have been identified and broadly detected in human tissues. These transporters non-specifically deliver choline for phospholipid synthesis (Wang, 2007).

Based on the kinetics of choline uptake, increased choline transporter activation can contribute to phosphocholine accumulation (Eliyahu, 2007).

1.22 Choline kinases

Choline kinase (ChoK) is primarily located in the cytoplasm of cells. Three isoforms of ChoK (ChoKα1, ChoKα2 and ChoKβ) exist in mammalian cells and are encoded by two separate genes: ChoKα and Chokβ. Homodimeric or heterodimeric forms of ChoK are enzymatically active (Aoyama, 2004). ChoK catalyses the phosphorylation of choline using ATP (adenosine triphosphate) as a phosphate donor, producing phosphocholine (Aoyama, 2004). This step using ChoK can be rate-limiting and can take a regulatory role in phosphatidylcholine

(PtdCho) synthesis under some circumstances (Aoyama, 2004). The upregulation of ChoK activity in cancer probably results from an increase in ChoKα expression. Moreover, the activity of ChoKα was shown to be increased in human breast carcinomas compared with normal breast tissue (Ramirez de Molina, 2002). This overexpression has been reported in several human tumor derived cell lines of multiple origins: lung, colon prostate and others (Gallego-Ortega, 2009; Ramirez de Molina, Rodriguez-Gonzalez, 2002). Increased enzymatic activity and overexpression of ChoKα is correlated with advanced histological tumor grade in breast carcinoma (Ramirez de Molina, 2002). ChoKα expression and activity is directly associated with increased cancer cells proliferation and malignancy, making of it a potential prognostic marker of some cancers (Ramirez de Molina, 2007).

ChoKα and ChoKβ are similar in their primary sequence but they are implicated in different metabolic pathays. While ChoKα1 affects into both phosphatidylcholine and phosphatidylethanolamine synthesis, ChoKβ affects only phosphatidylethanolamine synthesis. Furthemore, the transformation capacity seems to be exclusive to the ChoKα isoform. ChoKβ overexpression is not sufficient to induce *in vitro* cell transformation or *in vivo* tumor growth. The proliferative and oncogenic activities are linked with ChoKα and this isoform is one of the major targets of the choline pathway for antitumoral treatment (gallego-ortega, 2009).

1.23 Phosphocholine cytidylyltransferase (CTP)

This enzyme catalyses the synthesis of CDP-choline from phosphocholine (PCho) and cytidine triphosphate. CDP-choline is an active choline intermediate of the choline pathway which forms the membrane lipid phosphatidylcholine

(PtdCho). Phosphocholine cytidylyltransferase catalyses a regulatory step in PtdCho synthesis in normal cells as well as in cancer cells (Kent, 1997). Four homologous isoforms of CTP exist in mammalian cells. The control of CTP activity is very complex and this control is linked to oncogenic signaling. For example, CTP activity is increased in liver tumorigenesis and in colon cancer which results in elevated PtdCho levels (Bell, 1998; Dueck, 1996). An increase in CTP activity could decrease the phosphocholine levels. However several enzymes as ChoK can increase intracellular PCho and counteract a possible depletion of cellular PCho levels, thereby facilitating enhanced cell growth (Bell, 1998).

1.24 Phosphatidylcholine hydrolysis

Specific phospholipase D (PLD) hydrolyses PtdCho to phosphatidic acid and choline; this hydrolysis produces intracellular free choline (Cho). PLD1 and PLD2 are crucial in cell proliferation, survival signaling, cell transformation and tumor progression (Buchanan, 2005). High levels of PLD activity can be correlated with aggressiveness in human breast cancer cells (Imamura, 1993).

Specific phospholipase C (PLC) can hydrolyse PtdCho producing PCho and diacyl-glycerol. The activation of PLC can partially cause a higher PCho levels linked to ovarian carcinogenesis (Spadaro, 2008).

1.3 Aberrant metabolism of choline in cancer

During malignant transformation and growth, there is a reprogrammation of lipid metabolism, in particular fatty acid synthesis (Swinnen, 2006; Menendez, 2007). The ultimate goal of these modifications is

to provide cellular biomass for accelerated tumoral growth (Hsu, 2008). This is also called the “cholinic phenotype” of tumors.

Phospholipids play a dual role of basic structural components of membranes and substrates of reactions involved in key regulatory functions in mammalian cells (Vance, 2004). PtdCho, the most abundant phospholipid in eukaryotic cell membranes, can generate second messengers and mitogens, such as diacylglycerol (DAG), phosphatidic acid (PA), which is, in turn, a precursor of DAG and lysophosphatidic acid (LPA), arachidonic acid (AA) and lysophosphatidylcholine (LPtdCho), through three major catabolic pathways mediated by specific phospholipases of types C (PLC) and D (PLD), acting at the two distinct phosphodiester bonds of the PtdCho headgroup, and by phospholipase A2 (PLA2) in the deacylation reaction cascade (Fig. 3). PCho, either produced by choline kinase (ChoK) in the first reaction of the three-step Kennedy biosynthetic pathway, or via PLC-mediated PtdCho catabolism, has also been shown to be mitogenic by acting as a mediator of growth factor-associated cell proliferation (Podo, 2011).

1.31 Regulation of choline metabolism by oncogenic signaling

Choline metabolism is known to be regulated by oncogenic signaling (Glunde 2011). Many studies indeed emphasize the complex reciprocal interactions between oncogenic signaling and choline metabolism. But, how and where PCho is involved in the growth signaling cascade, and its relationship with the induction of ChoK activity downstream of Ras activation, remain to be determined (Podo, 2011). Several relationships therefore exist between the PtdCho cycle and cell receptor-activated signal transduction pathways, with implications for the biogenesis and utilization of other lipids and phospholipids

(Podo, 2011). Some of the existing links between ChoK activation and Ras-GTP-stimulated phosphorylation cascades, mediated by Ras-effector serine/threonine-specific protein kinase encoded by RAF-1 gene (Raf-1), Ral guanine nucleotide dissociation stimulator (Ral-GDS) and phosphoinositide 3-kinase (PI3K) effectors, are depicted schematically in Fig. 3.

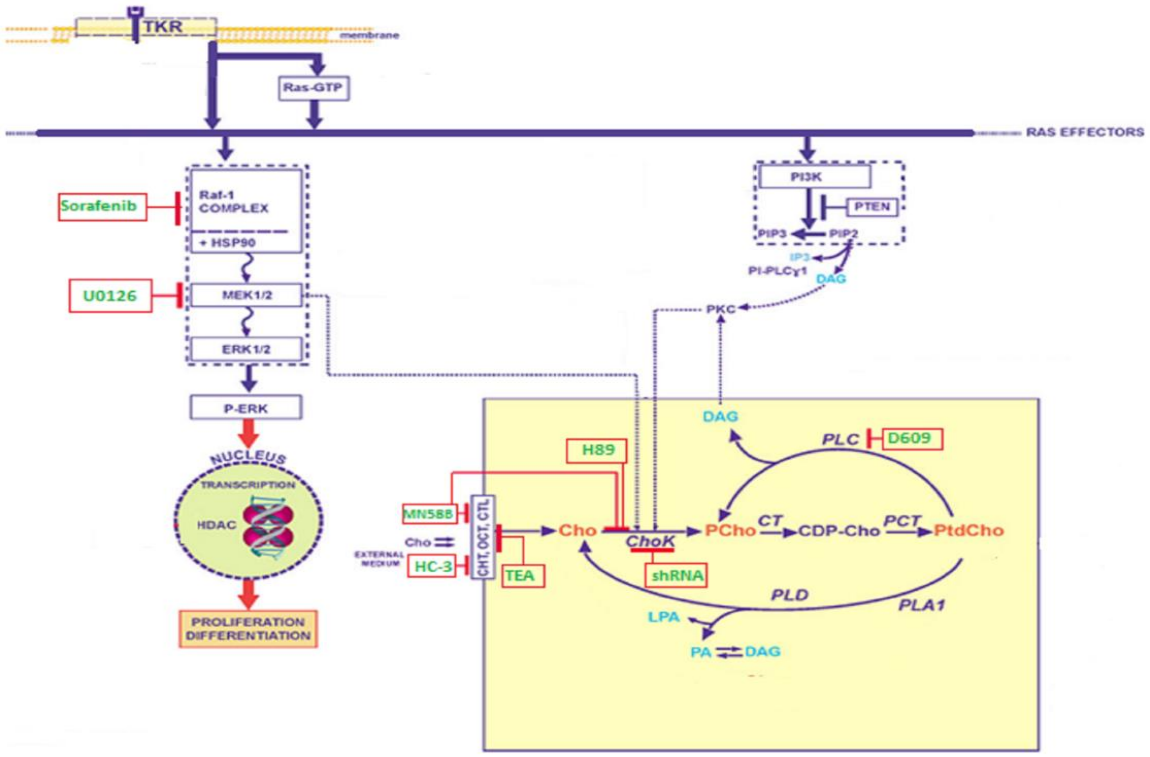

Fig.3. Schematic representation showing links between phosphatidylcholine (PtdCho) de novo biosynthesis and catabolism (yellow box) and some signal transduction pathways. PtdCho cycle metabolites: CDP-Cho (cytidine diphosphocholine); Cho (free choline); DAG (diacylglycerol); GPCho (glycerophosphocholine); Gro3P (sn-glycerol 3-phosphate); LPtdCho (lysophosphatidylcholine); PA (phosphatidic acid); PCho (phosphocholine). Adapted from Podo, 2011.

Importantly, Yalcin et al. found in 2010 that small interfering RNA (siRNA) silencing of choline kinase expression in transformed HeLa cells (epitheloid cervix carcinoma cells) completely abrogated the high concentration of phosphocholine, which in turn decreases phosphatidylcholine, phosphatidic

acid and signaling through the MAPK and PI3K/AKT pathways. These simultaneous reductions decreased the anchorage-independent survival of HeLa cells. In addition, they confirmed the relative importance of phosphatidic acid for the pro-survival effect as phosphatidic acid supplementation fully restored MAPK signaling and partially rescued HeLa cells from choline kinase inhibition. Taken together, these data indicate that the pooling of phosphocholine in cancer cells may be required to provide a ready supply of phosphatidic acid necessary for the feed-forward amplification of cancer survival signaling pathways (Yalcin, 2010).

a. MAPK pathway and choline cycle

MAPK signaling is involved in key cellular functions, including proliferation, motility and apoptosis. A major component of MAPK signaling is represented by the reaction cascade involving Ras, c-Raf, the MAPK/ERK kinases MEK1/2 and the extracellular signal-regulated kinases ERK1/2 (Fig.3). This pathway, following Ras mutation, results in an aberrant activation of target proteins and transcriptional factors in about 30% of human cancers.

Each of the enzymes involved in choline metabolism is known to be affected by the RAS pathway. Oncogenic RAS can activate ChoK and controls the transcription of CTP through the activation of the MAPK pathway (Ramirez Molina, Penalva, 2002; Bakovic, 2003). In addition, several oncogenes including RAS increase ChoKα activity, resulting in higher intracellular levels of phosphocholine (Ramirez de Molina, 2005). These elevated expressions can lead to enhanced PtdCho synthesis, enabling rapid cell proliferation and tumor growth. Moreover, platelet derived growth factor (PDGF) can stimulate the phospholipase expression to elevate PCho levels. This high level of expression is

combined with increased ChoK activity to activate the choline pathway (Plevin, 1991).

In the purpose, it has been shown that U0126, a MAPK inhibitor, induces a drop in phosphocholine by inhibition of choline uptake and phosphorylation (Beloueche-Barbari, 2005). Also, this MAPK inhibitor is able to block phosphocholine formation in human colon carcinoma cells by interfering with choline uptake and phosphorylation via choline kinase (Liu, 2002). These studies have shown that pharmacological inhibition of MAPK signaling in cancer cells can be associated with modulations of choline pathway, reduced tCho level that precedes effects on cell cycling.

Another inhibitor of the MAPK pathway was shown by our group to significantly decrease the total choline peak after 2 days of treatment with sorafenib (Karroum 2013). This observation suggests that the action of Sorafenib as MAPKinases inhibitor could result in an indirect inhibition of the choline pathway. Indeed, inhibition of MAPK signalling can result indirectly in reduced PCho and tCho levels; this effect is primarily mediated by ChoK inhibition as a result of its reduced expression downstream of Hypoxia Induced Factor 1 activation (Glunde 2008). Sorafenib, also named BAY 43-9006 and Nexavar, is used for the treatment of renal cell carcinoma and hepatocellular carcinoma (Pratilas, 2010). It is a small molecule multi-targeted kinase inhibitor that blocks RAF/MEK/ERK pathway. This inhibitor has other biologically relevant targets including vascular endothelial growth factor receptors, platelet derived growth factor receptors, fibroblast growth factor receptor,… (Wilhelm, 2004). Sorafenib is therefore able to affect both tumor signaling and angiogenesis. Preclinically, Sorafenib shows broad-spectrum antitumor activity in renal, colon, hepatocarcinoma, breast, non–small cell lung, ovarian, thyroid,

pancreatic, and melanoma xenograft models, involving either antiproliferative and/or antiangiogenic effects of the drug (Wilhelm, 2006). Sorafenib has potential toxicities as cardiotoxicity, hand-foot skin reaction and rash, hypertension, gastrointestinal perforations,… The more common undesirable effects of Sorafenib are described as : infection, lymphopenia, anorexia, haemorrhage,… This multi kinase inhibitors has many targets and must be used with caution.

b. PI3K pathway and choline cycle

The type I PI3K pathway triggered by cell receptor stimulation and Ras activation, and also involving chemokines and adhesion molecules, mediates the conversion of phosphatidylinositol 4,5-bisphospate (PIP2) into phosphatidylinositol 3,4,5-trisphosphate (PIP3), which, in turn, acts as an effector of downstream cell signaling, including AKT phosphorylation (Fig.3) (Cantley, 2002). An aberrant PI3K pathway and altered expression of the antagonizing phosphatase and tensin homolog (PTEN) are involved in tumor progression, angiogenesis, invasion and cell survival (Vivanco, 2002) .

Phosphoinositide-3-kinase (PI3K) pathway can also affect the choline metabolism and has an action on choline uptake in lung carcinoma cell lines (Wang, 2007). PI3K-AKT also affects ChoK activation (Ramirez de Molina, Penalva 2002). Knockdown of ChoKα with small interfering RNA leads to the attenuation of MAPK and PI3K-AKT signaling and is associated with the inhibition of cell proliferation (Yalcin 2010). Contrarily, ChoKα contributes through a positive feedback to increased MAPK and PI3K signaling (Glunde, 2011). The inhibition of PI3K using PI-103, results in a significant decrease in treated prostate and colon carcima cells volume compared to controls. Monitoring the changes in phosphocholine and tCho levels by MRS may

provide noninvasive pharmacodynamic biomarkers of PI3K pathway inhibition and potentially of tumor response (Al-Saffar, 2010).

c. HIF and choline cycle

Stabilization of the subunit of hypoxia-inducible transcription factor-1 (HIF-1) and upregulation of its target genes play an important role in the metabolic machinery by which cancer cells undergo adaptive responses to hypoxic conditions and maintain a high proliferative rate in the presence of an altered bioenergetic balance between downregulated oxidative phosphorylation and increased glycolytic rate (Semenza, 2013). HIF-1 can increase ChoKα expression within hypoxic environments, consequently increasing cellular PC and tCho levels within these environments. Cells that survive in a hypoxic environment are likely to demonstrate elevated PCho levels (Glunde, 2008). Glunde et al indicated that MRSI detection of tCho might prove to be a useful biomarker not only of tumor aggressiveness and progression but also of tumor hypoxia (Glunde, 2008). On cells, Glunde et al observed a significant increase of ChoK and phosphocholine at exposure to hypoxia. There is a colocalization between the ChoK and the hypoxia in tumors (Glunde, 2008). This study suggests that the hypoxia inducible factor (HIF-1) can bind the hypoxia response elements of ChoKα promoter to increase ChoKα expression within hypoxia environments (Glunde, 2008). This suggestion was confirmed by Bansal et al; the transcriptional control of choline phosphorylation is largely mediated via HIF-1α binding to the newly identified hypoxia response element 7 of the ChoKα (Bansal, 2012). The inhibition of the MAPK signaling pathway resulted in reduced tCho levels mediated by ChoK inhibition as a result of its reduced expression of HIF-1 activation. HIF-1 is activated under hypoxic condition and degraded under normoxic condition. A

correlation was observed between region of high tCho levels and hypoxia in vivo due to the regulation of choline kinase by HIF-1 (fig.4) (Glunde, 2008).

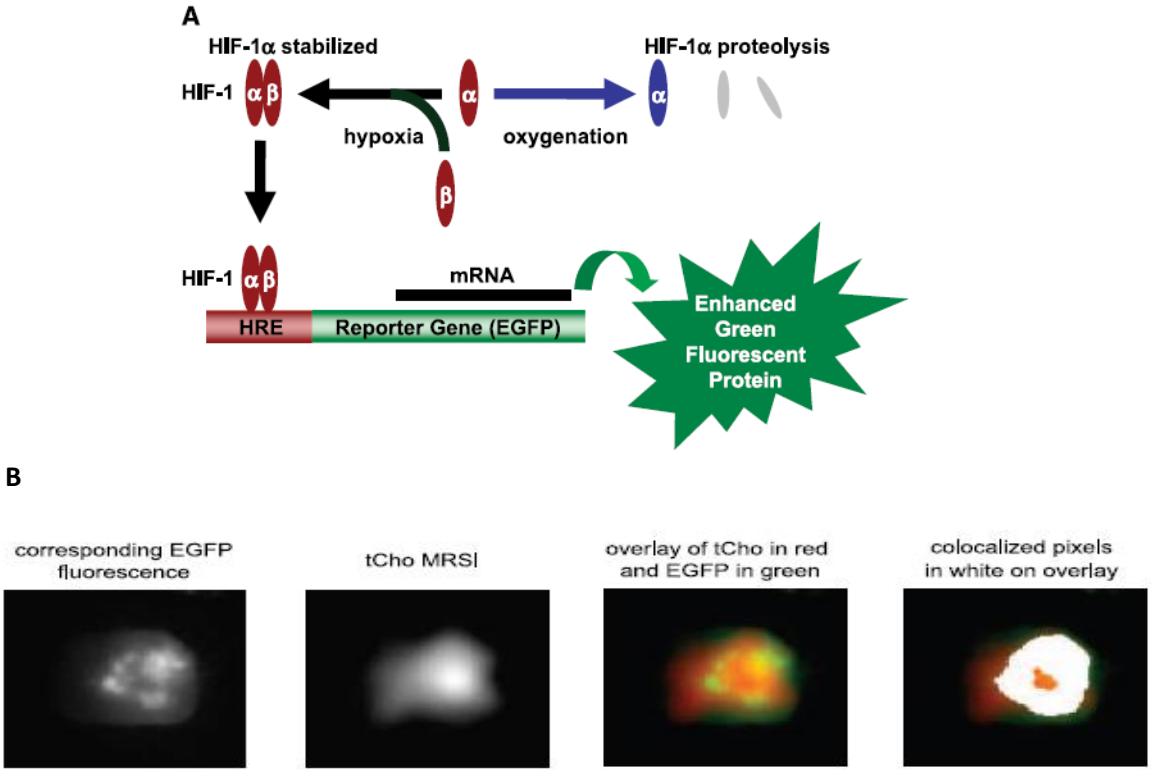

Fig.4. (A)The hypoxia response element linked with the enhanced green fluorescent protein is activated by HIF-1 under hypoxic conditions. HIF-1α is degraded under normoxic conditions. The binding of HIF-1 with the hypoxia element results in green. (B) The green fluorescence and the corresponding spectroscopy imaging of tCho were coregistered. In the resulting overlay image, the tCho image has been rendered in red, whereas green fluorescence is shown in green so that colocalization becomes yellow. Adapted from Glunde, 2008.

1.32 The choline cycle as a target in oncology

a. Inhibition of ChoKα

ChoKα is an important potential target in the cholinic cycle. Lacal and al suggested ChoKα inhibition as an antitumour therapy (Hernandez-Alcoceba,

1997). Lacal group developed the drug MN58b, a specific inhibitor of ChoKα (Rodrigez-Gonzalez, 2003).

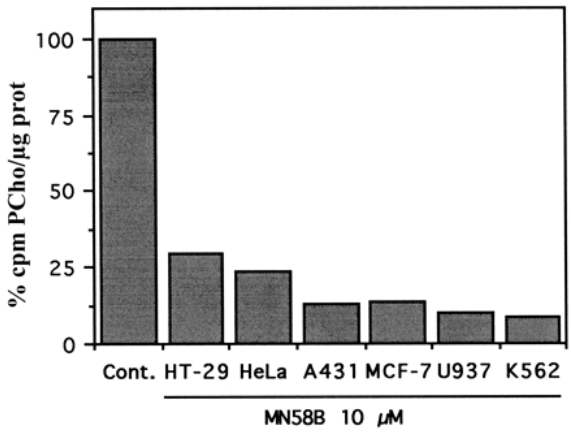

Fig.5. Inhibition of PCho production by MN58B on different human cell lines, this effect is correlated with the inhibition of proliferation. Adapted from Hernandez-Alcoceba 1999.

This compound exhibits significant antiproliferative activity and induces a strong reduction of tumour growth in nude mice xenografts (Rodrigez-Gonzalez, 2003; Rodrigez-Gonzalves, 2004). MN58b shows more than 20-folds higher efficiency towards ChoKα1 than ChoKβ (Gallego Ortega, 2009). The treatment of a MDA-MB-231 (breast) carcinoma with this inhibitor results in a specific decrease of phosphocholine and tCho levels in tumors (Al-Saffar, 2006). These changes in metabolites have the potential to be qualified as non-invasive pharmacodynamic biomarkers for detecting tumor response following treatment with choline kinase inhibitors (Al-Saffar, 2006). The induction of apoptosis by inhibition of ChoKα is related to the specific and significant increase of intracellular pro-apoptotic ceramides (a product of sphingomyelin metabolism) in tumor cells (Rodríguez-González, 2005). Moreover the PI3K/AKT and ERK (Extracellular signal-regulated kinases from the MAPK pathway) signaling pathways can be inhibited by ChoK inhibitors (Chua, 2009). In vivo,

the ChoK inhibition slowed tumor growth through the inhibition of Akt phosphorylation (Chua, 2009). Pharmacological inhibitors targeting ChoKα result in tumor growth inhibition and apoptosis. Targeting ChoKα results in decreased PCho and tCho levels. A significant decrease of cell proliferation and induction of differentiation in human breast cancer cells and tumors xenografts was observed with ChoKα downregulation (Glunde, 2005). ChoK is required for breast tumor progression and pharmacological inhibition of ChoK reduced tumor growth in breast cancer (Ramirez de Molina 2004). Moreover the down regulation of ChoK using siRNA resulted in low uptake and retention of choline (Nimmagadda, 2009). These results support the targeting of choline kinase and show the potential ability of non-invasive MRS and radiolabeled choline to detect choline pathway modulation and tumor sequestration of choline. ChoK silencing may provide an alternative to enhance the effect of anticancer drugs in malignant cells as 5-fluorouracil (5-FU) treatment. In colorectal cancer ChoKα inhibitors induce a down regulation of the levels of both thymidilate synthase (TS) and thymidine kinase (TK), contributing to the induction of apoptosis triggered by 5-FU treatment. The mechanistic basis for the synergism seems to rely on the finding that ChoKα inhibitors are modulating the levels of TS and TK1 enzymes which are related to 5-FU metabolization (de la Cueva, 2013).

N-[2-bromocinnamyl(amino) ethyl]-5-isoquinolinesulphonamide (H-89) is a molecule used as a specific cyclic-AMP-dependent protein kinase A (PKA) inhibitor. It has been used extensively for evaluation of the role of PKA in the heart, osteoblasts, hepatocytes, smooth muscle cells, neuronal tissue, epithelial cells, …(Lochner, 2006). It has also been shown that H89 inhibits at least 8 other kinases (MAPKAP-K1b, MSK1, KBα, SGK, S6K1, ROCK II, AMPK, and CHK1), while having a relatively large number of PKA-independent effects (Lochner, 2006; Davies, 2000). H-89 has been reported to inhibit

phosphocholine production and ChoK activity in HeLa cell lysates (Aboagye, 1999). In the presence of 10 microM H-89, choline kinase activity was inhibited by 36 +/- 7.6% in vitro (Wieprecht, 1994). However in plasmodium falciparum, the inhibition of ChoK using H89 failed and ChoK catalized the formation of phosphocholine as efficiently as control cells (Choubey, 2007). In his study Gabellieri et al tested the effect of H-89 on samples of purified ChoK and showed that H-89 is capable of directly inhibiting ChoK activity independently of PKA or any other targets in cell lysates of MDA-MB-231 breast, PC-3 prostate and HeLa cervical cancer cells and in solutions of purified human ChoK. This is an off-target effect for H-89 (Gabellieri, 2009).

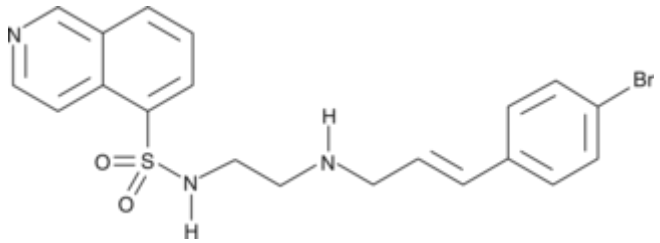

Fig.6. Chemical structure of Protein Kinase Inhibitor H-89; 5-Isoquinolinesulfonamide (CAS 127243-85-0)

b. Inhibition of choline transporters

The choline transport is also proposed as a potential therapeutic anticancer agent. Choline transport is required for cellular membrane construction and is a rate-limiting step for acetylcholine production (Lockman, 2002). The choline transport can be inhibited using specific pharmacological inhibitors of the choline transporters as Hemicholinium-3 (HC-3) and Tetraethylammonium (TEA) (fig.7). HC-3, which inhibits low affinity sodium independent choline transport is not specific to choline transport and also inhibits ChoK (Hernandez-Alcoceba, 1997). TEA inhibits the organic cation

transporters. In prostate cancer cells, the choline uptake is reduced by 95% using hemicholinium-3 and by 20% using TEA. In prostate cancer cells, the uptake of choline is mediated by selective choline transporters other than by the OCT (Muller, 2009).

C. Other modulations

The inhibition of CTP activity is proposed to prevent CTP translocation to the membrane and as anti neoplasic therapy. This inhibition increases cellular PCho levels and decreases PtdCho level (Geilen, 1992; Jimenez-Lopez, 2002). The Miltefosine treatment, an inhibitor of CTP, has been approved for the topical treatment of cutaneous metastases of mammary carcinomas (Clive, 1999)

Phospholipase-D is involved in cell proliferation and oncogenic signaling; PLD can be a valuable target for therapeutic intervention in cancer (Glunde, 2011). The anti oestrogen drug tamoxifen activates PLD and PLC and increases levels of DAG, PCho and phosphoethanolamine which may lead to change in cell growth (Cabot, 1997).

Phospholipase-C inhibition reduced HER2 expression on the plasma membrane and induces antiproliferative effects. The D609 was shown to be a potent inhibitor of PLC in a dose-dependent manner and reduced PCho levels (fig.7) (Amtmann, 1996). D609 showed promising results in various animal and human cancer cells lines and transformed cells in vitro (Amtmann, 1987). However, in in vivo animal studies D609 exhibited only a little antitumor activity (Schick 1989).

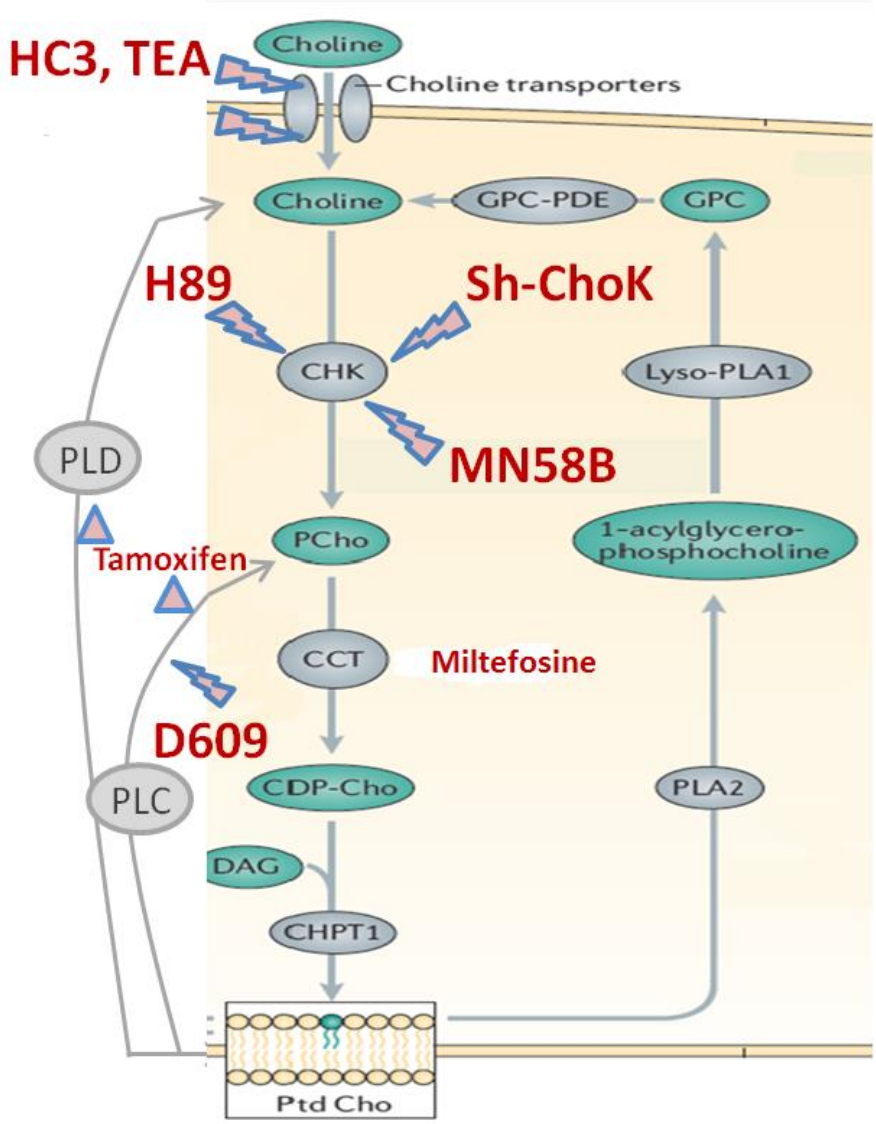

Fig.7. *Inhibition of choline cycle using pharmacological molecules or shRNA. Adapted from glunde, 2011.*

1.4 Imaging markers of response to treatment

In oncology, tumor size measurements before and after treatment is the most widely used method for evaluating tumor response to treatment (Afaq, 2010). However, reduction in tumor size usually occurs late after the start of treatment and is insensitive to early treatment effects. Moreover many of new

treatments are targeted towards specific metabolic pathway. Many of these drugs can be clinically active but may not result in significant reduction in tumor size (Afaq, 2010). For these reasons the RECIST size criteria (Response Evaluation Criteria in Solid Tumors) have potential limitations to evaluate the effectiveness of a treatment. If there is a reduction in tumor size, this may not necessarily translate to improved survival for the patient.

There is therefore a crucial need to use non-invasive imaging to facilitate the evaluation of the responsiveness of experimental tumors in preclinical therapeutic studies. Because molecular and cellular changes precede macroscopic changes in tumor size, it would be ideal to have an assay that could quantify these changes in both clinical cancer therapeutics and preclinical drug trials. Early indicators of treatment response that could also provide information on the spatial heterogeneity of response would be of significant benefit for both experimental and clinical trials.

In the purpose, molecular imaging has the potential to assess tumor response to anticancer treatment by addressing metabolic or hemodynamic changes that will occur earlier than changes in tumor size. Molecular imaging techniques may involve magnetic resonance imaging, computed tomography scan (CT), ultrasound, optical and radionucleide techniques. In the purpose, measurement of tumor metabolism, vascularity, cellularity, and proliferation can be considered for assessing tumor response to anticancer treatment (Afaq, 2010).

1.41 Imaging tumor metabolism

a. FDG-PET

Glucose metabolism can be assessed using Positron Emission Tomography and the uptake of the ^{18}F-fluorodeoxyglucose (FDG) tracer (Shields, 2006). This is based on the observation by Warburg, Wind, and Negalein (1927) that glucose metabolism is increased in many tumors. To date, FDG-PET is widely used in diagnosis, staging, and monitoring of therapy, as the method has unsurpassed sensitivity for detecting occult metastases (Shields, 2006; Culverwell, 2011). By comparing the degree of tracer uptake on sequential studies before and after treatment, tumor response can be determined (Afaq, 2010). It is routinely used in the staging of lung cancer at many centers, and has found regular use in the assessment of melanoma, lymphoma, colon, breast, head and neck, esophageal cancer,… (Valk, 2003). In the clinical setting, FDG-PET is usually associated with an x-ray computed tomography (CT) to combine metabolic data with anatomic imaging obtained by CT scanning. More over PET/CT can be used as a predictor of early response to chemotherapy in locally advanced breast cancer patients, lymphoma, pediatric cancer, lung cancer, ... PET/CT plays important role in early assessment of treatment response in various cancer patients. A positive PET/CT scans after the completion of therapy is a strong predictor of residual disease, whereas, a negative study is associated with complete remission in these patients (Kumar, 2010).

A limitation of FDG, however, is the fact that enhanced glucose metabolism is not specific for tumors alone. Indeed, enhanced FDG uptake has also been observed in muscle, brain, infected and inflammatory tissue (Direcks, 2008). Also, importantly, some tumor types are non-glucose avid and lead to false negatives (Culverwell, 2011).

b. Magnetic Resonance Spectroscopy

Metabolic activity can also be evaluated using MR spectroscopy (MRS), a technique that can identify and quantify tumor metabolites. MRS uses the same general principles and equipment as MRI. However, while MRI builds images using signals from ^{1}H nuclei in tissue water, present at high concentrations, MRS measures signals from magnetic nuclei of tissue metabolites such as choline, creatine, and lactate that are present at much lower concentrations. A number of nuclear magnetic resonance (NMR)-active isotopes are available for interrogation in vivo. The most common nuclei used are ^{31}P and ^{1}H, which generate spectra that are dominated by resonances from endogenous metabolites (Gillies, 2005). ^{13}C-MRS however is used to monitor the uptake and metabolism of ^{13}C-enriched metabolites and serves as a tool for monitoring the fate of the label, as it is incorporated into other metabolic intermediates such as glutamine and lactate in the case of ^{13} C-labeled glucose. When used in combination with imaging strategies, multinuclear MRS methods provide detailed biochemical information that can be directly correlated with anatomical features (Li, 2015).

^{1}H-MRS has the highest sensitivity and can detect many metabolites including lipids, creatine/phosphocreatine (PCr), glycolytic intermediates such as glucose, glutamine/glutamate and lactate, in addition to choline-containing compounds such as phosphocholine (PCho) and glycerophosphocholine (GPC) (Table 1). ^{31}P-MRS, on the other hand, has particular value for studies concerned with tissue bioenergetics, pH and membrane turnover, it can detect the presence of bioenergetic metabolites such as nucleotide triphosphates (NTP), PCr and inorganic phosphate (Pi), in addition to membrane phospholipid metabolites including phosphomonoesters (PME), which comprise PCho and

phosphoethanolamine (PE), and phosphodiesters (PDE), which comprise GPC and glycerophosphoethanolamine (GPE) (Belouche-Babari, 2010).

Istope	Resonance frequency (MHz) at 2.3 T	% Natural abundance	Sensitivity relative to ^{1}H	Monitoring of metabolite levels/fluxes and physiological parameters
^{1}H	100	99.985%	100	Choline phospholipid metabolism Glycolysis and products (lactate, alanine) Neutral lipid metabolism Amino acids pH intra- and extracellular
^{31}P	40.5	100%	6.6	Bioenergetics (NAD^-) Phospholipid metabolism pH intra- and extracellular
^{13}C	25.1	1.107%	1.6	Flux of metabolites in biochemical pathways (glycolysis, metabolism,…)
^{19}F	94.1	100%	83	Fluorinated drug uptake and pharmacokinetics Metabolic pathways with ^{19}F substrate Oxygen tension pH

Table 1. *Summary of commonly utilized isotopes to monitor cancer cell metabolism by MRS. Adapted from Podo, 2011.*

MRS profiles greatly contributed in the 1990s to the identification of the characteristics of altered choline-phospholipid metabolism in cancer cells and tissues, as a potential source of novel indicators of tumor progression and response to therapy (Podo, 1999). Elevation of the ^{1}H-MRS resonances band at 3.2 ppm, mainly as a result of the trimethylammonium headgroup of Cho-containing metabolites. Therefore arising from the nine chemically equivalent protons in the highlighted choline–$N(CH_3)_3$ groups of Cho, PCho and GPC has been reported as a common feature in a large variety of cancers (fig.8). Changes in the MRS tCho spectral profile reflect altered contents and metabolic fluxes of phosphocholine (PCho), glycerophosphocholine (GPC) and free choline

(Cho) through the biosynthetic and catabolic pathways of the phosphatidylcholine (PtdCho) cycle (Podo, 2011). The two main contributors, phosphorylcholine and glycerophosphocholine cannot be separated due to the small chemical shift difference relative to the spectroscopic linewidths (de Graaf, 2007).

Alterations in the levels of PCho and GPC can also be detected in the ^{31}P-MRS frequency ranges typical of phosphomonoester (PME) and phosphodiester (PDE) compounds, respectively, together with those of phosphatidylethanolamine (PtdE) derivatives, phosphoethanolamine (PE) and glycerophosphoethanolamine (GPE) (Podo, 2011).

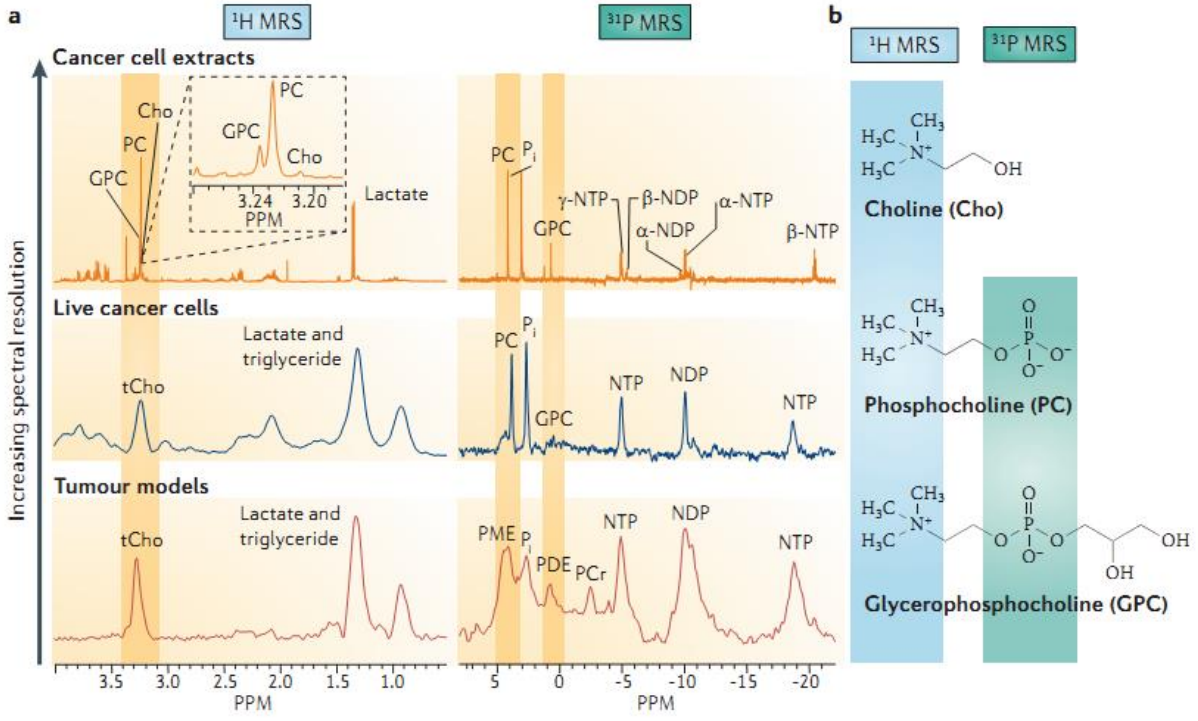

Fig.8. *Choline metabolism investigated with ^{1}H and ^{31}P-MRS in tumour models, live cancer cells and cancer cells extracts (a). Chemical strucuctures of choline metabolites (b). The 3.2 ppm "total choline"(tCho) peak consists of choline (Cho), phosphocholine (PCho) and glycerophosphocholine (GPC), which can be resolved in high-resolution ^{1}H-MRS spectra of tissue and cell extracts. Adapted from Glunde, 2011.*

The interest in choline (tCho peak, detectable with both ^{1}H and ^{31}P-MRS) primarily comes from its utility as a biomarker for cancer staging and diagnosis. This was first documented by Negendank (1992) who provided strong evidence for elevated phosphomonoesters in lymphomas and head and neck cancers. As stated above, choline compounds are precursors of acetylcholine and cells membrane; they are involved in phospholipid synthesis and reflect membrane turnover. However the interpretation of change in choline spectroscopy is complicated due to the multiple contributions (de Graaf, 2007). Nevertheless, elevated choline (reflecting increased membrane synthesis and a higher cell turnover) has been confirmed for breast, prostate, colon, cervical, and brain cancers and metastases, among others. Changes in choline are associated with positive responses in cancers in vitro (Podo, 2011) and in animal models (Gillies, 2005; Beloueche-Babari, 2010; and Podo, 2011), summarized in table 2.

The table below shows the described impact of different targeted therapies on major molecular targets cited in this work and their impact on metabolites measured by MRS.

Therapy	**Molecular target**	**Metabolites changes in cells**	**Metabolite changes in vivo/ex vivo**	**Reference**
MN58b (derivative from HC-3)	ChoK	↓phosphocholine	↓tCho ↓ phosphocholine	Al-Saffar, 2006
PX-478	Hif-1α		↓tCho ↓ phosphocholine ↓Glycerophosphocholine	Jordan, 2005
LY294002 & wortmannin	PI3K	↓ phosphocholine ↑glycerophosphocholine		Beloueche-babari, 2006
U0126	MEK1	↓ phosphocholine		Beloueche-babari, 2005
Sorafenib	MAPK		↓tCho	Karroum, 2013
H89	PKA, ChoK	↓ phosphocholine		Gabellieri, 2009
D609	PC-PLC	↓ phosphocholine		Iorio, 2010
Docetaxel	Antimitotic chemotherapy – stabilization of microtubules		↑ choline metabolites shortly after treatment (1-2 days) in sensitive tumors	Van Asten, 2015
suberoylanilide hydroxamic acid	Histone deacetylase inhibitor	↑ choline kinase α ↑ phosphocholine ↑glycerophosphocholine		Ward, 2013

Table 2. Non exhaustive summary list of MRS studies used to assess response to different classes of molecular-targeted therapies in pre-clinical tumour models.

Note that, if most of the time, decrease in choline metabolites is observed in response targeted agents, some inhibitors do show an increase in choline metabolites. Adapted from Beloueche-Babari, 2010.

Even if there is an accumulation of in vitro and in vivo data suggesting choline as a marker of response to treatment, interpretation of the tCho spectral profile in terms of pharmacodynamics biomarkers of targeted therapies is, however, made rather complex by the dual role of each tCho component as both substrate and product in PtdCho cycle pathways. Indeed, Cho can enter the Kennedy pathway following transport from the external medium, or PLD-catalyzed PtdCho hydrolysis, or phosphodiesterase (PD)-mediated GPC degradation; PCho, either synthesized by Cho phosphorylation or produced by PLC-mediated PtdCho degradation, acts as a substrate for the second reaction of the Kennedy pathway, catalyzed by CTP: phosphocholine transferase or cytidylyltransferase in the key regulatory step of PtdCho biosynthesis; and, finally, GPC, generated by PtdCho deacylation, can also act as a substrate for PD-mediated hydrolysis into Cho and sn-glycerol 3-phosphate (Gro3P) (Fig. 3). Therefore, elevation or reduction in the contents of PCho and tCho in cancer cells during tumor progression, or in response to therapy, may actually reflect a multiplicity of alterations taking place at the genetic, transcriptional, epigenetic and post-transcriptional levels (Podo, 2011).

From a clinical perspective, choline ^{1}H-MRS is also considered for tumor staging and monitoring. Most of clinical magnetic resonance scanners are equipped with sequences for spectroscopy measurements. The addition of spectroscopy to standard MRI techniques can significantly increase the sensitivity up to 88%, the specificity to greater than 90%, and the diagnostic accuracy up to 91% (Glunde and Bhujwalla, 2011). Choline metabolites can be a robust biomarker and can help to identify a lesion or to evaluate the efficacy of

a treatment. The proton spectroscopy of tCho can assist in diagnosing cancer and in specifying the margin of a breast tumor (Jacobs, 2004). The tCho spectrospy of the brain permits to distinguish tumor recurrence from necrosis (Wald, 1997).

Detecting the early response of a tumor to treatment is very important to reduce damage with normal tissue in patient with non-responding tumors (Glunde and Bhujwalla, 2011). Changes in tCho can help to detect early response after a treatment and possibly predict tumor response based on tCho signal in patients with advanced breast cancer who responded or not to neoadjuvant chemotherapy (Danishad, 2010). Anticancer treatments leading to apoptosis or necrosis induced characteristic decreases in choline metabolites (Evelhoch gillies, 2000).

tCho and other metabolite intensities can be translated into metabolomic profile and help to determine the tissue type. Metabolomic has the potential to detect lesions, guide biopsy, and to identify other conditions of malignancy, such as tumor aggressiveness (Wu, 2010).

1.42 Imaging cell death

As the cell undergoes apoptosis, there are a number of potential steps in the process that could be imaged: increase in cellularity with DW-MRI, or cytoplasmic lipid droplets associated with changes in the lipid structure during programmed cell death using ^{1}H-MRS.

Among those techniques, diffusion weighted MRI can assess tumor cellularity non-invasively (see section 1.54). DW imaging has indeed become a major contrast for tissue assessment by MRI (Bammer,2003; Norris, 2001) since the demonstration of the remarkable sensitivity of water diffusion to ischemia

in the brain, which prompted clinical interest in this novel MRI contrast. This technique is based on the mobility of water (or Apparent Diffusion Coefficient of water, ADCw) in a tissue. ADCw values are dominated by the presence of diffusion barriers (restriction effects). DW-MRI depends on the random small movements of water in the body. In the absence of barriers, these Brownian movements are totally free. The movement of water molecules in biological tissues is influenced by the cellular environment and by the integrity of membrane. The degree of restriction to water diffusion in vivo can be inversely correlated to tissue cellularity (Koh, 2007). The physical diffusion coefficients of intra- and extracellular water are not known with certainty. Nevertheless, because water is 'trapped' (on the NMR timescale) inside of the cells, the apparent diffusion of water within the cells is lower than that in the extracellular space. Hence, the measured ADCw is sensitive to cellularity. DW-MRI primarily reports on loss of cellularity (fig.9), which is the ultimate outcome not only of extensive necrosis (Koh, 2007) but also of other types of cell death, including apoptosis and mitotic catastrophe (Morse, 2007). Early and significant changes in ADCw can occur in case of mitotic catastrophe, lytic necrosis or apoptosis. All the changes in ADCw may be considered as a generalized measure of cytotoxic response to chemotherapy (Morse, 2007), although no assumption can be made on the type of cell death involved.

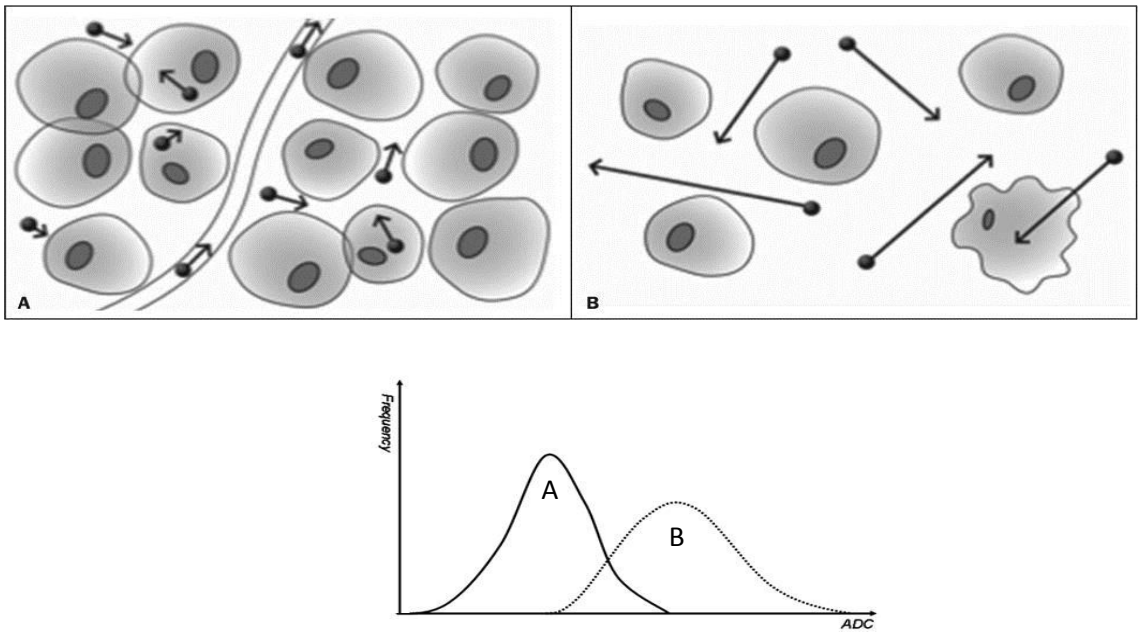

Fig.9. A restricted motion of water due to high cellularity (situation A) can influence the ADCw to lower value. The situation B represents a lower cells density and a higher ADCw. Adapted from Guimaraes, 2014.

Treatment of tumors may result in damage and/or killing of cells, thus altering the integrity of cell membranes or size of cells, thereby increasing the fractional volume of the interstitial space. These changes have been shown to increase the diffusion of water in the damaged tumor tissue (Kauppinen, 2002; Moffat, 2004; Ross, 2003). Successful anticancer therapies are correlated to early increases in tumor ADCw in both animals and humans (Jordan, Runquist, 2005). This is likely a consequence of reductions in cell volume, which are a general response to effective chemotherapy. Thus, by quantifying tumour ADCw before and after anticancer therapies, tumor response or lack of response to treatment can be determined. (Afaq, 2010).

Changes in the ADCw of tumors often precede any measurable change in tumor size or volume (Koh, 2007). Hence, determination of ADCw changes could be an advantageous tool for evaluating changes in the tumor

microenvironment before and after treatment (Koh, 2007). Moreover, in the clinical practice, the measure of ADCw allows much earlier adjustments in cancer therapy. In many cancers, an increase in ADCw has been reported within the first two weeks after the start of chemotherapy, radiotherapy or novel therapeutics and was correlated with tumor response to treatment (Afaq, 2010). Animal and clinical studies have shown that efficient treatments in many tumor types can be detected as an increase in tumor ADCw values due to the loss of cellular density (Thoeny, 2010). Many studies showed this characteristic increase of ADCw after different treatments, but a decrease of ADCw can also be observed. In different physiological or pathological conditions, cell swelling and shrinking changes the volume fractions of intra and extracellular spaces and lead to a drop in ADCw soon after initiation of a treatment, as summarized in Fig.10 (Jones, 2010 ; Afaq, 2010).

In general, any pharmacologic or radioactive process that causes necrosis, mitotic catastrophe or apoptosis will lead to increase the water diffusion in extra-cellular spaces and the corresponding ADC value. Cell death in response to treatment precedes size change; therefore, DW-MRI may be an early biomarker of response for therapies that induce mitotic catastrophe, apoptosis or necrosis. However, changes in ADC may depend upon treatment as shown in the following figure.

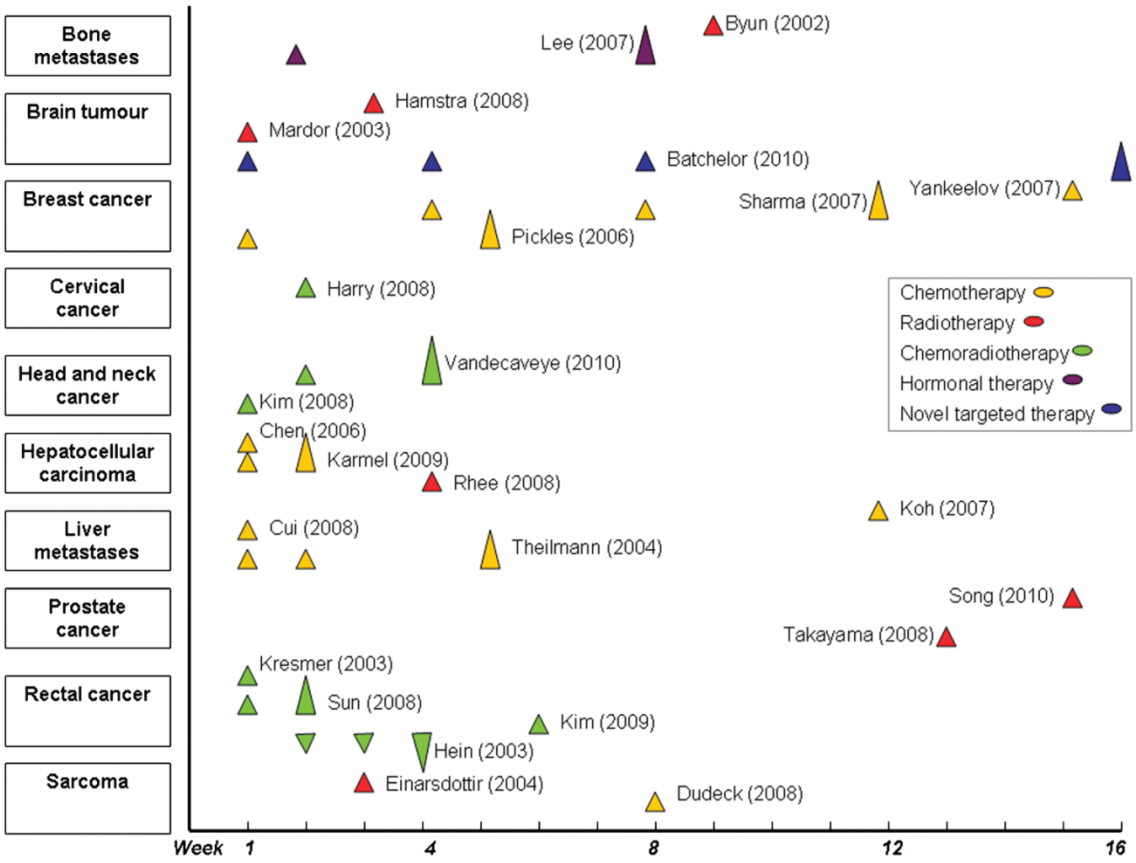

Fig. 10. *Chart summarises published studies using ADCw values to assess tumour response to chemotherapy (yellow), radiotherapy (red), chemoradiotherapy (green), hormonal therapy (purple) and targeted treatment (blue). The vertical axis shows tumour types and the horizontal axis indicates the timing of ADCw measurements (in weeks) after starting treatment. Each study is displayed across from top to bottom according to tumour types and indicated on the chart (author, year). Upward arrowheads indicate an increase in ADCw and downward arrowheads indicate a decrease in ADCw. In studies in which multiple ADCw measurements were taken, larger symbols indicate maximum ADCw change. Note that many studies showed an increase in ADCw values within 4 weeks of treatment. Furthermore, a number of studies showed a significant increase in ADCw values within 1 week of commencing therapy. Adapted from Afaq, 2010.*

1.43 Imaging proliferation

Thymine is the only nucleotide that is exclusively incorporated into DNA and not RNA, making of it and its nucleoside thymidine appropriate for studying DNA metabolism. In thymidine salvage, thymidine is transported across the cell membrane and phosphorylated by TK1 into thymidine monophosphate (TMP). The thymidine is further phosphorylated into thymidine diphosphate (TDP) and thymidine triphosphate (TTP) and then incorporated into DNA. Alternatively, using the de novo synthesis pathway, deoxyuridine monophosphate (dUMP) is converted to TMP which can then be further phosphorylated and incorporated into DNA. Similarly to thymidine, [^{18}F]-Fluorothymidine (FLT) is transported into the cell and phosphorylated into [^{18}F]-FLT monophosphate ([^{18}F]-FLTMP) and trapped by TK1. [^{18}F]-FLTMP can be further phosphorylated into [^{18}F]- FLT diphosphate ([^{18}F]-FLTDP) and [^{18}F]-FLT triphosphate ([^{18}F]-FLTTP). However, due to the substitution of OH with ^{18}F in the 5-prime position, [^{18}F]-FLTTP is not incorporated into the DNA. [^{18}F]-FLT is trapped after phosphorylation by thymidine kinase 1, whose expression is increased in replicating cells (Muzi, 2005).

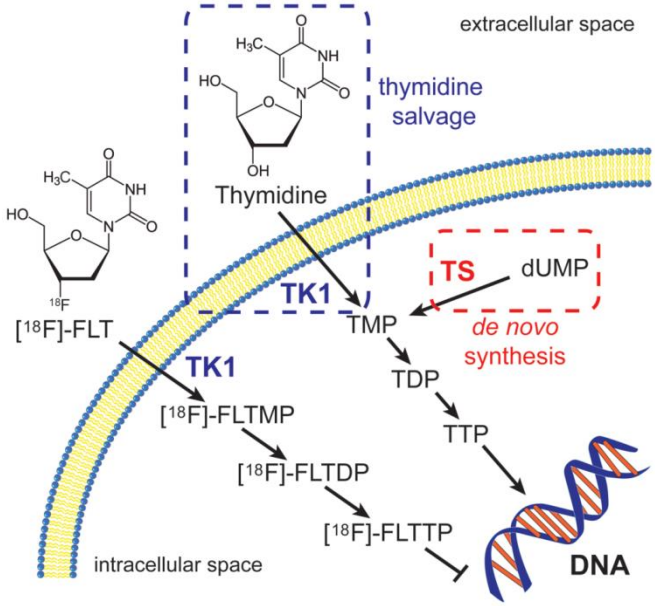

Fig.11. [^{18}F]-FLT PET serves as a surrogate of proliferation by targeting the activity of thymidine salvage, supplying DNA precursors to dividing cells. Adapted from McKinley, 2013.

Studies on breast, lung, and brain tumors have demonstrated that retention of [^{18}F]-FLT correlated with tumor proliferation (Tehrani, 2013). However, background uptake is high in the liver, bone marrow, and renal system, limiting the use in these organs.

1.44 Imaging tumor hemodynamic parameters

Since anticancer agents are sometimes targeted at the tumor vasculature, such as anti-angiogenic or anti-vascular drugs, there is a strong interest in monitoring response to these agents using non-invasive techniques that are able to assess tumor perfusion/vasculature or oxygenation status.

Useful imaging systems have been developed to monitor angiogenesis and the microvasculature in vivo, including dynamic contrast enhanced magnetic resonance imaging (DCE-MRI) (Choyke, 2003; Afaq, 2010), PET and single photon emission computed tomography (SPECT), CT, Doppler ultrasound, and optical imaging methods (Jennings, 2008; Afaq, 2010).

DCE-MRI is the acquisition of serial MR images before, during, and after the administration of an intravenous contrast agent (CA) that produces time series images that enable pixel-by-pixel analysis of contrast kinetics within a tumor. The change in signal intensity after contrast administration is used to evaluate vascular parameters. DCE-MRI is used to evaluate the effects of drugs that modulate tumor vasculature, such as anti-angiogenic and anti-vascular treatments (Padhani, 2005).

Non-invasive MR techniques are also able to assess tumor oxygenation, including 19F-MR oximetry and Electron Paramagnetic Resonance Oximetry. An adequate blood circulation is necessary for adequate supply of oxygen to all tissues.

1.45 Imaging tumor metabolism

MR spectroscopy (MRS) can be used to investigate biochemical changes associated with disease, but a limitation is the low sensitivity of this method for nuclei other than proton (Radda, 1986). ^{13}C-MRS is a method of choice to image metabolic substrates. Dynamic nuclear polarization (DNP) can increase the sensitivity of in vivo ^{13}C-MRS. For this, ^{13}C labelled metabolites must be hyperpolarized; this method increases the ^{13}C signal by >10 000 folds (fig.16) (Ardenkjaer-Larsen 2003). DNP transfers high electron spin polarization to nuclear spins via microwave irradiation in a strong magnetic field and at cryogenic temperature. Using this technique, dynamic changes in metabolic processes can be monitored (Jeffrey, 1991). The first clinical trial using ^{13}C-MR metabolic imaging has been successfully performed in patients with biopsy-proven prostate. There were no dose limiting toxicities observed with hyperpolarized ^{13}C pyruvate (Nelson, 2013). This emerging method is able to

assess disease activity and contribute to decisions concerning patient care. It constitutes the basis for designing additional human studies in other cancers and for evaluating response to therapy. Because hyperpolarized MRI does not require a radiation dose for the patient, it could be used for serial monitoring to detect recurrence at early stage (Brindle, 2011). The principal drawback of the method is the short half-life of the polarization which is maximum 1 minute.

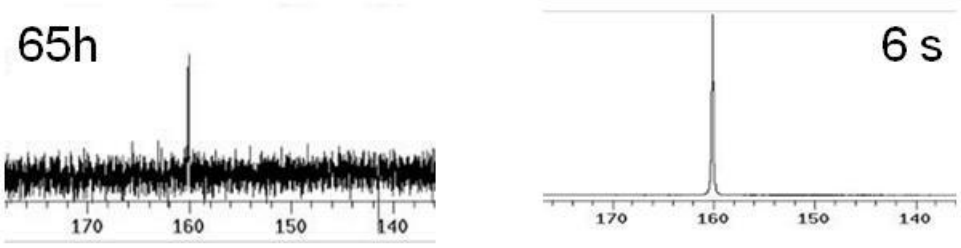

Fig.16. ^{13}C spectrum of urea (natural abundance ^{13}C) at 9.4 T and room temperature after an acquisition of 65 hours and the same sample hyperpolarized by the DNP-NMR method after an acquisition of 6 seconds. Adapted from Ardenkjaer-Larsen 2003.

Practically, after hyperpolarization of the ^{13}C enriched substrate, the enriched liquid is immediately injected into the mouse and the tumor is imaged in the MR magnet (fig.17) (see section 1.53 for technical aspects of hyperpolarization).

a. ^{13}C-pyruvate to ^{13}C-lactate conversion

To date, pyruvate has been the most commonly marker used for DNP. Pyruvate is a diagnostic marker in cancers because he is abundantly converted to lactate through anaerobic glycolysis in these conditions (fig.18) (Golman,

2006). Lactate labelling results from the reaction catalysed by the enzyme lactate dehydrogenase (LDH). The velocity of this reaction will depend on the delivery of hyperpolarized pyruvate to the tumor, the rate of pyruvate transport across the cell membrane and the kinetic of LDH (Brindle, 2011). The decrease in LDH-catalysed reaction can be explained by a loss of coenzyme NAD(H) due to the decrease in tumor cellularity, and reduced LDH concentrations (Brindle, 2008). There are increasing evidences for an early reduction in pyruvate-lactate exchange in a range of cancer models following treatment with cytotoxic chemotherapy (Witney, 2010 ; Day, 2007), targeted drug (Bohndiek, 2010 ; Dafni, 2010 ; Ward, 2010), radiotherapy (Day, 2011) and MAPK inhibitor (Lodi, 2013). A lot of studies support the pyruvate to lactate ratio as a biomarker of cancer aggressiveness, metastatic potential and response to treatment (Sriram, 2015). In another study, the response to treatment detected using hyperpolarized pyruvate is compared with the response detected from measurements of FDG uptake. After 24 hours of treatment the decrease in FDG uptake and the decrease in pyruvate to lactate ratio were comparable (Witney, 2009). Moreover, in prostate cancer cells significant changes of lactate/pyruvate (Lac/Pyr) are used to evaluate early response to radiotherapy. The decrease in Lac/Pyr ratio is mainly attributed to the decrease in LDH activity due to cell death caused by irradiation (Saito 2015).

Pyruvate, the end product of glycolysis, can be reduced by the NADH produced in the pathway to generate lactate, in the reaction catalyzed by the enzyme LDH. Alternatively, pyruvate undergoes transamination with glutamate to form alanine. Both reactions are readily reversible in the cell. A third reaction involves the irreversible decarboxylation of pyruvate to hyperpolarized ^{13}C-labeled carbon dioxide (Kurhanewicz, 2011). In pancreatic cells, the p53

status can be used as a biomarker to predict the sensivity to LDH inhibition. A mutant p53 tumor exhibited increased apoptosis, a lower ^{13}C-lactate production after administration of treatment and reduced proliferation (Rajeshkumar, 2015).

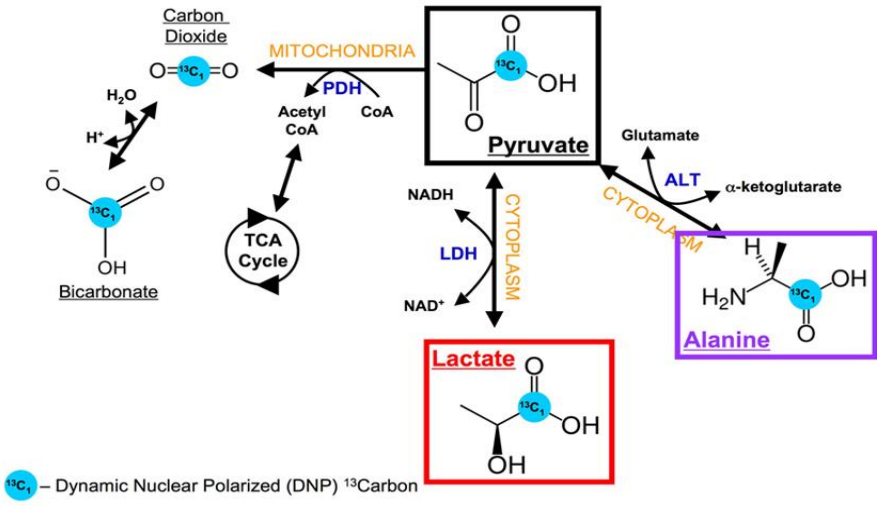

Fig.17. Transformation of ^{13}C pyruvate in ^{13}C lactate using the enzyme lactate dehydrogenase, in ^{13}C alanine by alanine transaminase , in ^{13}C carbon dioxide in a reaction catalysed by pyruvate dehydrogenase. Adapted from Kurhanewicz, 2011.

In cancer cells, the aerobic glycolysis is often enhanced (Warburg effect) with increased transcriptional regulation of a number of glycolytic enzymes including lactate dehydrogenase (LDH). Increased regulation has been shown to drive both tumor growth and the spread of metastases. Moreover, Warburg effect is associated with poor outcome in cancer (Hanahan, 2011). The reduction in the Warburg effect during PI-103-induced autophagy (PI3K / mTOR inhibitor) could result in a concomitant reduction in intracellular and excreted lactate. The autophagy induced in cancer cells by PI-103 could affect glycolytic metabolism reducing the formation of lactate. The measurements of the rate constant of pyruvate to lactate exchange by DNP and ^{13}C-MRS could provide a

valuable biomarker to monitor the effects of the PI-103 drug in longitudinal studies. The change in lactate could provide an indicator of metabolic processes accompanying drug induced autophagy. The drug-effects can be monitored through the use of hyperpolarized pyruvate (Lin, 2014).

The injected hyperpolarized ^{13}C-labeled pyruvate generates a ^{13}C signal that is linearly proportional to its concentration. The conversion of pyruvate to its metabolites, including lactate occurs within a minute of injection. This timing is short and corresponds to the unrecoverable decay of hyperpolarized products due to T1 relaxation and radio frequency excitation. The rate constant for pyruvate to lactate conversion can be significantly influenced by metabolic activity in tissues, by perfusion and by a rapid reduction of tumor oxygenation (Khegai, 2014 ; Bluff, 2015). Importantly, recent findings indicated that lactate labeling could result not only from net conversion of pyruvate into lactate, but also from exchange of the hyperpolarized ^{13}C label between the injected hyperpolarized ^{13}C pyruvate and the endogenous lactate pool (Brindle, 2015). There is now considerable evidence for a significant exchange contribution (Brindle, 2011). The chemical shift value is 183 ppm for lactate and 171 ppm for pyruvate (fig.19).

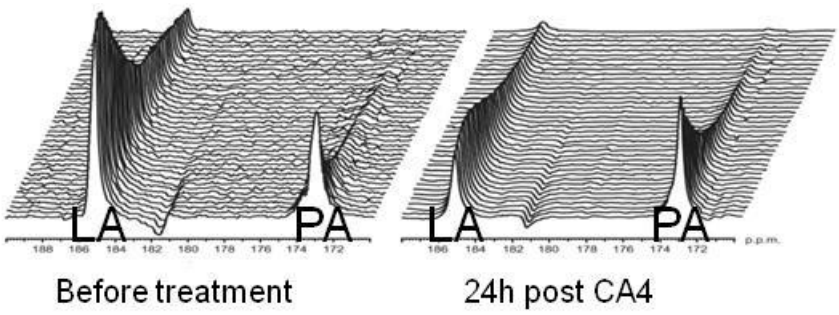

Fig.18. Evolution of lactate and pyruvate peaks before and after treatment with Combrestatin-A4, a vascular targeting-agent. Adapted from Bohndiek, 2010.

b. ^{13}C-fumarate to ^{13}C-malate conversion

There are currently no techniques for directly and specifically imaging necrosis in vivo. ^{13}C-magnetic resonance spectroscopy (MRS) can detect hyperpolarized fumarate to malate conversion catalysed by fumarase (fig.20). This reaction has been suggested as a marker of drug-induced cellular necrosis and treatment response in tumors (Gallagher, 2009). The malate outside of the tumor may reflect loss of tumor fumarase into the extracellular space of the surrounding tissue. Necrotic areas are likely to have poor perfusion and high extracellular fumarase activity where the plasma membrane permeability barrier has been compromised. In these particular conditions, the fumarate can be rapidly converted to malate (Gallagher, 2009). Healthy cells demonstrate slow fumarate transport through plasma membrane transport. Consequently, there is little detectable conversion of fumarate to malate within the short lifetime of the polarisation (Brindle, 2011). For example, the treatment of MDA-MB-231 cells with doxorubicin (a DNA intercalator) resulted in the production of significant levels of labelled malate by 72 h after drug treatment. There was no detectable labelled malate produced in untreated cells (Witney, 2010). The levels of malate produced correlated with the levels of necrosis in vitro and in vivo (Gallagher, 2009; Witney, 2010). This method could therefore be used as a very early marker of necrosis (fig.21) (Bohndiek, 2010). The fumarase reaction is suitable as an in vivo biomarker of tissue necrosis because no coenzymes are required for the reaction, so even during cell death the

enzyme will continue to function (Gallagher, 2009). After injection of the fumarate, the signals from (1,4-$^{13}C_2$)fumarate, (4-^{13}C) malate and (1-^{13}C) malate were seen at 176 ppm 181 ppm and 182 ppm respectively.

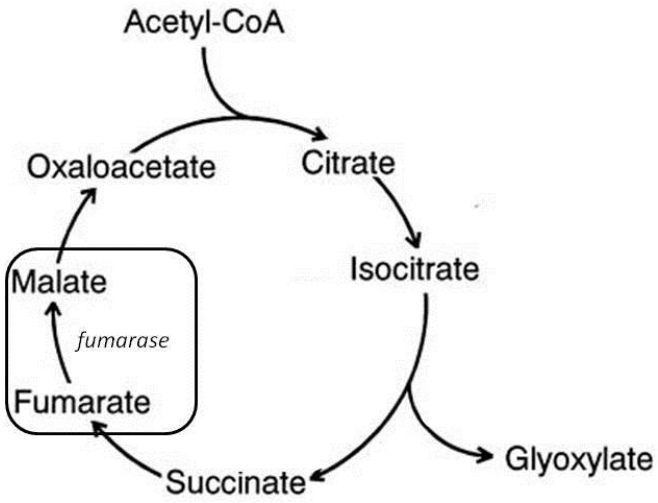

Fig.19. Krebs cycle with a focus on the transformation of fumarate into malate catalysed by fumarase. Adapted from Munir, 2001

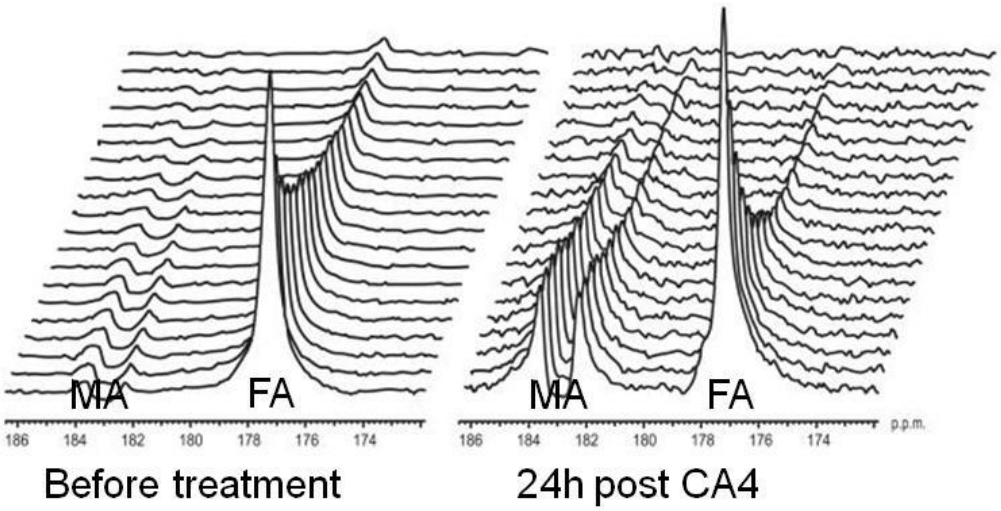

Fig.20. Evolution of malate and fumarate peaks before and after treatment with Combrestatin-A4. Adapted from *Bohndiek, 2010.*

c. Other major hyperpolarised substrates valuable in cancer monitoring

Another hyperpolarised substrate that could be valuable in detecting tumor treatment response is ^{13}C glutamine. Tumors show upregulated glutamine utilization due to the use of this amino acid for the generation of metabolic intermediates in the biosynthesis process, which supports the increased growth rate of tumor cells and the synthesis of anti-oxidant as glutathione (Cairns, 2011). The cellular oncogene *MYC* encodes a transcription factor which promotes cell proliferation. MYC up-regulates the expression of the glutamine transporters and the glutaminase activity (Gao, 2009). ^{13}C glutamine can be used as a surrogate for MYC expression and to assess inhibition of tumour cell proliferation (Brindle, 2012).

The metabolism of hyperpolarized glutamate to α-ketoglutarate, catalyzed by the enzyme alanine transaminase, may influence HIF-1 expression. HIF-1 is a transcription factor that facilitates tumor growth when oxygen is low and whose stability is regulated by α-ketoglutarate (Zhao, 2009). Hyperpolarised ^{13}C glutamate can detect α-ketoglutarate in a tumor in vivo, raising the possibility to investigate on the role of α-ketoglutarate in controlling gene expression and HIF-1 stability in a tumor (Gallagher 2011 ; Brindle, 2012).

The tumor extracellular pH can be imaged from the ratio of the signal intensities of hyperpolarised bicarbonate $H^{13}CO_3^-$ and $^{13}CO_2$ following intravenous injection of hyperpolarised $H^{13}CO_3^-$. The technique was demonstrated in a mouse tumor model, which showed that the average tumor interstitial pH was significantly lower than the surrounding tissue. This technique can be used to image cancer which can be associated with alteration in tissue pH (Gallagher, 2008).

The tumor redox state can be determined by monitoring the oxidation and reduction of hyperpolarised ^{13}C ascorbate and ^{13}C dehydroascorbate, the reduced and oxidised forms of vitamin C. ^{13}C ascorbic acid may find application in diseases, as inflammation, that lead to a high level of extracellular reactive oxygen species. The ascorbate oxidation is impossible in cancer because tumors have upregulated anti-oxidant systems to cope with the increased reactive oxygen species (ROS).^{13}C dehydroascorbic acid provides a hyperpolarized probe to observe the rapid reduction to ascorbate and to hightlight redox status (Brindle, 2012).

The technological improvements in nuclear magnetic resonance allow the analysis of biomarkers, which characterize tumor developments and tumor response. These techniques improve morphological data and diagnostic performances in oncology. For example, spectroscopy combined with diffusion weighted MRI allow to distinguish benign lesion from malignant tumor (Elshafey, 2014). Since those developments involve technological knowledge, the following section will briefly address the techniques underlying the parameters that have been described here above.

1.5 Techniques

1.51 ChoKα silencing using short hairpin RNA (shRNA)

These RNA molecules are used to silence target gene expression. The introduction of shRNA into mammalian cells through infection with viral vectors allows for stable integration of shRNA and long-term knockdown of the targeted gene (Moore, 2010). Once the small hairpin RNA is integrated in the

host genome, it is transcribed by the polymerase and exported from the nucleus by exportin 5. The mechanism of RNA interference is based on a post-transcriptional process which leads to the sequence-specific degradation of host mRNA through the cytoplasmic introduction of double-stranded RNA identical to the target sequence (Fire, 1998). The double-stranded RNA is cleaved by Dicer generating small interfering RNAs formed by a guide strand and a passenger strand (fig.22). The endonuclease Argonaute 2 (Ago) catalyzes the unwinding of the small interfering RNA duplex. One strand of this duplex (the guide strand) is loaded into the RNA Interference Specificity Complex (RISC) while the passenger strand is released. The RISC then localizes the guide strand to the mRNA that has a complementary sequence leading to the endonucleolytic cleavage of the target (Elbashir, 2001). The target cleaved mRNA is further degraded by other endogenous nucleases.

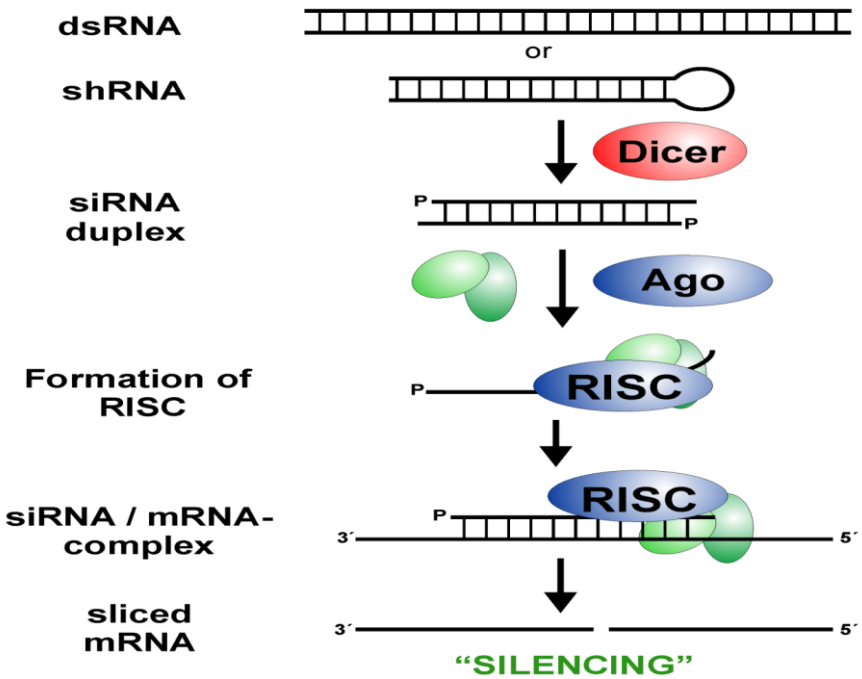

Fig.21. Gene silencing : The shRNA is cleaved by Dicer. The "passenger strand" is cleaved by Ago and released. The "guide strand" is integrated in RISC. RISC

localizes the "guide strand" to the mRNA of interest leading to the cleavage of the target. Adapted from Kumar 2000.

In our work, HEK293FT cells were transiently transfected with lipofectamine using a third-generation lentiviral system for lentivirus preparation. After 24h and 48h, viral supernatants were harvested, titrated, and used to infect target MDA-MB-231 cells. Selection was realized with puromycin (2 μg/mL). MDA-MB-231 cells were infected with lentivirus containing five short hairpin RNA's (shRNA) targeting ChoKα (ThermoFisher Scientific ABgene; Epsom, Surrey – United Kingdom) (Porporato, 2014). The most effective shRNA (ID TRCN0000006050) was selected by western blot for in vivo experiments. Inhibition of ChoKα in MDA-MB-231 cells was compared with cells transduced with shRNA's with a scrambled sequence (scr). Using shRNA, the inhibition of the ChoKα is very efficient and specific; it's the best way to gene silencing. The use of a lentiviral vectors to target ChoK in a human breast cancer xenograft is very efficient. The downregulation of ChoK, which can be detected non-invasively with ^{31}P or ^{1}H-MRS, results in a reduction of cell proliferation and tumor growth (Krishnamachary, 2009).

1.52 Magnetic Resonance and ^{1}H-MRS

The information measured with magnetic resonance includes images, spectroscopy and spectroscopic imaging. The magnetic resonance is the absorption or emission of electromagnetic radiation by atoms in response to the application of a magnetic field. This technic is used to analyze the properties of matter and tissues. All atoms have an intrinsic nuclear motion of the nucleus call the spin. The manipulation of the spin orientation by a radiofrequency pulse is the basis of MR measurements. The MR signal is

obtained by placing a sample into an external field B0. In these conditions spins rotate about an axis with a specific frequency called the Larmor frequency proportional to the magnetic field B0. At the Larmor frequency the nuclei absorb energy causing the proton to change its alignment and to be detected in a magnetic field. The MR signal intensity is reflected in the amount of energy emitted. To excite the nuclei in a required frequency range a radio frequency pulse with a selected bandwidth can be applied. When the radio frequency field matches the Larmor frequency at which the nuclear magnets naturally precess in the magnetic field B0, some of the nuclei are promoted from the low energy state to the high energy state. This single powerful pulse covers the whole frequency range and is commonly applied perpendicular to the applied magnetic field. The magnetization, disturbed from its orientation along the B0 axis, precesses in the XY plane, generating an oscillating signal, which is to be picked up by a receiver coil. This signal is called the free induction decay (FID). The MR signal is proportional to the number of nuclei contributing to it. The electron density in a molecule varies according to the type of nuclei and bonds in the molecule, therefore the net magnetic field vary with each nucleus. This phenomenon is also known as chemical shift and is the reason why different molecules are distinguishable in the MR spectrum as different peaks (Osorio-Garcia, 2011).

MRS is used to obtain metabolic information in the form of a spectrum. The clinical applications of MR spectroscopy are the exploration of tissue's metabolites to diagnose diseases or to monitor treatment response. For this in-vivo approach we use spatial localization techniques to detect a signal from a specific volume of tissue within an anatomical region of the body (Salibi, 1998). Single voxel spectroscopy acquires a spectrum from a defined volume of tissue. This voxel of interest is defined by the intersection of three orthogonal planes.

There is an excitation of this volume of interest with frequency selective radio frequency (rf) pulses in techniques like point resolved spectroscopy (PRESS). Slice selective-rf pulses excite three intersecting orthogonal planes. The first slice is selected with a gradient and excited by a frequency selective 90° rf pulse. The second slice is selected using a 180° pulse; this pulse rephrases spins in the intersecting with slice 1. The third slice is select with gradient and a 180° pulse. Only spins at the intersection with the third slice are excited by three pulses: a 90° excitation and two 180° refocusing pulses. Their net magnetization produces the final echo which is sampled and processed during PRESS frequency (Salibi, 1998). The signals obtained during the PRESS frequency correspond to a sum of complex-damped exponentials in the time-domain, called the Free Induction Decay (FID) (Osorio-Garcia, 2011).

To improve the acquisition many parameters of the FID can be modulate:

- Repetition time : it's the time between two excitation pulses applied on the same slice.
- Echo time: It's the time between the application of the excitation pulse and the beginning of the signal's peak in the coil. Depending echo time, we observe more slowly decaying components or metabolites. When the echo time is high (150 ms) the metabolites selected have a long T2. When the echo time is shorter (10ms) more metabolite resonances will appear in the spectra. There is superposition of number of peaks.
- T1 or longitudinal relaxation time (fig.23): After a 90° pulse, the T1 relaxation time is a measure of the return of magnetization following an exponential growth process to recover its ground state in the

direction of B0. Precisely the T1 is the time required to return to 63% of initial magnetization.

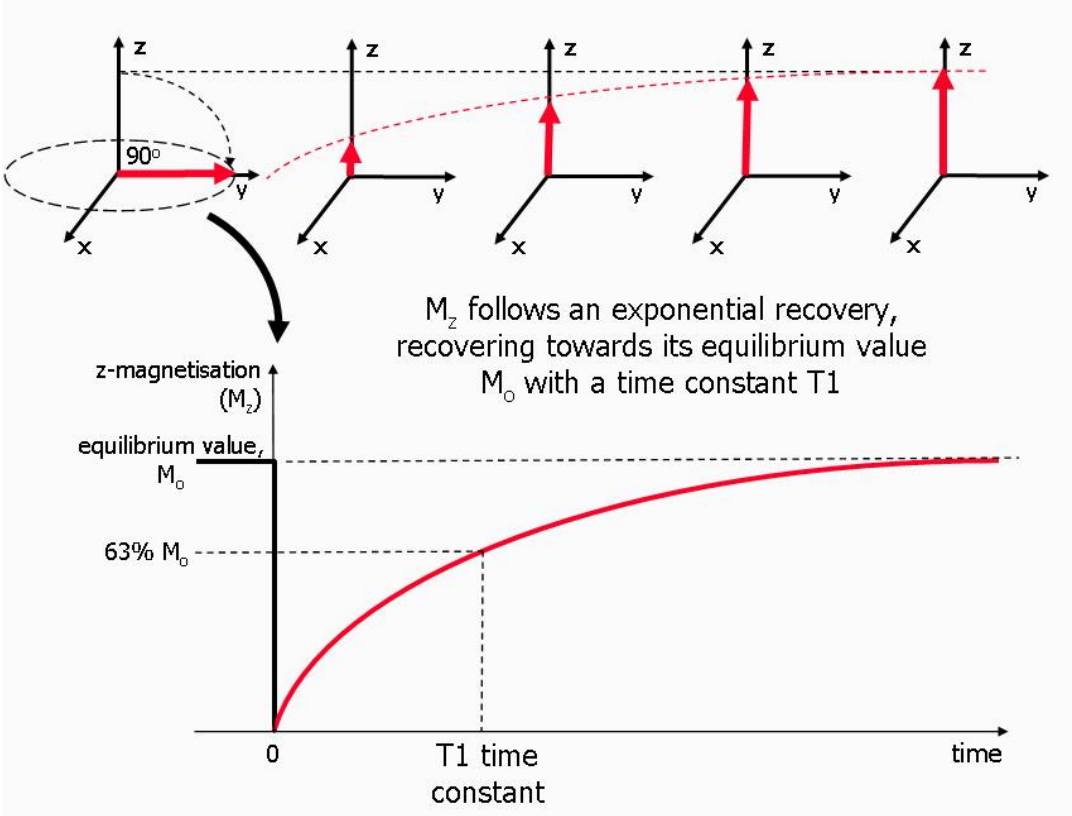

Fig.22. T1 relaxation after a 90° pulse or longitudinal relaxation curve. The recovery of magnetization is an exponential process with a time constant T1. This is the time at wich the magnetization has recovered to 63% of its value at equilibrium. Adapted from Ridgway, 2010

- T2 or transverse relaxation time (fig.24): After a 90° pulse, the T2 relaxation time measures the progressive dephasing of spins. T2 is the decay to 37% of initial transverse magnetization.
- T2* is the effective transverse relaxation time (fig.24). This parameter includes the transverse relaxation and inhomogeneities of magnetic field. These fluctuations are especially due to main field inhomogeneity and magnetic susceptibility in a sample.

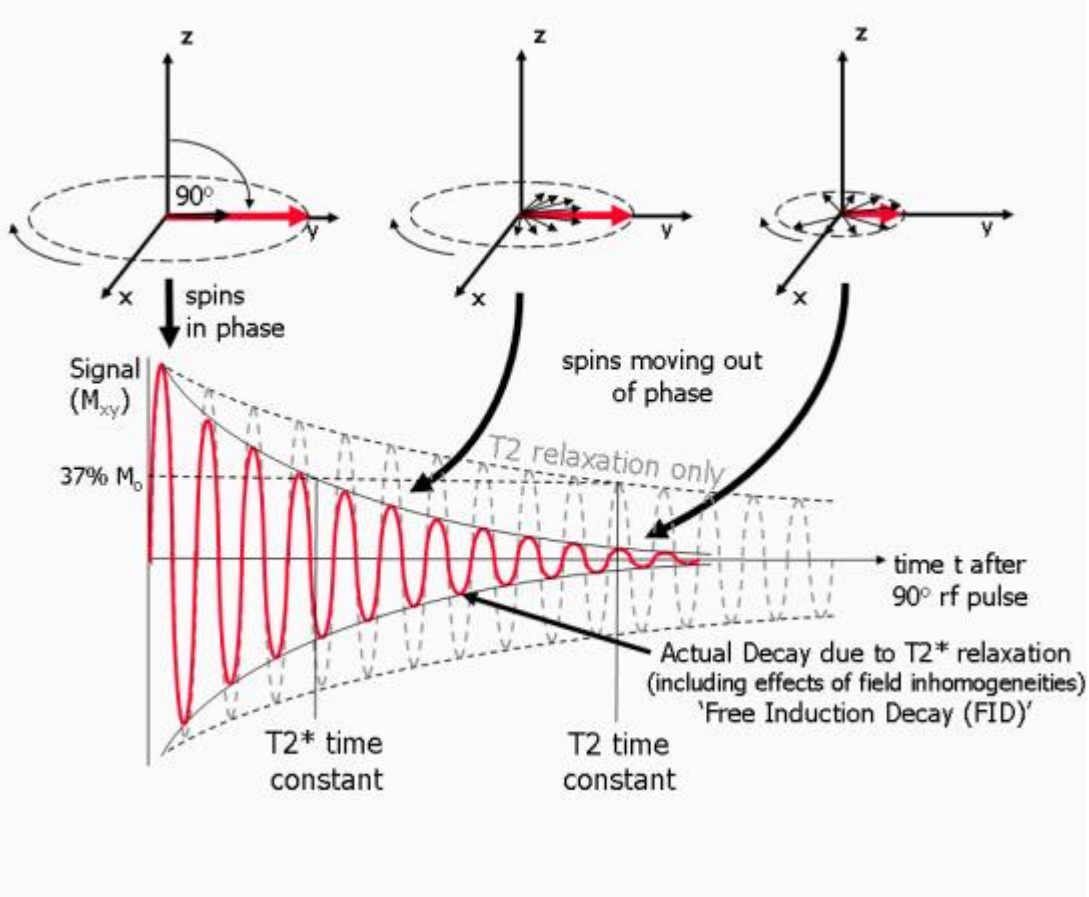

Fig.23. Transverse (T2 and T2) relaxation. Both T2 and T2* are exponential processes with times constants T2 and T2* respectively. This the time at which the magnetization has decayed to 37% of its initial value immediately after the 90° rf pulse. Adapted from Ridgway, 2010*

- Number of average: number of spectra acquired. This number can be increased to improve the quality of the spectrum and specially the signal to noise ratio.
- Shimming: this step is crucial to correct the inhomogeneities of magnetic field. The tuning of different gradients pulses will improve the spectral resolution and permit to segregate the different metabolite resonances. The homogeneity of the field B0 is dependant of the first and second order shimming. The field homogenization is

also dependant of the size of the region to analyze and the tissues homogeneity.

- Suppression of the water peak: to visualize the weak metabolites, a suppression of the big water peak is essential. Without this step, the water peak covers by his larger all the metabolite peaks. To suppress the water signal, specific radio frequency pulses centered on the resonance frequency of the water peak are applied in association with dephasing gradient.
- Other parameters like magnetic field strength, type of coil used, distance between the region of interest and the coil or size of the lesion can influence the Free Induction Decay (Fayad, 2010).

The transformation of the Free Induction Decay (time domain) in the frequency domain using the Fourier transform is necessary to observe the different peaks corresponding to the excited nuclei. The area under each peak allows the computation of the metabolite concentrations. In the spectrum, the variation in magnetic field strengths experienced by each molecule is related to their chemical shift, also called resonance frequency (Osorio-Garcia, 2011). Frequency differences are known as chemical shifts, are expressed in parts per million (ppm) and are independent of B0. On a spectrum, the X axis represents the chemical shifts of different metabolites. The Y axis represents the amplitude of the peak and is proportional to the among of metabolite.

Moreover an in vivo spectroscopy measure must go along with an unsuppressed water signal. This water spectrum is used as reference for quantification. Relative concentration of the peak of interest is obtained by dividing the amplitude of peak by the water peak.

1.53 ^{13}C-MRS and Dynamic nuclear polarization (DNP)

The hyperpolarization is a method to obtain strongly polarized nuclear spins (Ardenkjaer-Larsen, 2003). The dynamic nuclear polarization (DNP) is one of the most effective methods to polarize a wide range of systems. This DNP method enhances nuclear polarization using transfer of magnetization from electron to nuclear spins. This is a consequence of the strong coupling of the electron spin to the surrounding nuclei (Barnes, 2008). In 1953 Overhauser proposed that it was possible to transfer polarization to nuclei from electrons by saturating the electron transition (Overhauser, 1953). However this idea has been accepted 3 years later with the experimental verification of Carver and Slichter (Carver, 1956). This controversial mechanism is active when the electron resonance has a linewidth of the same order than the nuclear Larmor frequency. The shift in energy levels produced between spins is a hyperfine coupling; using this method the polarization of substrate will increase.

Dynamic Nuclear Polarization is based on polarizing the nuclear spins in the solid state. The mechanism requires the presence of unpaired electrons added as free radical in a substrate. This free-radical doping agent is OX63 and must be present in the sample at micromolar concentrations during microwave irradiation in order to provide the needed nuclear polarization for intermolecular transfer (de Graaf, 2007). In order for the DNP process to be totally effective, the free radical must be homogeneously mixed within the sample. After cooling the sample, the high electron spin polarization is in part transferred to the nuclear spins by microwave irradiation (Ardenkjaer-Larsen, 2003). Under irradiation with microwave at the electron Larmor frequency, the transitions are stimulated and the nuclear polarization is increased. This transfer is increase at very low temperature (Ardenkjaer-Larsen, 2003). Indeed

the nuclear polarizations of ^{13}C can be increased in a sample to almost 50% by placing him in a strong magnetic field at low temperature close to 0 Kelvin (de Boer, 1974).

To illustrate the principle of DNP, consider nuclei at Larmor frequency ωN and electron spins with Larmor frequency ωe positioned in an external magnetic field B0 (fig.25A). When the nuclei and electrons will be completely separated, nuclear transitions can be achieved at frequency ωN. Electronic transitions are achieved at frequency ωe. However, when the electron generates a finite magnetic field at the nuclei, the two become dipolar-coupled. The solid effect is represented by this dipolar interaction between an electron and a nuclear. This so-called hyperfine interaction will lead to a mixing of the states of energy, which in turn will lead to simultaneous electron and nuclear spin transitions or flips (de Graaf, 2007). The system is now irradiated at the microwave frequency (ωe − ωN). Besides a flip of the electron spin, the nuclear spin flips from an antiparallel to a parallel orientation (Fig.25B). However, due to fast electron T1 relaxation the spin quickly returns to the lowest energy level. Therefore, the combined effect of microwave irradiation and fast electron relaxation has led to a slight increase in polarization, as a single nuclear spin has been transferred from an antiparallel to a parallel orientation (Fig.25C). Continuing this process will lead to a complete depletion of the antiparallel state, giving complete or 100 % nuclear polarization (de Graaf, 2007).

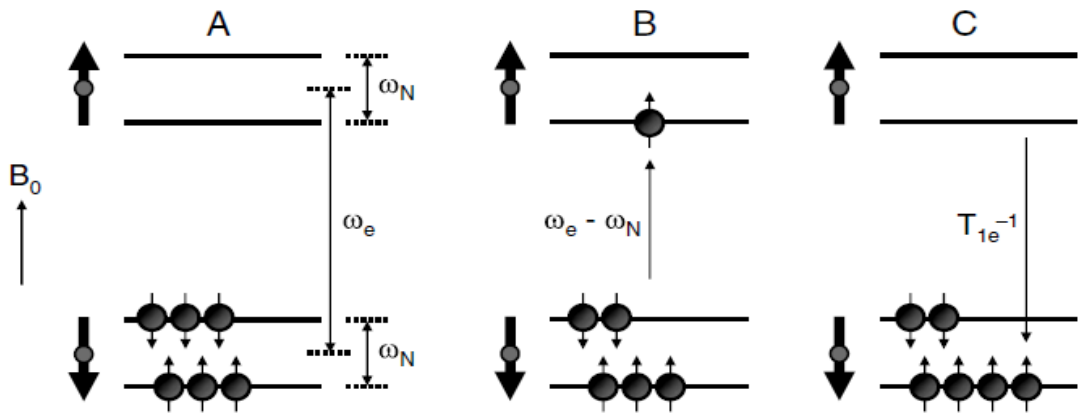

Fig.24. Scheme of the population of energy levels before and after hyperpolarization. The spectroscopic signal is proportional to the difference between the populations of nuclei in distinct energy levels. The hyperpolarization increases the NMR signal. Adapted from de Graaf, 2007

During polarization the sample must be kept cold while irradiated by microwaves in a strong magnetic field. DNP has been used as a polarization technique for organic molecules in the solid state. However, in vivo applications require the polarized material in the liquid state for injection into the subject. Ardenkjaer-Larsen *et al.* have offered a solution to this challenging problem (Ardenkjaer-Larsen, 2003). After polarization, the polarized solid material is brought into the liquid state by dissolution in an appropriate solvent, while preserving the large nuclear polarization (de Graaf, 2007). The polarized liquid is transferred to an injection syringe for immediate magnetic resonance acquisitions. The sample produced by DNP is an hyperpolarized ^{13}C labeled compounds and allows the observation of reactions and metabolism in vivo and in vitro.

1.54 Diffusion Weighted-MRI

Water diffusion sequence is adapted from a T2-weighted spin echo sequence. For this, a symmetric diffusion-sensitizing gradient around 180° refocusing pulse is applied (fig.26). Stationary molecules are unaffected by gradients and measured signal intensity is preserved. By contrast, moving water molecules acquire phase information from first gradient, which is not entirely rephased by second gradient, thereby leading to signal loss. Hence, water diffusion is detected as attenuation of measured MR signal intensity (Koh, 2007). The degree of water motion is proportional to the degree of signal attenuation (Koh, 2007).

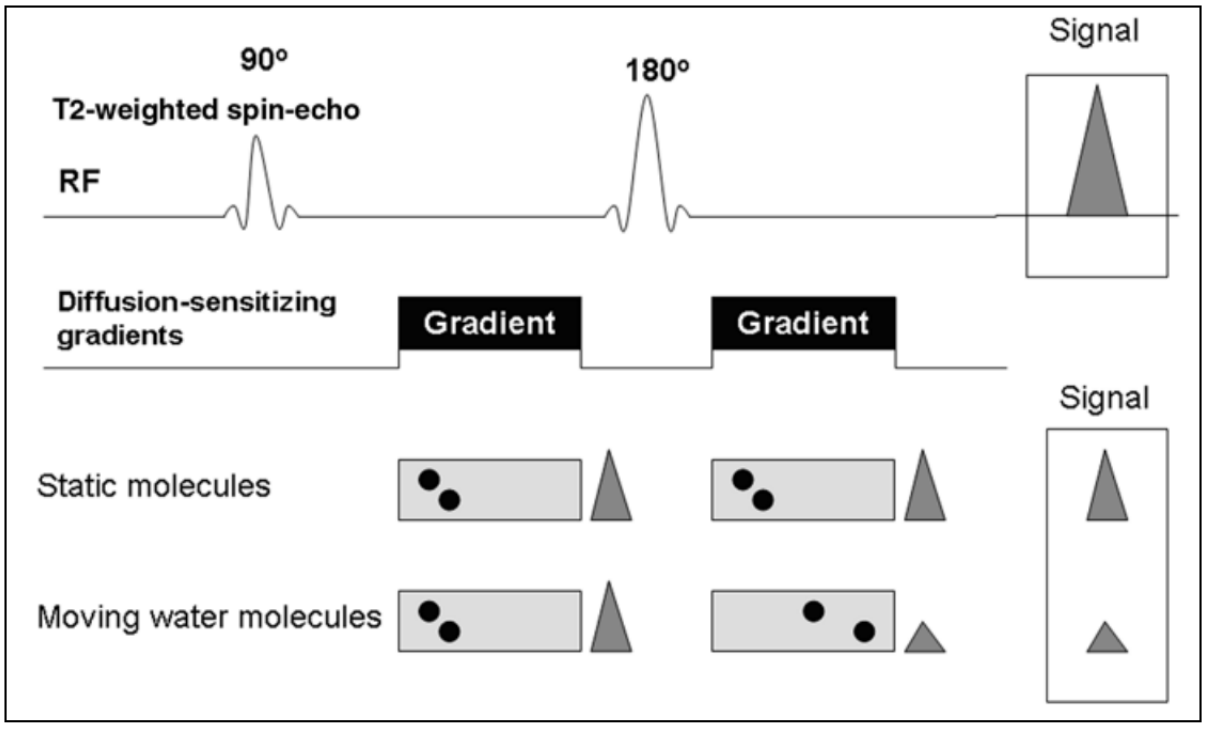

Fig.25. Diffusion sequence and measurements of water motion are realised by the application of two gradients on either side of the refocusing 180° pulse. Adapted from Koh, 2007.

The sensitivity of diffusion is dependant of b-values. These parameters measure the degree of diffusion weighted applied, thereby indicating the gradient amplitude, the time of applied gradient, and the duration between the paired gradient (Koh, 2007). The change of b-values alters mostly the gradient amplitude. Water molecules with a large degree of movement will show signal attenuation with small b-values. By contrast, large b-values are usually required to perceive slow-moving water molecules or small diffusion distances in a high cellularity tissue (Koh, 2007).

Using multiple b-values, the quantitative analysis can be performed and result in the calculation of the Apparent Diffusion Coefficient of water (ADCw). ADCw can be calculated by plotting the logarithm of the relative signal intensity of the tissue on the Y axis. The b-values are plotting on the X axis. A line can be fitted through the plots and the slope of this line describes the ADCw. The fit can be improved by using more b-values to reduce the error in ADCw calculation. The ADCw is calculated for each pixel and can be displayed as a parametric map (Koh, 2007).

Chapter II : Objectives of the thesis

Objectives of the thesis:

The major goal of this study is focused on the validation of early in-vivo markers of response to therapies targeting the modulation of the choline pathway. These modulators are pharmacological inhibitors and specific shRNAs targeting choline kinase. Modulating the choline pathway, using specific targeted agents, represents a major challenge for current research efforts in oncology since this pathway is involved in tumor progression. Conventional anatomically based endpoints may be inadequate to monitor the tumor response to these targeted agents that usually do not result in tumor shrinkage while used as monotherapy. Therefore, the identification and use of more appropriate, combined biomarkers are needed to optimize the choice of treatments. These non-invasive biomarkers are particularly adapted for longitudinal monitoring and could be the key factor for treatment individualization and for managing tumor resistance. Among them, three non-invasive imaging markers of tumor response are being benchmarked in response to choline targeted agents in the current work, and compared with classic histological methods and with therapeutic outcome in vivo in tumor xenografts:

(i) ^{1}H Magnetic Resonance Spectroscopy is used to assess the total choline level in tumors, wich is an indicator of the activity of choline pathway and membrane turnover.

(ii) Diffusion Weighted Magnetic Resonance Imaging is used to assess cell density and as a potential early indicator of therapeutic response.

(iii) The dynamic monitoring of the conversion of hyperpolarized ^{13}C-fumarate into ^{13}C-malate, and of hyperpolarized ^{13}C-

pyruvate into ^{13}C-lactate, considered as emerging in vivo markers to evaluate treatment efficacy.

Chapter III : Results

1. MR spectroscopy can be used to investigate biochemical changes associated with cancer. This study validates the use of ^{1}H Magnetic Resonance Spectroscopy and Diffusion Weighted Magnetic Resonance Imaging as early in-vivo markers of response to therapies targeting the modulation of the choline pathway in the breast cancer**.**

I Non-invasive *in vivo* imaging of early metabolic tumor response to therapies targeting choline metabolism

Lionel Mignion, Pierre Danhier, Julie Magat, Paolo E. Porporato, Julien Masquelier

Vincent Gregoire, Giulio G. Muccioli, Pierre Sonveaux, Bernard Gallez, Bénédicte F. Jordan

Under review in International Journal of Cancer: minor revision

Short report

Non-invasive *in vivo* imaging of early metabolic tumor response to therapies targeting choline metabolism

Lionel Mignion[1], Pierre Danhier[1], Julie Magat[1], Paolo E. Porporato[2], Julien Masquelier[3]

Vincent Gregoire[4], Giulio G. Muccioli[3], Pierre Sonveaux[2], Bernard Gallez[1], Bénédicte F. Jordan[1]

[1] Université catholique de Louvain (UCL), Louvain Drug Research Institute, Biomedical Magnetic Resonance Group, Avenue Mounier 73 box B1.73.08, 1200 Brussels, Belgium.

[2] Université catholique de Louvain (UCL), Pole of Pharmacology, Institut de Recherche Expérimentale et Clinique (IREC), Avenue Mounier 52 box B1.53.09, 1200 Brussels, Belgium.

[3] Université catholique de Louvain (UCL), Louvain Drug Research Institute, Bioanalysis and Pharmacology of Bioactive Lipids Research Group, Avenue Mounier 72 box B1.72.01, 1200 Brussels, Belgium.

[4] Université catholique de Louvain (UCL), Institut de Recherche Expérimentale et Clinique (IREC), Pole of Molecular Imaging, Radiotherapy and Oncology. Avenue Hippocrate 55 box B1.55.02 , 1200 Brussels, Belgium.

Corresponding author:

Prof. Bénédicte F. Jordan, PhD - Biomedical Magnetic Resonance Unit (REMA) - Université Catholique de Louvain - Louvain Drug Research Institute,

Avenue E. Mounier, 73 box B1.73.08 - 1200 Brussels (Belgium) - **email:** benedicte.jordan@uclouvain.be fax : +32 27647390

Novelty and impact statement:

Sensitive and non-invasive biomarkers that correlate with efficacy are highly required in the transition towards individualized therapy in cancer. The current study identifies early markers of response to therapies targeting choline signaling, including ^{1}H-choline spectroscopy as a pharmacodynamic biomarker, and DW-MRI as a marker of tumor response. Our data suggest that DW-MRI combined to choline spectroscopy may provide a useful non-invasive marker for the early clinical assessment of tumor response to therapies targeting choline signaling.

Abstract

The cholinic phenotype, characterized by elevated phosphocholine and a high production of total-choline (tCho)-containing metabolites, is a metabolic hallmark of cancer. It can be exploited for targeted therapy. Non-invasive imaging biomarkers are required to evaluate an individual's response to targeted anticancer agents that usually do not rapidly cause tumor shrinkage. Because metabolic changes can manifest at earlier stages of therapy than changes in tumor size, the aim of the current study was to evaluate ^{1}H-MRS and diffusion-weighted MRI (DW-MRI) as markers of tumor response to the modulation of the choline pathway in mammary tumor xenografts. Inhibition of choline kinase activity was achieved with the direct pharmacological inhibitor H-89, indirect inhibitor sorafenib and down-regulation of choline-kinase α (ChKA) expression using specific short-hairpin RNA (shRNA). While all three strategies significantly decreased tCho tumor content *in vivo*, only sorafenib and anti-ChKA shRNA significantly repressed tumor growth. The increase of apparent-diffusion-coefficient of water (ADCw) measured by DW-MRI, was predictive of the induced necrosis and inhibition of the tumor growth in sorafenib treated mice, while the absence of change in ADC values in H89 treated mice predicted the absence of effect in terms of tumor necrosis and tumor growth. In conclusion, ^{1}H-choline spectroscopy can be useful as a pharmacodynamic biomarker for choline targeted agents, while DW-MRI can be used as an early marker of effective tumor response to choline targeted therapies. DW-MRI

combined to choline spectroscopy may provide a useful non-invasive marker for the early clinical assessment of tumor response to therapies targeting choline signaling.

Introduction

Choline phospholipid metabolism is significantly increased in cancer cells. This specific cholinic phenotype is a new metabolic hallmark of cancer associated to elevated phosphocholine (PC) and increased production of total choline (tCho)-containing metabolites.[1, 2] Choline kinase (ChK) is the first cytosolic enzyme of the choline pathway.[3] This enzyme catalyzes the ATP-dependent phosphorylation of choline to form PC, initiating the choline pathway for phosphatidylcholine (PtCho) biosynthesis[3]. In cancer, accumulation of intracellular PC is believed to reflect increased ChK activity. Chk induction is a general cellular response to growth factor stimulation, and is essential for cell growth and viability. Malignant transformation, facilitated by both ChK activity and PC production, is therefore characterized by abnormal choline metabolism.[4] At least three ChK isoforms exist in mammalian cells, which are encoded by two genes: choline kinase α (*ChKA*) and choline kinase β (*ChKB*). At least one isoform, probably ChKA, is involved in the promotion of cell growth during carcinogenesis. Therefore, inhibition of ChK activity may provide a novel strategy for the development of new families of targeted anticancer drugs.[5]

In animal models, various pharmacological anticancer agents have an effect on phospholipid metabolism. In particular, ChK inhibition by RSM-932A and MN58b significantly decreases PC levels,[6, 7] vascular disrupting agents such as 5,6-dimethyl-xanthenone-4-acetic acid induce a decrease in tCho,[8] gene therapy as a treatment of glioma induces early apoptosis with a significant

accumulation of glycerophosphocholine (GPC) and PC,[9] and radiation therapy can decrease tCho levels, as observed 24 hours after a 20 Gy X-ray dose.[10]

Effective methods to characterize an individual's response to treatment are mandatory to assess the therapeutic benefits of novel targeted therapies. Conventional, anatomically-based endpoints are deemed inadequate to monitor a tumor response to targeted agents that usually do not affect tumor size when used as a monotherapy. As an alternative, *in vivo* proton MR spectroscopy (^{1}H-MRS) is a non-invasive technique that can provide information on tumor metabolism for experimental investigation and, potentially, for tumor diagnosis and monitoring.[11, 12] Metabolic changes can manifest at earlier times during therapy with respect to changes in tumor size.[13] Hence, a rapid reduction in tCho levels (comprising mixed signals from choline, GPC and PC) has been proposed as a non-invasively marker of the tumor status and of inhibition of cellular proliferation.[13] In this context, ^{1}H-MRS imaging of tCho levels in many cancers, including breast cancer,[14] have been performed and linked to tumor evolution and diagnostic performance.

Besides ^{1}H-MRS, diffusion-weighted MRI (DW-MRI) is another non-invasive method than can be used to monitor the evolution of a tumor and its response to treatment. DW-MRI primarily reports on loss of cellularity, which is the ultimate outcome not only of extensive necrosis[15] but also of other types of cell death, including apoptosis and mitotic catastrophe.[16] Changes in the Apparent Diffusion Coefficient of water (ADCw) of tumors often precedes any

measurable change in tumor size or volume.[15] Hence, determination of ADCw changes may influence clinical practice by allowing much earlier adjustments in therapy.[17] In many cancers, an increase in ADCw has been reported within the first two weeks after the start of chemotherapy or radiotherapy and was correlated with tumor response to treatment.[17]

The aim of the current study is to evaluate tCho (detected with ^{1}H-MRS) and ADCw (detected with DW-MRI) as markers of the response of mammary tumor xenografts to the modulation of the choline pathway using direct and indirect ChK inhibitors in mice.

Material and methods

Targetingof ChK activity

MDA-MB-231 tumor-bearing mice (tumor volume: 0.2 ± 0.1cm^3, see supplementary for tumor induction protocol) were intraperitoneally treated daily with a direct inhibitor of ChK activity (H89: 20mg/kg dissolved in 35µl of DMSO) for 5 days, an indirect inhibitor of ChK activity (sorafenib: 40mg/kg dissolved in 35µl of DMSO) for 5 days, or vehicle (DMSO, 35µl). H89 is used in this study for his direct and independent inhibition of ChK activity[18], whereas sorafenib is a well-documented multi-kinase inhibitor.[19] For ChKA silencing, we used short hairpin (sh)RNA (clone ID TRCN0000006050) from ABgene (Epsom, Surrey, United Kingdom). Scramble shRNA (shSCR) was used as a negative control. Cells were transfected as reported previously[20] (see supplementary). Reduction in choline kinase expression was assessed by western blotting analysis (see supplementary).

^{1}H-MR choline spectroscopy

Animal experiments were performed with an 11.7-Tesla, 16-cm inner diameter bore system (Bruker, Biospec, Ettlingen, Germany) equipped with a quadrature volume coil (40-mm inner diameter). Animals (tumor volume: 0.2 ± 0.1cm^3) were anesthetized by isoflurane inhalation (3% in air for initiation and 1–2% in air for maintenance). They were laid on a warm water blanket connected to a circulating water bath to maintain body temperature (checked using a rectal temperature probe). A pressure cushion was used to monitor breathing.

For single voxel spectroscopic data acquisition, volumes of interest were placed inside tumors according to T2-weighted reference images. Optimalization of magnetic field homogeneity (localized shimming) was performed until achieving a linewidth of water resonance below 50Hz. Automatic shimming and manual water suppression (VAPOR) were used. ^{1}H-MR spectra were acquired using a point-resolved spectroscopy (PRESS) localization technique. Typical acquisition parameters were repetition time (TR)=2.5s, echo time (TE)=20ms, averages=256, voxel size=4x4x4 mm^3, and total acquisition time=10min50s. MR spectra were analyzed using jMRUI software version 5.0. Metabolite model signals used in quantitation based on quantum estimation (QUEST) were simulated in NMR-SCOPE (NMR spectra calculation using operators; jMRUI). Signals were imported in jMRUI, pretreated by Hankel Lanczos Singular Value Decomposition (HLSVD) in order to eliminate any residual water peak, and rephased. Model fitting was performed using the QUEST routine of jMRUI. Peak areas were measured for tCho peak (δ=3.21ppm) and normalized with the water peak area (δ=4.7ppm) from the non-water suppressed scans using a same volume of interest and geometry.

DW-MRI

For DW-MRI, a transverse echo planar imaging sequence was used with the following acquisition parameters: TR/TE=3000/27ms, duration of diffusion gradients (d)=7ms, separation of diffusion gradients (Δ)=14ms, slice number=12; slice thickness,=1mm, interslice distance=1.2mm, acquisition

time=5min24sec. DW images were acquired using b-values of 0-100-200-400-600-800-1000-1200-1500s/mm 2. The b-value is equal to $\gamma^2 G_d^2\ \delta^2 \left(\Delta - \left({}^{\delta}/_{3} \right) \right)$, where Gd is the strength of the diffusion-weighting gradient, and g is the gyromagnetic ratio for protons. Mean apparent diffusion coefficients (ADCw) were calculated from DW images and averaged for every slice where the tumor was found using a homemade program in Matlab software (The MathWorks Inc., Natick, MA, USA) to define regions of interest (ROI). The exponential decay of the signal as a function of the b-value was measured according to the Stejskal–Tanner equation. ADC maps were generated by nonlinear least squares regression of a mono-exponential to the experimental signal intensity for all b values.

Results

Direct (H89) and indirect (sorafenib) targeting of ChKA decreases tumor choline content

In mice bearing a MDA-MB-231 human breast cancer, we first quantified tumor tCho content non-invasively using single voxel ^{1}H-MR choline spectroscopy. A significant decrease in the tCho to water ratio was observed after 48 hours of treatment with H89 (*, CI 0.06-0.72; n=6) and with sorafenib (**, CI 0.095-0.5, n=7) (Fig.1A). Decreases were still significant after 5 days (measurement at 108 hours) of treatment (*, CI 0.02-0.7 and *, CI 0.027-0.41, respectively). In the control group (n=8), there was no significant change of the tCho peak during the 5 days of monitoring (Fig.1A). Corroborating these *in vivo* data, *ex vivo* quantification of PC by mass spectrometry (*HPLC-ESI-MS*, see supplementary methods) of 4 tumors of each group did confirm the significant difference between control tumors and tumors treated with sorafenib or H89 (*, CI 0.17-2.51; **, CI 0.67-3.00 respectively) (Fig.1B). The decrease in tCho and PC demonstrate a modulation of the choline cycle. In this regard, ChKA expression was shown to be significantly decreased to 49,7% after treatment with sorafenib (**; n=4, independent experiments), and to 71,9% after treatment with H89 (*, n=4, independent experiments), with respect to control cells (supplementary Fig.1).

In mice bearing shRNA-transfected MDA-MB-231 tumors, a significant decrease (p=0.003, n=9) was also observed in the tCho to water ratio when

comparing anti-ChKA *versus* SCR shRNA-expressing tumors (n=10) (Fig.1C). Again, *ex vivo* quantification of PC by mass spectrometry of 4 tumors of each group did confirm the significant difference between shSCR and shChKA tumors (***, CI -4.52/-1.80) (Fig.1B). ChKA expression was efficiently silenced by the specific shRNA, as shown by Western blot analysis in vitro on MDA-MB-231 cells (Fig.1C). Typical ^{1}H- MRS spectra from *in vivo* shSCR and shChKA tumors are shown in Fig.1D. Thus, both direct and indirect pharmacological inhibition of the choline cycle activity, as well as genetic targeting of ChKA expression, all significantly reduced the tCho content of MDA-MB-231 tumor xenografts in mice. Relative decreases in tCho tumor content were of -54.4% after 48h using H89, -49.3% after 48h using sorafenib, and -57.2% using anti-ChKA shRNA. Importantly, the results also illustrate the high heterogeneity in the basal tCho/water ratios from one tumor to another (large standard errors of the mean).

Sorafenib, but not direct ChK targeting, decreases intratumoral cellularity

In MDA-MB-231 tumor-bearing mice, intratumoral cellularity was assessed using DW-MRI and quantified from ADCw calculation[15]. No significant change in ADCw was observed following treatment with H89 (n=6), whereas sorafenib induced a progressive increase in ADCw that was significant after 5 days of treatment (**, CI -0.54-0.07, n=9) (Fig.2A), which is generally described to reflect a decrease in cellularity. Typical ADCw maps pre and post-sorafenib treatment are shown in Fig.2B. Similarly to H89 ChK inhibition, MDA-MB-231

tumor expressing an anti-ChKA shRNA had similar ADCw compared to those expressing SCR shRNA (data not shown). Thus, only sorafenib increased ADCw in MDA-MB-231 xenografts.

Direct and indirect ChK targeting can induce tumor necrosis

Tumors were harvested after 5 days of treatment. Hematoxylin and eosin staining of tumor slices revealed a significant increase in necrosis with sorafenib treatment (*, p=0.048, n=4; Fig.2C) with respect to control tumors (n=6). Anti-ChKA shRNA also caused a significant tumor necrosis (*, n=4; p=0.015), but not H89 (n=6) after 5 days of treatment (only a non-significant trend towards increased necrosis was seen). Typical H&E stained tumor sections with or without treatment with sorafenib are shown on Fig. 2D.

Direct and indirect ChK targeting can delay the tumor growth

The impact of daily sorafenib and H89 administration on MDA-MB231 tumor growth was compared for 10 days with the growth of tumors in vehicle-treated mice. A significant tumor growth retardation was observed for sorafenib *versus* control treatment (*, p=0.02; n=3-4/group), but not for H89 *versus* control (n=10) (Fig.3A). A significant tumor growth delay was also observed in anti-ChKA *versus* SCR shRNA tumors (***, CI -686.5-134.5; n=8-10/group) (Fig.3B). Thus, sorafenib and anti-ChKA shRNA, but not H89, impacted MDA-MB-231 tumor volume progression.

Discussion

Most targeted therapies for cancer cause tumor stabilization rather than shrinkage, thus reducing the sensitivity or rendering inappropriate the standard metrics of response, including Response Evaluation Criteria in Solid Tumors (RECIST).[21] There is therefore a need for alternative quantitative biomarkers of response. Among these, our study shows that tCho (measured using ^{1}H-MRS) and ADCw (measured using DW-MRI) can be used to noninvasively assess metabolic tumor responses to treatments *in vivo*.

Our data document that intracellular tCho levels can be determined non-invasively in tumors with ^{1}H-MRS in order to evidence ChK target inhibition. This pharmacodynamic parameter was suitable to demonstrate that treatments were acting on their targets. However, it was not suited to predict the response of a tumor to choline-targeted treatment, and additional imaging markers should be considered to predict the response of a tumor to treatment. This is illustrated in our study by the fact that, when targeting ChK activity with a direct inhibitor (H89), a significant decrease of tCho and PC was observed that was not associated with a drop of cellularity and a stabilization of tumor growth. Comparatively, we used sorafenib, a well-documented clinical multi-kinase inhibitor that primarily decreases the phosphorylation of extracellular signal-regulated kinase (ERK) in the mitogen-activated protein kinase (MAPK) pathway,[19] and also targets ChK activity. Daily injections of sorafenib at high dose induced a rapid (48-h) decrease in the tumor content of tCho and PC, which preceded decreased cellularity (measured with DW-

MRI), necrosis and, ultimately, a reduction of tumor size (which became significant only 5 days post-treatment). In line with our findings, inhibition of MAPK signaling with the U0126 MEK inhibitor has been previously reported to cause a drop in intratumoral tCho and PC levels in tumors.[22] Finally, targeting ChKA with a specific shRNA decreased tCho and PC levels in tumors. We found that the knock-down of the ChKA induces tumor necrosis and tumor growth retardation. We did not observed any significant difference in basal ADCw values between MDA-MB-231 tumor expressing an anti-ChKA shRNA compared to those expressing SCR shRNA. Indeed, Diffusion-Weighted MRI is adapted to a longitudinal follow up of individual tumors before and after treatment, which is not possible with this approach. Of note, our DW-MRI results were interpreted as a drop of cellularity, while other factors can contribute to ADCw changes, including tissue disorganization, extracellular space tortuosity, and integrity of cellular membranes that can also impact on motion of water molecules.[23]

Publically available ^{1}H-MRS data support variable independent conclusions regarding the usefulness of *in vivo* spectroscopy for monitoring the response of breast cancer to therapy. One source of variability is that choline transport rates and ChK activity are increased in breast cancer cells that express elevated levels of PC.[24] Another source of variability could be attributed to the significant induction of ChK expression with the histological tumor grade.[25] Consistently, the association between ChK overexpression and tumor aggressiveness has been reported for ChK inhibition by small interfering RNAs[26]

and by the specific inhibitor MN58b.[6] These studies nevertheless concluded that ChK inhibition significantly reduces PC and tCho levels in breast cancer cells, and proposed MRS to be used as a potential non-invasive marker of ChK inhibition and of tumor response to treatment. However, authors also pointed out limitations to the use of the composite choline signal as a marker of response, which notably included a large inter-subject variability in the level of metabolites detected using ^{1}H-MRS.[14] Here, we show that tCho level quantification *in vivo* with ^{1}H-MRS is a sensitive pharmacodynamic marker of a tumor to choline targeted treatment. However, this measurement was not per se predictive of the tumor response to a treatment as tumors were responsive to sorafenib and not to H89. Longitudinal pre- and post-treatment measurements of ADC values were more consistent in terms of response as there was a close agreement between ADC values, tumor growth and tumor necrosis for both H89 and sorafenib treatments.

Of note, besides the multiple kinases inhibited by Sorafenib, the drug has also shown significant anti-angiogenic properties that could also be responsible for changes in tumor ADCw. In this context, we previously showed that, while the anti-angiogenic effect of sorafenib can be quantified as soon as 48h post-treatment using anti-CD105 antibody, it is not reflected in terms of ADCw at this time point, and only becomes significant at day 5.[19,27] Moreover, tumor cell proliferation assessed *in vivo* using ^{18}F-FLT with a similar protocol does significantly increase at day 2. All these data do suggest that the anti-angiogenic property of the drug is not the major factor responsible for the change in ADCw. Finally, regardless the major

factor influencing the change in ADCw in response to treatment with sorafenib, the current results do still demonstrate that tCho can be modified with no consecutive effect in terms of tumor growth.

In conclusion, DW-MRI combined with choline spectroscopy may provide a useful non-invasive marker of response for choline signaling-targeted therapies, with the ultimate goal of improving *individualized drug therapy*.

Acknowledgments

The authors acknowledge Morgane Tardy and Thibaut Vazeille for technical assistance. This study was supported by grants from the Belgian National Fund for Scientific Research (F.R.S.-FNRS), the *Communauté Française de Belgique* (Actions de Recherches Concertées (ARC) 09/14-020 & ARC 14/19-058), a Starting Grant from the European Research Council (ERC No. 243188 TUMETABO to P. Sonveaux) and the UCL *Fonds Spéciaux de la Recherche* (FSR). B.F. Jordan is Senior Research Associate of the F.R.S.-FNRS and P. Sonveaux is Research Associate of the F.R.S.-FNRS, P.E. Porporato is a Postdoctoral Researchers of the F.R.S.-FNRS. P. Danhier is a Télévie post-doctoral fellow and L. Mignion is a Télévie PhD Fellow.

References:

1. Glunde K, Bhujwalla ZM, Ronen SM. Choline metabolism in malignant transformation. *Nat Rev Cancer* 2011;**11**: 835-48.

2. Glunde K, Serkova NJ. Therapeutic targets and biomarkers identified in cancer choline phospholipid metabolism. *Pharmacogenomics* 2006;**7**: 1109-23.

3. Wittenberg J, Kornberg A. Choline phosphokinase. *J Biol Chem* 1953;**202**: 431-44.

4. Aboagye EO, Bhujwalla ZM. Malignant transformation alters membrane choline phospholipid metabolism of human mammary epithelial cells. *Cancer Res* 1999;**59**: 80-4.

5. Aoyama C, Liao H, Ishidate K. Structure and function of choline kinase isoforms in mammalian cells. *Prog Lipid Res* 2004;**43**: 266-81.

6. Al-Saffar NM, Troy H, Ramirez de Molina A, Jackson LE, Madhu B, Griffiths JR, Leach MO, Workman P, Lacal JC, Judson IR, Chung YL. Noninvasive magnetic resonance spectroscopic pharmacodynamic markers of the choline kinase inhibitor MN58b in human carcinoma models. *Cancer Res* 2006;**66**: 427-34.

7. Lacal JC, Campos JM. Preclinical Characterization of RSM-932A, a Novel Anticancer Drug Targeting the Human Choline Kinase Alpha, an Enzyme Involved in Increased Lipid Metabolism of Cancer Cells. *Mol Cancer Ther* 2015;**14**: 31-9.

8. McPhail LD, Chung YL, Madhu B, Clark S, Griffiths JR, Kelland LR, Robinson SP. Tumor dose response to the vascular disrupting agent, 5,6-dimethylxanthenone-4-acetic acid, using *in vivo* magnetic resonance spectroscopy. *Clin Cancer Res* 2005;**11**: 3705-13.

9. Valonen PK, Griffin JL, Lehtimaki KK, Liimatainen T, Nicholson JK, Grohn OH, Kauppinen RA. High-resolution magic-angle-spinning 1H NMR spectroscopy reveals different responses in choline-containing metabolites upon gene therapy-induced programmed cell death in rat brain glioma. *NMR Biomed* 2005;**18**: 252-9.

10. Dyke JP, Zakian KL, Spees WM, Matei C, Chen Y, Mao X, Shungu DC, Koutcher JA. Metabolic response of the CWR22 prostate tumor xenograft after 20 Gy of radiation studied by 1H spectroscopic imaging. *Clin Cancer Res* 2003;**9**: 4529-36.

11. Jagannathan NR, Kumar M, Seenu V, Coshic O, Dwivedi SN, Julka PK, Srivastava A, Rath GK. Evaluation of total choline from in-vivo volume localized proton MR spectroscopy and its response to neoadjuvant chemotherapy in locally advanced breast cancer. *Br J Cancer* 2001;**84**: 1016-22.

12. Kumar M, Arlauckas SP, Saksena S, Verma G, Ittyerah R, Pickup S, Popov AV, Delikatny EJ, Poptani H. Magnetic resonance spectroscopy for detection of choline kinase inhibition in the treatment of brain tumors. *Mol Cancer Ther* 2015.

13. Sharma U, Baek HM, Su MY, Jagannathan NR. In vivo 1H MRS in the assessment of the therapeutic response of breast cancer patients. *NMR Biomed* 2011;**24**: 700-11.

14. Katz-Brull R, Lavin PT, Lenkinski RE. Clinical utility of proton magnetic resonance spectroscopy in characterizing breast lesions. *J Natl Cancer Inst* 2002;**94**: 1197-203.

15. Koh DM, Collins DJ. Diffusion-weighted MRI in the body: applications and challenges in oncology. *AJR Am J Roentgenol* 2007;**188**: 1622-35.

16. Morse DL, Galons JP, Payne CM, Jennings DL, Day S, Xia G, Gillies RJ. MRI-measured water mobility increases in response to chemotherapy via multiple cell-death mechanisms. *NMR Biomed* 2007;**20**: 602-14.

17. Afaq A, Andreou A, Koh DM. Diffusion-weighted magnetic resonance imaging for tumour response assessment: why, when and how? *Cancer Imaging* 2010;**10**: 179-88.

18. Gabellieri C, Beloueche-Babari M, Jamin Y, Payne GS, Leach MO, Eykyn TR. Modulation of choline kinase activity in human cancer cells observed by dynamic 31P NMR. *NMR Biomed* 2009;**22**: 456-61.

19. Karroum O, Mignion L, Kengen J, Karmani L, Leveque P, Danhier P, Magat J, Bol A, Labar D, Gregoire V, Bouzin C, Feron O, et al. Multimodal imaging of tumor response to sorafenib combined with radiation therapy:

comparison between diffusion-weighted MRI, choline spectroscopy and 18F-FLT PET imaging. *Contrast Media Mol Imaging* 2013;**8**: 274-80.

20. Porporato PE, Payen VL, Perez-Escuredo J, De Saedeleer CJ, Danhier P, Copetti T, Dhup S, Tardy M, Vazeille T, Bouzin C, Feron O, Michiels C, et al. A mitochondrial switch promotes tumor metastasis. *Cell Rep* 2014;**8**: 754-66.

21. Milano A, Perri F, Ciarmiello A, Caponigro F. Targeted-therapy and imaging response: a new paradigm for clinical evaluation? *Rev Recent Clin Trials* 2011;**6**: 259-65.

22. Beloueche-Babari M, Jackson LE, Al-Saffar NM, Workman P, Leach MO, Ronen SM. Magnetic resonance spectroscopy monitoring of mitogen-activated protein kinase signaling inhibition. *Cancer Res* 2005;**65**: 3356-63.

23. Patterson DM, Padhani AR, Collins DJ. Technology insight: water diffusion MRI--a potential new biomarker of response to cancer therapy. *Nat Clin Pract Oncol*. 2008;**5**:220-33.

24. Ting YL, Sherr D, Degani H. Variations in energy and phospholipid metabolism in normal and cancer human mammary epithelial cells. *Anticancer Res* 1996;**16**: 1381-8.

25. Ramirez de Molina A, Gutierrez R, Ramos MA, Silva JM, Silva J, Bonilla F, Sanchez JJ, Lacal JC. Increased choline kinase activity in human breast carcinomas: clinical evidence for a potential novel antitumor strategy. *Oncogene* 2002;**21**: 4317-22.

26. Glunde K, Raman V, Mori N, Bhujwalla ZM. RNA interference-mediated choline kinase suppression in breast cancer cells induces differentiation and reduces proliferation. *Cancer Res* 2005;**65**: 11034-43.

27. Karroum O, Kengen J, Danhier P, Magat J, Mignion L, Bouzin C, Verrax J, Charette N, Starkel P, Calderon PB, Sonveaux P, Feron O, Grégoire V, Gallez B, Jordan BF. Tumor reoxygenation following administration of Mitogen-Activated Protein Kinase inhibitors: a rationale for combination with radiation therapy. *Radiother Oncol*. 2012;**105**:64-71.

Figures

Fig.1

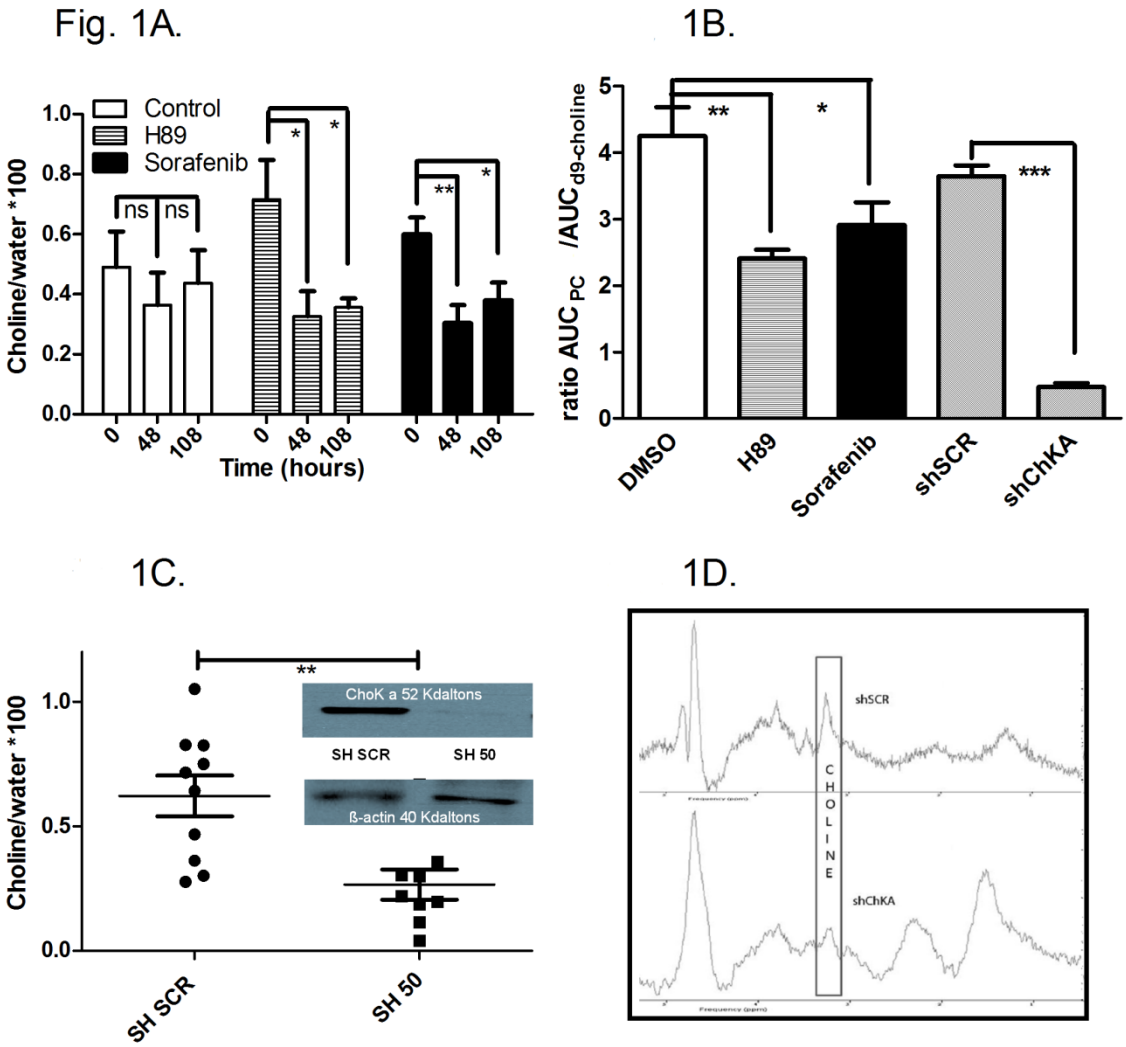

(A) Longitudinal and individual follow up of total choline to water ratio (tCho/water ratio) before and after direct (H89) and indirect (sorafenib) treatments targeting choline kinase. A significant decrease in the choline to water ratio was observed after 48 hours of treatment with H89 (*) and with sorafenib (**). (B) *Ex vivo* quantification of PC using mass spectrometry (*HPLC-ESI-MS)* in

control tumors vs H89 or sorafenib tumors, and in shChKA vs shSCR tumors. (C) tCho/water ratio in shChKA group vs shSCR (control) group (with confirmation of inhibition of ChKA expression in vitro on MDA-MB-231 cells by Western blotting analysis) (D) Typical in vivo 1H-MRS spectra of MDA-MB-231 tumors: control shSCR tumor and choline kinase downregulated shChKA tumor.

Fig.2

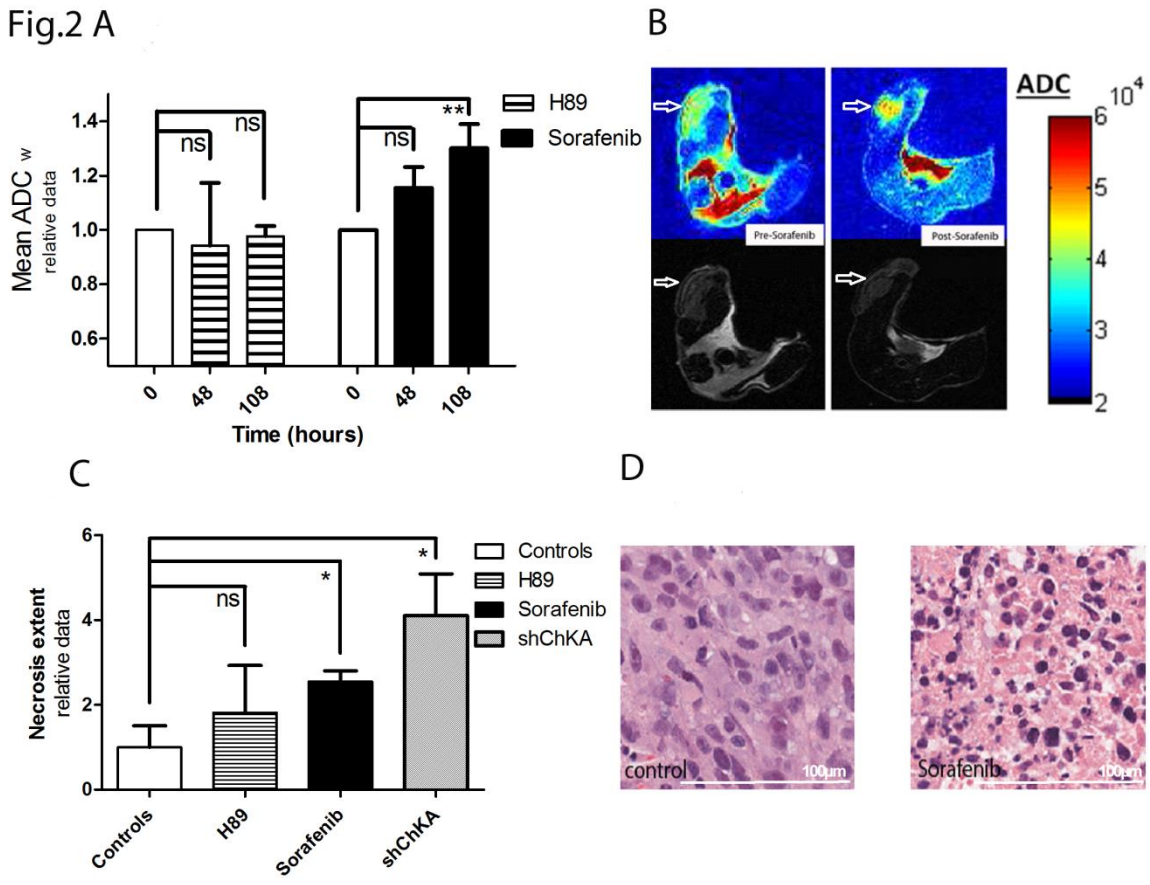

(A) Longitudinal and individual follow up of tumor ADCw following administration of H89 and sorafenib. A significant decrease in cellularity was observed after 5 days of sorafenib treatment.

(B) Typical ADCw maps and corresponding anatomical MR images of MDA-MB-231 tumors before (left image) and 5 days after treatment with sorafenib (right image). (C) Quantification of H&E staining in H89 or sorafenib treated tumors, choline-kinase downregulated (shCHKA) tumors, vs controls. (D) Typical H&E sections of MDA-MB-231 control (left) and 5 days-sorafenib treated tumors (right).

Fig.3

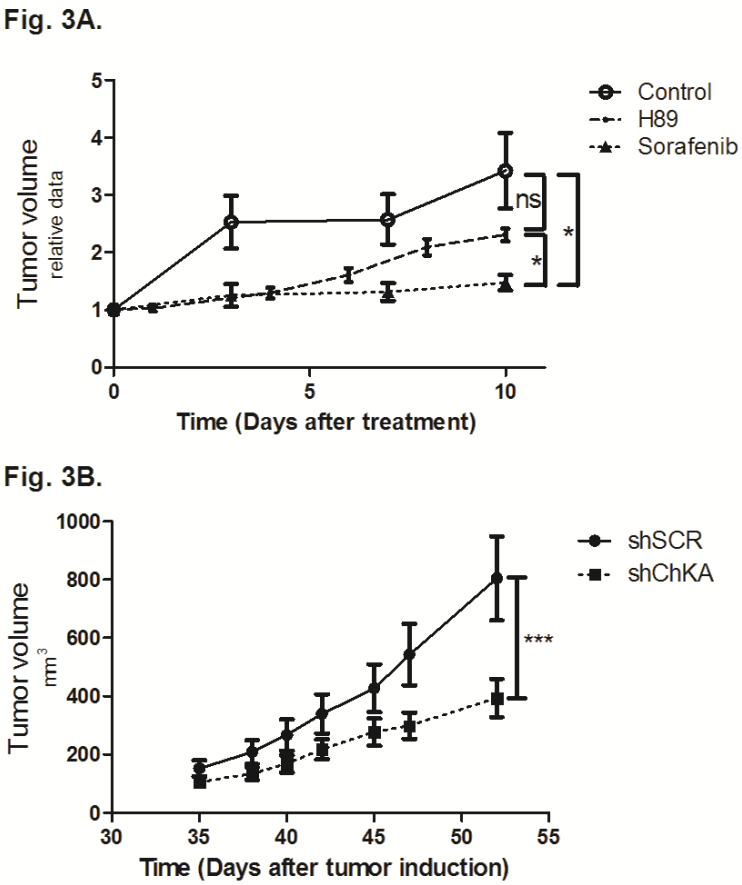

(A) Growth delay assays showed a significant tumor growth retardation 10 days after administration of sorafenib *versus* control treatment (*), but not for H89 *versus* control.

(B) A significant delay (***) in tumor growth was observed 52 days after tumor induction in MDA-MB-231 shChKA tumors in comparison with control group (MDA-MB-231 shSCR).

Supplementary methods

Tumor cells & animal model

MDA-MB-231 human breast cancer cells were grown in Dulbecco's modified Eagle's medium containing low glucose, GlutaMAX, pyruvate, 10% fetal bovine serum (v/v) and 1% penicillin-streptomycin (v/v). About 10 million cells resuspended in 100µl of NaCl 0.9% were injected into the hind limb of 5-6-week-old female NMRI nude mice. Tumors were allowed to grow up to a volume of 200 mm^3 at which time they were imaged (day 0 or 'pre-treatment' time point) and treated with Sorafenib, H89, or vehicle. Longitudinal imaging was then performed at day 2 and day 5. All *in vivo* experiments were conducted under approval of UCL authorities (*Comité d'Ethique Facultaire pour l'Expérimentation Animale*) according to national animal care regulations.

Cell transfection

For lentivirus preparation, HEK293FT cells were transiently transfected with lipofectamine using a third-generation lentiviral system. After 24h and 48h, viral supernatants were harvested, titrated, and used to infect target MDA-MB-231 cells. Selection was done with puromycin (2 µg/mL). MDA-MB-231 cells were infected with lentivirus containing five short hairpin RNA's (shRNA) tartgeting ChKA (ThermoFisher Scientific ABgene; Epsom, Surrey – United Kingdom). The most effective shRNA (ID TRCN0000006050) was selected by western blot for in vivo experiments. Inhibition of ChKA in MDA-MB-231 cells was compared with cells transduced with shRNA's with a scrambled sequence

(SCR). shRNA tumors were allowed to grow up to a volume of 200 mm^3 and were then imaged, SCR vs shRNA ChKA groups were compared. Reduction in choline kinase expression was assessed by western blotting analysis.

Western Blotting

To confirm ChKA inhibition in shRNA cells, as well as to confirm the effect of sorafenib and H89 on ChKA, western blot analysis was performed on MDA-MB-231 cells after 2 days of treatment with H89 (5µg/ml of medium) and sorafenib (10µg/ml of medium), in comparison with control cells. Cells were lysed and proteins were extracted in RIPA buffer. Proteins were separated on 4-20% gels (Biorad) and transferred to a PVDF membrane for detection with rabbit anti-ChKA (Sigma) and mouse anti-β-actin (Sigma) antibodies. Peroxidase-conjugated secondary antibodies anti-mouse or anti-rabbit were used. Chemiluminescense was visualized using Western lightning plus ECL (PerkinElmer). Quantification based on color density of ChKA expression vs B-actin expression was performed using Image J software.

Phosphocholine quantification in tumors by HPLC-ESI-MS

Tumor tissues were homogenized in distilled water (10mg/mL) before adding the internal standard (d_9-choline, 4 nmol), methanol (1 mL) and chloroform (1 mL). Following vigorous mixing the samples were centrifuged and the aqueous layer containing phosphocholine was recovered and evaporated under a stream of N_2. The resulting residues were solubilized in 100 µL of mobile phase and 25 µL were analyzed by HPLC-MS using an LTQ Orbitrap mass spectrometer

coupled to and Accela HPLC system (Thermo Fischer Scientific). Analyte separation was achieved using an HILIC guard pre-column and an HILIC Proshell 120 column (4µm, 4.6 x 150 mm) (Agilent). Separation was achieved by isocratic elution (0.4mL/min) using acetonitrile-water (50:50, v/v) containing 20 mM ammonium formate and adjusted to pH 4.4. An ESI source operated in the positive mode was used for the MS analysis. Data were normalized by tumor sample weight.

Histology

Tumors were excised 24-h after the end of treatment and fixed in 4% paraformaldehyde. Samples were paraffin-embedded and sliced in 5 µm-thick sections. Tissue slices were stained with hematoxylin and eosin, and photographed on a Zeiss MIRAX slide scanner for a global view of necrotic tumor areas. Quantification of necrotic regions was obtained using Panoramic Viewer and Image J software, and is expressed as % of whole tumor area. For that purpose, the percentage of necrosis was determined by detecting the number of pixels that satisfy a color and intensity predefined (necrotic), divided by the number of pixels in non-necrotic tissue.

Tumor Growth

At day 0 (mean tumor volume=0.2±0.1cm^3), tumor-bearing mice were injected with sorafenib (40mg/kg/day), H-89 (20mg/kg/day) or vehicle (DMSO, 35µl).

Tumor size was assessed using an electronic caliper for 10 days. Tumor established with shRNA-transfected cells were monitored for 52 days after tumor induction. Tumor volumes were estimated by determining the mean of the 3 tumor diameters *D* (mean of length, width and height), using the following equation: Tumor volume= $\pi * \left(\frac{D}{2}\right)^2$.

Statistical Analysis

Results are shown as means ± standard error of the mean (SEM). Confidence intervals (CI) are calculated for a measure of treatment effect. Comparisons between groups were made using Student's t-test or one-way ANOVA (post-hoc Dunnett's multiple comparison test) where appropriate. p-Values ≤ 0.05(*), ≤ 0.01(**) or ≤ 0.001(***) were considered to be significant.

Supplementary figures

Sup.Fig.1A

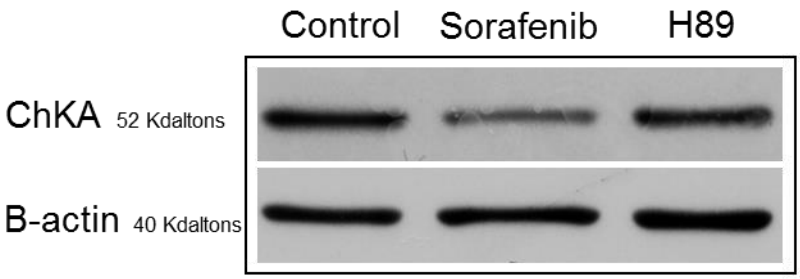

Sup.Fig.1B

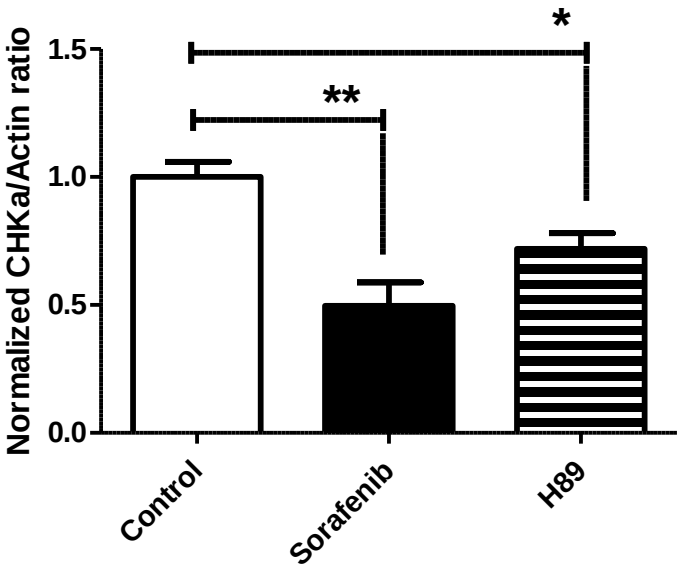

Legend : Fig.1A : Western blotting analysis of ChKA expression in control and treated (sorafenib, H89) MDA-MB-231 cells in vitro. Fig.1B : Expression of ChKA (normalized to B-actin) is decreased to 49,7%+/- 9,1% of the control after treatment with Sorafenib (** ; n=4, independent experiments) and 71,9%+/- 6,2% of the control after treatment with H89 (* ; n=4, independent experiments).

Addendum

Before to start the study, some preliminary experiments were realized to evalutate the efficacy of different treatments and to define different time points to visualize the treatment effects. During this preliminary phase, teatraethylammonium (TEA) an inhibitor of OCT (20mg/kg, intra peritoneal), was also tested to evaluate its potential action on the choline cycle.

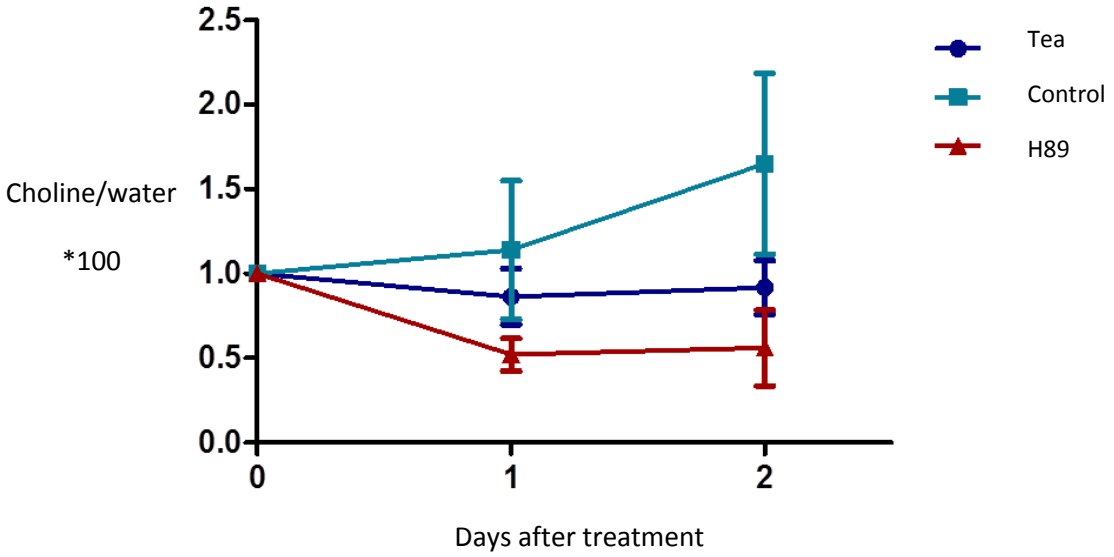

Longitudinal follow up of total choline to water ratio (tCho/water ratio) before and after direct inhibition of choline kinase α using H89 and before and after inhibition of organic cation transporters using TEA. A significant decrease in the choline to water ratio was observed after 48 hours of treatment with H89; that was not the case for TEA.

2. ^{13}C-MRS is a method of choice to image metabolic substrates. This emerging method is able to assess disease activity and contribute to decisions concerning the patient care. In this study, the dynamic monitoring of the conversion of hyperpolarized ^{13}C-fumarate into ^{13}C-malate, and of hyperpolarized ^{13}C-pyruvate into ^{13}C-lactate, is used as emerging in vivo markers to evaluate treatment efficacy.

II Monitoring chemotherapeutic response by hyperpolarized ^{13}C -fumarate MRS and diffusion MRI.

Lionel Mignion, Prasanta Dutta, Gary V. Martinez, Parastou Foroutan, Robert J. Gillies, Benedicte F. Jordan.

Cancer Research, 2014 Feb 1 ; 74 (3) : 686-694.

Integrated Systems and Technologies: Mathematical Oncology

Cancer Research

Monitoring Chemotherapeutic Response by Hyperpolarized ^{13}C-Fumarate MRS and Diffusion MRI

Lionel Mignion[1], Prasanta Dutta[2], Gary V. Martinez[2], Parastou Foroutan[2], Robert J. Gillies[2], and Benedicte F. Jordan[1]

Abstract

Targeted chemotherapeutic agents often do not result in tumor shrinkage, so new biomarkers that correlate with clinical efficacy are needed. In this study, we investigated noninvasive imaging protocols to monitor responses to sorafenib, a multikinase inhibitor approved for treatment of renal cell and hepatocellular carcinoma. Healthy cells are impermeable to fumarate, so conversion of this metabolite to malate as detected by ^{13}C-magnetic resonance spectroscopy (MRS) has been suggested as one marker for cell death and treatment response in tumors. Diffusion MRI also has been suggested as a measure of therapy-induced cytotoxic edema because viable cells act as a diffusion barrier in tissue. For these reasons, we assessed sorafenib responses using hyperpolarized ^{13}C-fumarate, diffusion-weighted MRI (DW-MRI) in a xenograft model of human breast cancer in which daily administration of sorafenib was sufficient to stabilize tumor growth. We detected signals from fumarate and malate following intravenous administration of hyperpolarized fumarate with a progressive increase in the malate-to-fumarate (MA/FA) ratio at days 2 to 5 after sorafenib infusion. The apparent diffusion coefficient (ADC) measured by DW-MRI increased in the treated group consistent with cytotoxic edema. However, the MA/FA ratio was a more sensitive marker of therapeutic response than ADC, with 2.8-fold versus 1.3-fold changes, respectively, by day 5 of drug treatment. Histologic analyses confirmed cell death in the sorafenib-treated cohort. Notably, ^{13}C-pyruvate-to-lactate conversion was not affected by sorafenib in the breast cancer model examined. Our results illustrate how combining hyperpolarized substrates with DW-MRI can allow noninvasive monitoring of targeted therapeutic responses at relatively early times after drug administration. Cancer Res; 74(3); 686–94. Ó2013 AACR.

Introduction

Sorafenib (Nexavar) was the first RAF kinase inhibitor to enter human clinical testing and is now approved for use in advanced or metastatic renal cell carcinoma and in unresectable hepatocellular carcinoma (1). This compound, initially developed as a selective inhibitor of RAF, has shown other biologically relevant targets, including VEGFR2/3, platelet-derived growth factor receptor (PDGFR), Flt-3, c-kit, and fibroblast growth factor receptor (FGFR-1; ref. 2). Sorafenib is therefore able to affect both tumor signaling and angiogenesis. Preclinically, Sorafenib shows broad-spectrum antitumor activity in renal, colon, hepatocarcinoma, breast, non–small cell lung, ovarian, thyroid, pancreatic, and melanoma xenograft models, involving either antiproliferative and/or antiangiogenic effects of the drug (3). Clinical studies using sorafenib as monotherapy have also been conducted in patients with malignant glioma (4), thyroid cancer (5–7), metastatic melanoma (8, 9), angiosarcoma (10), head and neck tumors (11), acute leukemias (12), and advanced soft tissue sarcomas (13).

The new targeted therapies and treatment options require timely and effective methods to evaluate an individual's response. Conventional anatomically based endpoints may be inadequate to monitor the tumor response to targeted agents that usually do not result in tumor shrinkage while used as monotherapy. Diffusion-weighted MRI (DW-MRI) seems to detect the loss of the cellularity, which is the end result of extensive necrosis (14), and has also been shown to be sensitive to other type of cell death, including mitotic catastrophe and apoptosis (15). However, tumor ADC (apparent diffusion coefficient) is not yet able to detect low levels of diffuse necrosis or early necrosis following administration of anticancer agents (16, 17). Therefore, the identification and use of complementary, earlier, and more sensitive noninvasive biomarkers are needed to optimize the schedule and dosage of novel therapeutics. Several novel imaging methods exploit altered metabolism and its normalization in treatment-responsive tumors as methods for the evaluation of the treatment response (18). Magnetic resonance spectroscopy (MRS) has been used to

Authors' Affiliations: [1]Biomedical Magnetic Resonance Research Group, Louvain Drug Research Institute, Universite Catholique de Louvain, Brussels, Belgium; and [2]Department of Cancer Imaging and Metabolism, H. Lee Moffitt Cancer Center and Research Institute, Tampa, Florida

L. Mignion and P. Dutta contributed equally to this work.

Corresponding Author: B. Jordan, Biomedical Magnetic Resonance Group, Louvain Drug Research Institute, Universite Catholique de Louvain, Avenue Mounier 73.08, 1200 Brussels, Belgium. Phone: 32-2-764-7364; Fax: 32-2-764-7390; E-mail: benedicte.jordan@uclouvain.be

doi: 10.1158/0008-5472.CAN-13-1914

investigate biochemical changes associated with disease, and tumor response to targeted therapies (19). However, a limitation of MRS is low sensitivity, especially for nuclei other than protons. Dynamic nuclear polarization (DNP) can be used to increase the sensitivity >10,000-fold of in vivo ^{13}C-MRS through hyperpolarization of nuclear spins of intravenously delivered ^{13}C labeled substrates (20, 21). DNP transfers high electron spin polarization to nuclear spins via microwave irradiation in a strong magnetic field (3,35T) and at cryogenic temperature (1.4 K). Metabolic fluxes have been followed in experimental tumors using hyperpolarized [1-^{13}C] pyruvate, [1,4-$^{13}C_2$] fumarate, or ^{13}C bicarbonate, among others (22, 23). The first clinical trial using hyperpolarized ^{13}C-MR metabolic imaging with [1-^{13}C] pyruvate has been successfully performed in patients with biopsy-proven prostate cancer and no dose-limiting toxicities were observed (24).

^{13}C-MRS–detectable conversion of hyperpolarized fumarate-to-malate, catalyzed by fumarase, has been suggested as a marker of drug-induced cellular necrosis and treatment response in tumors (25). Healthy cells are impermeable to fumarate, thus fumarate-to-malate conversion is thought to reflect the necrosis-mediated release of fumarase into the extracellular space of the surrounding tissue. Necrotic areas are poorly perfused and have high extracellular fumarase activity (25). Importantly, the background is low, as viable cells demonstrate slow uptake, and, consequently, there is little detectable malate production within the lifetime of the polarization (26). The levels of malate produced correlated with the levels of necrosis in vitro and in vivo (25, 27). This method could therefore be used as a very early marker of therapies that induce necrosis (28).

Pyruvate, an endogenous substrate, is generated by metabolism of glucose or oxidation of lactate (29). To date, this metabolite has been the most commonly used for DNP. The conversion of pyruvate-to-lactate may be used to help distinguish tumor from normal tissue (30) and can also serve as a diagnostic marker (31). The abnormality of pyruvate metabolism in diseased tissue can be detected by quantifying its downstream metabolites. Lactate conversion results from the reaction catalyzed by the enzyme lactate dehydrogenase (LDH). The conversion kinetics will depend on the delivery of hyperpolarized pyruvate to the tumor, the rate of pyruvate transport across the cell membrane and the activity of LDH (26). LDH activity, in turn, depends on the concentration of the enzyme and substrate ($NAD^þ$, NADH, pyruvate, and lactate) concentrations at steady state as well as the intracellular pH (26). There is increasing evidence for an early reduction in pyruvate–lactate exchange in a range of cancer models following treatment with cytotoxic chemotherapy (27, 32), targeted drug (28, 33, 34), and radiotherapy (35). In addition, ^{13}C-MRS–detectable hyperpolarized pyruvate-to-lactate conversion has recently been suggested as a response marker for LDH A (36) and MAPK inhibition (18) as well.

The aim of this study was to assess the response to sorafenib using ^{13}C-MRS of hyperpolarized fumarate and pyruvate in mammary xenografts, in comparison with DW-MRI and histologic markers.

Materials and Methods

Tumor model

All animals were maintained in accordance with Institutional Animal Care and Use Committee (University of South Florida, Tampa, FL) standards of care in pathogen free rooms, in the Moffitt Cancer Center (Tampa, FL) Vivarium. All imaging and measurements were performed within the facility. As a model for tumor therapeutic response, human tumor xenografts were grown in NMRI nude mice. MDA-MB-231 human breast cancer cells were grown in Dulbecco's Modified Eagle Medium-F12 media supplemented with 10% FBS and 1% penicillin–streptomycin. Cells were removed from flasks by either treating with trypsin. About 10 million cells in 100 mL of media were immediately injected into the leg of 3- to 6-week-old female severe combined immunodeficient mice. For imaging and histology, xenografts were allowed to grow 3 to 6 weeks into tumors of suitable volume. The ^{13}C-MRS study was initiated when tumor volume reaches about 200 mm^3. Mice were weighed and tumor volumes were measured twice-weekly using calipers and calculated as ðlength Â width Â widthÞ=2, with the length and width defined as the long and short diameters, respectively. Moreover, tumor volume was measured more precisely during MRI experimentation using T_2-weighted imaging (fast spin-echo). Only healthy mice were used for imaging and spectroscopy. Magnetic resonance (MR) experiments were carried out before injection of any drug, after 2 and 5 days of daily sorafenib treatment (40 mg/kg dissolved in dimethyl sulfoxide, DMSO). Drug was administered by intraperitoneal injection (35 mL).

MR experiments

Mice bearing MDA-MB-231 xenografts were imaged at day 0 (tumor size of 150–200 mm^3), day 2, and day 5 of daily treatment with 40 mg/kg of sorafenib. Mice were anesthetized with a mixture of 1.0 L/min O_2 and 3% isoflurane (AErrane; Baxter) for induction, and 1% isoflurane for maintenance. Body temperature was maintained constant (37 C Æ 0.5 C) in the gradient coils using an air heater and monitored using a rectal temperature probe.

[1-^{13}C] pyruvic acid or [1,4-$^{13}C_2$] fumaric acid, were mixed with 15 mmol/L trityl radical (OX63) and hyperpolarized by an Oxford DNP Polarizer (HyperSense). The polarized substrate was quickly dissolved in Tris/EDTA, NaCl, and NaOH solution at 37 C, yielding 80 mmol/L pyruvate or 20 mmol/L fumarate at neutral pH, before injecting into the mouse via jugular vein catheter. Mice were imaged using a double tuned ^{1}H-^{13}C–volume coil in an Agilent ASR 310 7T small animal imaging system. After administration of 0.45 mL of hyperpolarized fumarate, ^{13}C spectra were acquired with a T_R of 2,000 ms and flip angle 15 for 5 minutes from a 3- to 4-mm-thick slice across the tumor. After 1 hour of fumarate injection, 0.35 mL of hyperpolarized pyruvate was administered and ^{13}C spectra were acquired with a T_R of 1,000 ms and flip angle 9 for 5 minutes from the same tumor. Low flip angle pulses are required to preserve the polarization over the whole imaging period that allow more efficient use of the available polarization. DW-MRI was performed before the injection of

hyperpolarized substrate using a spin-echo sequence with three b values (50, 500, and 1,000), T_R ¼ 1,500 ms, T_E ¼ 36 ms. All the MRI data were compared before and after 2 or 5 days of treatment.

Histologic analysis

Tumors were excised at day 5 for histologic analysis and compared with untreated tumors. The center section of the subcutaneous tumor of each animal was fixed in 10% formalin and paraffin embedded before staining one 5-mm-thick cross-sectional sample per animal with hematoxylin and eosin (H&E) for histology. Another 5 mm slice was taken for cleaved caspase-3 (CC3) staining. Histology slides of both H&E and CC3 were scanned using the Aperio ScanScope XT with a 200Â/0.8NA objective lens at a rate of 8 minutes per slide via Basler trilinear array. Histologic pattern recognition was conducted using the Genie (Aperio) software platform to segment and classify necrosis, viable tumor, and other nontarget tissues (i.e., adipose, muscle, and skin; ref. 37). Furthermore, Spectrum algorithms were applied the entire slide's digital image and to determine the percentage of necrosis by detecting the number of pixels that satisfy a color and intensity predefined (necrotic), divided by the number of pixels in nonnecrotic tissue. Similar analyses were performed to evaluate the number of positive nucleus in CC3 slides. All the training algorithms developed above were quality controlled by a practicing pathologist.

Statistical analysis

All results are expressed as mean Æ SEM. ANOVA and Bonferroni post-test, t test were performed to assess the statistical significance between the different groups and timings. Statistical significance was considered at the $P < 0.05$ level.

Results

Daily intraperitoneal sorafenib injections (40 mg/kg) for 9 days were able to significantly reduce MDA-MB-231 tumor growth. Tumor volumes were measured twice-weekly using calipers (n ¼ 4). We observed a significant difference at days 2, 6, and 9 (P value < 0.001) between the sorafenib-treated group and the control group, which received only DMSO vehicle (Fig. 1A).

By day 5, we observed a significant increase in tumor ADC_w during Sorafenib treatment ($P < 0.01$; one-way ANOVA, Bonferroni post-test). These results suggest a significant decrease in cellularity in the tumor after 5 days of treatment (Fig. 1B). ADC_w values within the segmented tumor regions of interest were also used to generate histograms. As shown in Fig. 1C, a right shift in tumor water diffusion was observed at 5 days of treatment. ADC maps from a representative animal before and after treatment with sorafenib (day 0 vs. day 5) are shown on Fig 1D. This is better displayed using cumulative (Fig. 1E) and cumulative difference histograms (Fig. 1F).

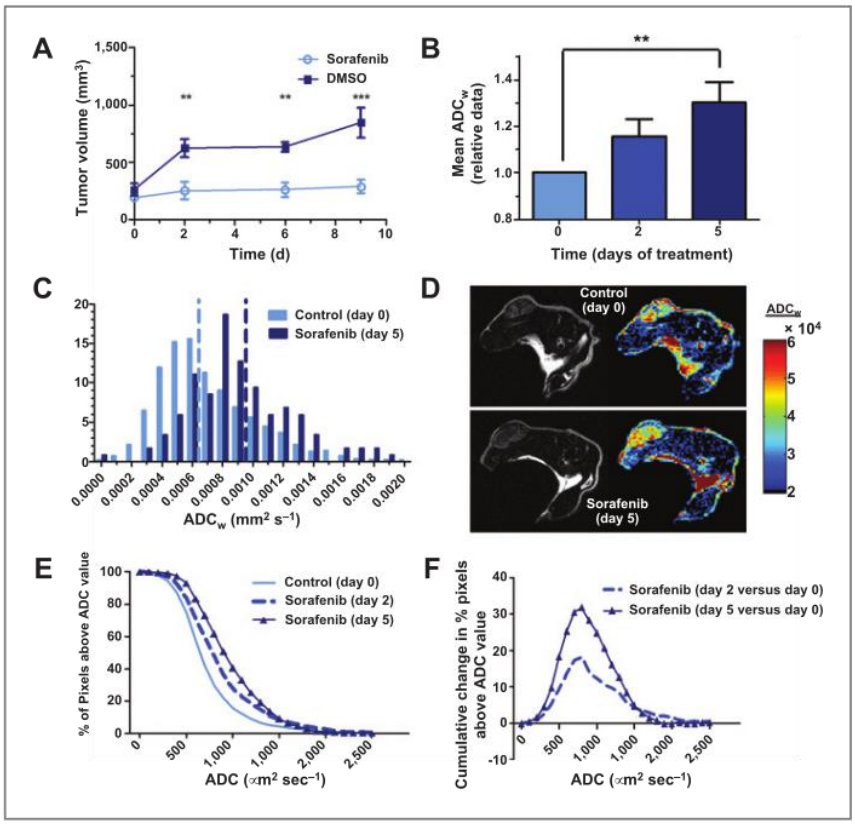

Figure 1. A, MDA-MB-231 tumors growth curve with or without sorafenib treatment (ÃÃ, $P < 0.01$). B, average tumor ADC_w following administration of sorafenib (ÃÃ, $P < 0.01$ after 5 days of treatment). C, typical ADC_w histograms of control and treated tumors (day 5). A right shift in tumor. D, typical diffusion maps before treatment and after 5 days of treatment with sorafenib. ADC_w is observed after 5 days of treatment with sorafenib. E, cumulative histograms before and after treatment, percentage pixels above ADC value. F, cumulative change in percentage pixels above ADC value after 2 days and 5 days of treatment.

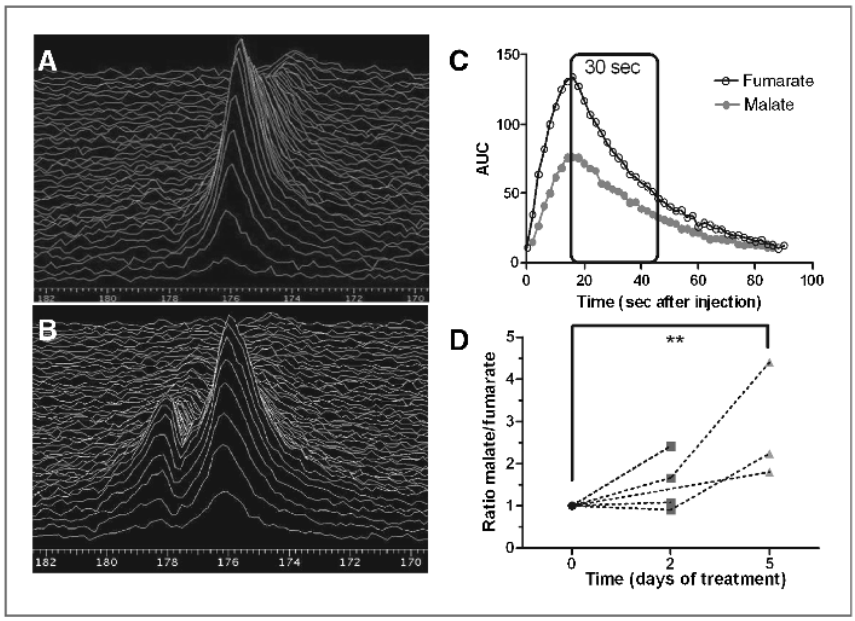

Figure 2. A, typical ^{13}C-MRS spectra from an MDA-MB-231 untreated tumor after hyperpolarized fumarate injection. B, ^{13}C-MRS spectra from a treated tumor: fumarate (176 ppm) and malate (179 ppm) peaks. C, corresponding areas under the curves for fumarate and malate signals. D, ^{13}C flux modifications in the malate/fumarate ratio after sorafenib treatment ($P < 0.01$).

Intravenous administration of hyperpolarized fumarate resulted in detectable signals from fumarate (176 ppm) and malate (179 ppm) following 2 days of treatment (Fig. 2B). No detectable malate was observed before treatment (Fig. 2A). Because the two ^{13}C carbons of [1,4-$^{13}C_2$] fumarate are equivalent, they give a single peak. However, [1,4-$^{13}C_2$] malate should yield two peaks. These are merged into a single anisotropic peak in this study, likely because of low spectral resolution resulting from the 4 mm tumor slice from which the spectra were obtained. In our study, 3 ppm chemical shifts between fumarate and malate were observed in vivo, which is consistent with the results of Witney and colleagues in similar tumors (27). However, larger chemical shifts have been described in other studies between malate and fumarate, especially in vitro (25). There was a time-dependant change in fumarate-to-malate conversion that became significant after 5 days of treatment with sorafenib (n ¼ 3). The flux ratio of tumor malate and fumarate was assessed as a drug therapy response marker in this study. The evolution of this ratio reflects the evolution of cell death in response to sorafenib treatment. The malate-to-fumarate (MA/FA) ratios calculated as the 30-second integrals following peak (Fig. 2C) progressively increased from day 2 (n ¼ 5) until day 5 (n ¼ 3), time at which the relative increase of the ratio is significant ($P < 0.01$, one-way ANOVA; Bonferroni post-test; Fig. 2D). The MA/FA ratio reached its highest value at 2.8 after 5 days of sorafenib treatment.

Notably, the ADC_w changes in sorafenib-treated tumors at day 2 (n ¼ 9) and day 5 (n ¼ 5) were in accordance with changes observed with MA/FA ratio. Indeed, a positive correlation was observed between the relative change in MA/FA and the relative change in ADC_w over time (Pearson correlation test, $P < 0.05$; Fig. 3). In comparing the sensitivities of the two methods, a 2.8-fold increase was observed for ^{13}C fumarate/malate versus 1.3-fold for ADC_w. However, the reproducibility of ADC_w measurements is expected to be higher than those of MA/FA, as they do not require injection of exogenous substrate.

One hour after fumarate injection, hyperpolarized ^{13}C pyruvate was administered and resulted in two detectable peaks: lactate (183 ppm) and pyruvate (171 ppm; Fig. 4A and B). Pyruvate-to-lactate conversion and their quantitative analysis for pretreated and treated animals were performed. The flux ratio (Lac/Pyr) were calculated from area under the curve of total pyruvate pool and lactate pool with time and this ratio did not change in pre- and post-treated tumors as shown in Fig 4C. In addition, we calculated the apparent rate

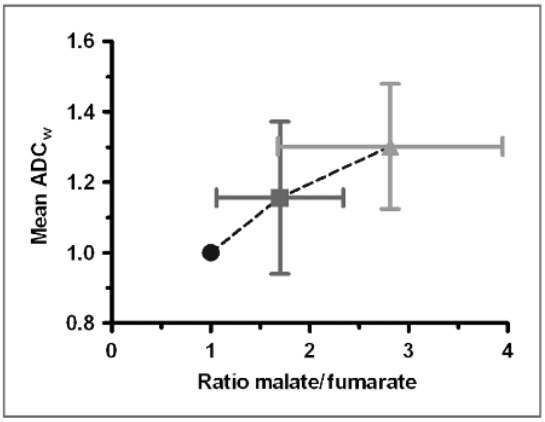

Figure 3. Positive correlation (Pearson correlation test) between malate/fumarate and ADC_w.

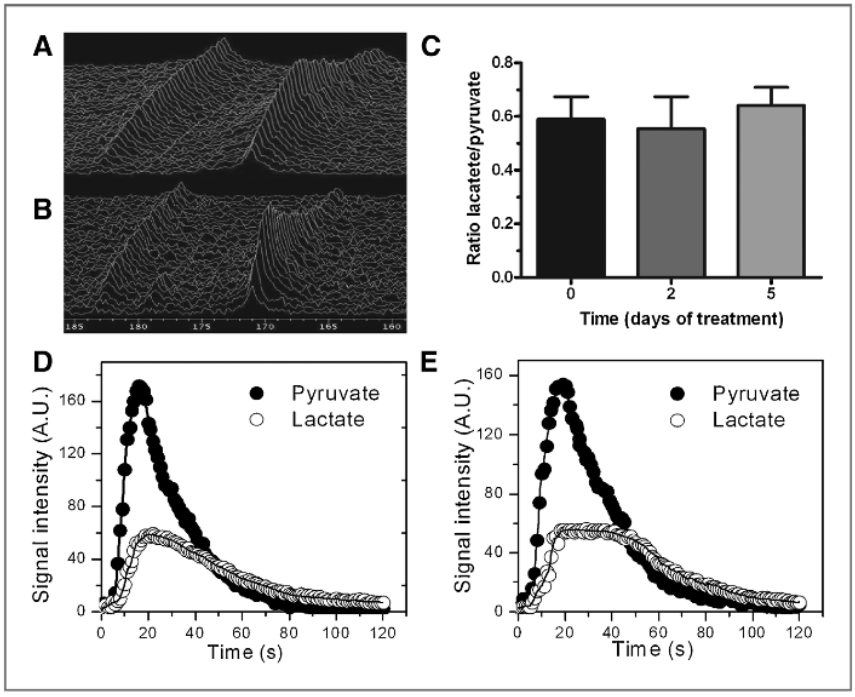

Figure 4. A, typical ^{13}C-MRS spectra from an MDA-MB-231 untreated tumor after hyperpolarized pyruvate injection. B, ^{13}C-MRS spectra from a treated tumor: pyruvate (171 ppm) and lactate (183 ppm) peaks. C, ^{13}C flux modifications in the lactate/pyruvate ratio after sorafenib treatment. D and E, pyruvate and lactate fluxes with time for pre- (D) and post- (day 5; E) sorafenib–treated tumors. Solid lines represent the fits to modified Bloch equations.

constants k_P (pyruvate-to-lactate) and k_L (lactate-to-pyruvate) using modified Bloch equations (32, 34) as shown in Fig. 4D and E. The fitting results indicated that the rate constants did not change significantly between pre- and post-treated tumors as shown in Table 1.

This result was also confirmed ex vivo by lactate measurements of tumor extracts. There were no significant differences in lactate concentrations between control (7.6 Æ 1.1 mmol/g) and treated (6.1 Æ 1.1 mmol/g) tumors (P ¼ 0.41). Moreover, regardless of the tracer used, the times to maximum peak of the signals after tracer injection were not significantly different between control and sorafenib tumors. For pyruvate, the times to peak were 13 s Æ 1.0 s versus 11 s Æ 1.0 s for control and treated tumors, respectively, (P ¼ 0.22). For fumarate, the times to peak were 14.0 s Æ 2.0 s versus 16.0 s Æ 2.0 s for control and treated tumors, respectively, (P ¼ 0.58). These observations indicate that the delivery of hyperpolarized substrates, and hence the vasculature and perfusion, were not modified by sorafenib treatment.

Table 1. Fitted values of apparent rate constants k_P (pyruvate-to-lactate) and k_L (lactate-to-pyruvate) using modified Bloch equations for the pre- and post-sorafenib–treated tumors (n ¼ 4; P < 0.05, Student t test)

Tumors	k_P (per second)	k_L (per second)
Pre-sorafenib (day 0)	0.054 Æ 0.004	0.023 Æ 0.003
Post-sorafenib (day 2)	0.055 Æ 0.003	0.022 Æ 0.004
Post-sorafenib (day 5)	0.053 Æ 0.004	0.021 Æ 0.003

Histologic studies of tumor sections were obtained post-mortem on control mice and mice treated with daily sorafenib for 5 days. These included H&E and caspase-3 analysis. H&E histologic analysis showed a significant (P < 0.008) increase in tumor necrosis (40.7 % increase) between untreated tumors and tumors treated with sorafenib for 5 days (Fig. 5A and B). Differences in CC3 staining probing apoptotic cell death were also observed between treated and control tumors. Quantitative analyses showed that average CC3 stained–positive pixel values normalized by constant area of tissue section were much larger (P < 0.0001) following 5 days of treatment with sorafenib compared with control (untreated) tumors (Fig. 5C and D). Notably, tumor size did not change between day 0 and day 5 under sorafenib treatment, whereas it did in the controls (Fig. 1A). This suggests that the lack of tumor volume change was associated with an increase in apoptotic and necrotic cell death.

Discussion

The introduction of new drugs and targeted treatments to individual patient has led to the need for specific biomarkers of treatment response that are good predictors of final outcome (38). Indeed, targeted therapies usually result in tumor stabilization rather than in tumor shrinkage, at least in monotherapy, reducing the sensitivity of standard metrics of response, such as Response Evaluation Criteria in Solid Tumors (39). There is therefore a need for quantitative biomarkers to assess treatment response. Noninvasive imaging can provide sensitive and specific measures of tumor response in the absence of

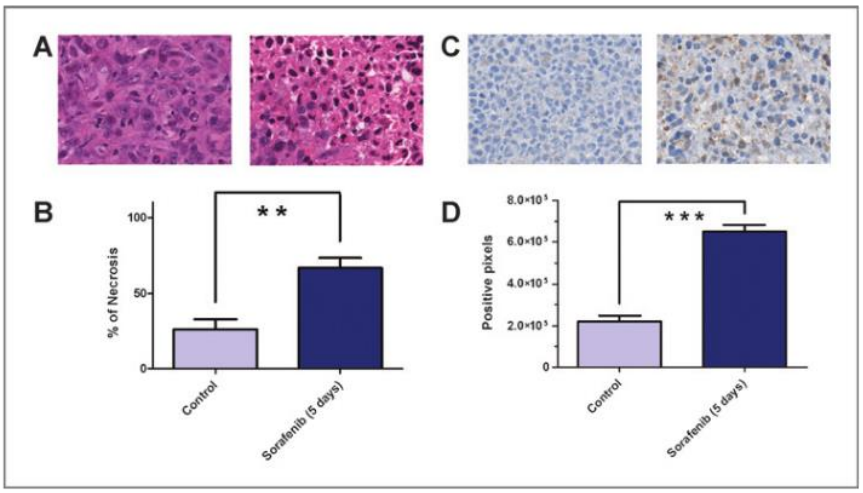

Figure 5. A, H&E staining in untreated tumors (left) and treated tumors (right). B, note the significant increase in tumor necrosis after sorafenib treatment ($P < 0.01$). C, cleaved caspase-3 staining in untreated tumors (left) and treated tumors (right). D, note the significant increase in tumor apoptosis after sorafenib treatment ($P < 0.001$).

change in tumor size. Such methods include DNP and DW-MRI, which alone or in combination can noninvasively assess metabolic or oedematous responses in vivo.

Tumor response to sorafenib has been assessed using overall survival, time to symptomatic progression and time to progression in phase II and III clinical studies in hepatocellular carcinoma (40). Objective evidence of tumor shrinkage has been seen in renal cell carcinoma (41), melanoma (42), pancreatic, and papillary thyroid carcinoma (43). More sensitive and quantitative biomarkers that correlate with clinical efficacy are required in the transition toward individualized therapy; especially given the financial and patient costs of targeted treatments, such as sorafenib. Notably, response biomarkers can also serve as nonresponse biomarkers, to spare patients cycles of futile therapy, and possibly allow them to move to other, possibly experimental therapies.

Imaging techniques to quantify response have included 2[18F]fluoro-2-deoxy-D-glucose–positron emission tomography to assess metabolism (44), dynamic contrast enhanced MRI (DCE-MRI) to assess tumor blood flow and perfusion (45), and DW-MRI to assess cellularity (14). Newly emerging techniques include hyperpolarized ^{13}C-MRI, which cannot only measure catabolism and trapping of tracer, but can also measure metabolic conversion. ^{13}C fumarate provides positive contrast and is described to be a marker of cellular necrosis (25). In necrotic cells, the plasma membrane permeability barrier is compromised; fumarate is therefore rapidly transformed into malate. In viable cells, however, there is a very slow plasma membrane transport and thus, no detectable conversion of fumarate-to-malate within the short lifetime of the ^{13}C polarization is observed (27). The rate of labeled malate production has shown good correlation with the level of tumor cell necrosis (25). The lack of a malate signal in the absence of cell death makes this a highly sensitive measurement. In this study, we observed a 280% increase of the malate/fumarate ratio following sorafenib treatment. These results were consistent with the decrease in cellularity assessed using DW-MRI. Because there is water diffusion in normal tissues, there is a higher background and hence, a smaller magnitude change of only 30% Both the increase in malate and ADC were consistent with the increase of necrosis and apoptosis measured by H&E and caspase-3 analyses, respectively. The level of tumor cell necrosis after treatment has been described both in preclinical and in clinical studies as a good prognostic indicator for treatment outcome in the absence of any change in tumor size (46). Our results show that the net change in ^{13}C fumarate conversion into malate marker was more sensitive than DW-MRI. However, it must be remembered that the value of a biomarker is directly related to the magnitude of change, normalized to its test–retest reproducibility, and this has yet to be assessed in a larger cohort and others tumor models before generalization, although our results are in agreement with other recent preclinical studies comparing fumarate with pyruvate and ADC_w (28, 47). Also, ADC_w has been reported to be highly reproducible within a single institution. No such data are yet available for fumarate, yet the real-time availability of the input function can mitigate the greatest source of error for an injectable kinetic model (48). Bohndiek and colleagues showed that the changes in fumarate conversion were earlier and more sensitive than the changes in ADC_w in lymphoma tumors treated with combrestatatin-A4-phosphate (28). In this model, they did not observe any change in ADC_w at 6 hours after treatment, although there was a 32% increase in necrotic fraction at 24 hours. This was consistent with the fact that in xenograft tumors with small or diffuse regions of necrosis, there may be no change in ADC with necrotic fractions of up to 40% (17). We also do see a more sensitive response using fumarate than ADC_w, but in our case, timing of response is similar and even positively correlated at day 2 and day 5. So, in this study, the major advantage of fumarate is the higher dynamic range, which might be balanced by the disadvantage of requiring the injection of an exogenous substrate with respect to DW-MRI.

Cohyperpolarized pyruvate and fumarate preparations could not be used in vivo as malate production is masked by

overlapping signals from lactate and the pyruvate hydrate formed from labeled pyruvate (27). However, injections of hyperpolarized fumarate and pyruvate were performed one hour apart and were consecutive to the DW-MRI scans, so that all measurements were performed on the same tumors during the same MRI session.

Importantly, the monitoring pyruvate-to-lactate flux did not show any sensitivity to treatment with sorafenib in this study on MDA-MB-231 xenografts. This is in contrast with other studies that have shown significant effects of targeted and nontargeted chemotherapy on pyruvate-to-lactate fluxes. For example, the LDH-catalyzed interconversion of hyperpolarized label between pyruvate and lactate was observed to decrease early after etoposide chemotherapy (32), which was explained by a loss of the coenzyme NADH, decreases in tumor cellularity, and reduced LDH concentrations (23). Also, with respect to targeted therapies, inhibition through the phosphoinositide 3-kinase (PI3K/Akt/mTOR) pathway was shown to correlate with a drop in hyperpolarized [1-^{13}C] lactate levels in breast cancer and glioblastoma cells and xenografts (34). This was attributed to a drop in LDH expression as a result of reduced levels of the transcription factor, hypoxia-inducible factor-1a , which regulates expression of the LDH gene (23). Finally, the pyruvate-to-lactate flux observed in transgenic prostate tumors has been shown to be consistent with tumor cellularity and necrosis (23).

Two studies reporting a lack of change in pyruvate-to-lactate conversion (18, 49), attributed the lack of response to a putative role played by the monocarboxylate transporters (MCT) 1 and MCT4, in pyruvate-based molecular imaging and the concomitant low MCT1 expression in their tumor cell lines. MCT1 is not detected in MDA-MB231 cells (50). However, the hypothesis that the expression of the transporter is rate limiting is not consistent because other groups observed a decrease in lactate-to-pyruvate ratio in MDA-MB-231 tumors in response to doxorubicin (27) or to PI3K inhibition (34).

A factor that could be involved in the lack of change in pyruvate-to-lactate ratio is a potential normalization effect of sorafenib. Indeed, this could be the result of compensating effects between an increase in delivery of pyruvate (due to potential normalization effects of sorafenib) and a potential decrease in pyruvate-to-lactate conversion. Pyruvate results have been discussed in the same context in other studies: Bohndiek and colleagues (47) had similar results using bevacizumab in colorectal cancer xenograft (HT29). In this study they observed a significant increase in apoptotic and necrotic areas (5%-10% at 72 hours) accompanied by a paradoxical increase in ^{13}C flux from hyperpolarized pyruvate. In contrast, the same treatment in another colorectal cancer model that was more sensitive to the anti-VEGF therapy showed a decrease in ^{13}C pyruvate flux. The likely explanation of these discrepancies was the difference in the antiangiogenic response and in pyruvate delivery depending on the tumor type. In our study, normalization effects of sorafenib were not directly assessed, although the time to maximum peak intensity (reflecting the delivery of the substrates) in both fumarate and pyruvate studies did not differ significantly from day 0 to day 5. Time-to-maximum is, however, not as robust as is DCE-MRI or ex vivo studies of microvessel density to assess spatially explicit change in delivery/perfusion that can be induced by sorafenib. With this regard, the literature reports that the MDA-MB-231 breast cancer model was shown to be sensitive to sorafenib treatment in terms of normalization. Daily oral administration of a 30 or 60 mg/kg dose of sorafenib for 5 days strongly decreased the number and area of microvessels in the sorafenib-treated tumors, showing significant inhibition of angiogenesis in this tumor model, as shown by ex vivo staining of CD31 (2). A hypothesis is therefore that a potential vessel normalization could contribute to an increase in delivery of pyruvate at day 2 of 5, which could in turn compensate for a potential decrease in the pyruvate-to-lactate conversion. Notably, a decrease in pyruvate-to-lactate conversion has been described by other groups in response to doxorubicin or PI3K inhibition in this same tumor model (27, 34). If this were the case, the final lactate-to-pyruvate ratio would not be modified. Although we did observe a trend for ex vivo lactate levels to decrease at day 5, these were not significant. This would also require further "normalization" studies, such as DCE-MRI, to attest this hypothesis. Finally, the malate/fumarate ratio is a more direct measure of cell death than is the lactate/pyruvate ratio. For example, dying cells are permeable and, unless this results in a loss of cofactor NADH, the LDH reaction may continue to proceed in a MCT-independent fashion. This same increase in permeability allows access of fumarate to fumarase and subsequent conversion to malate. The fumarate results are coherent with histologic results, whereas pyruvate results seem to be also influenced by the vascularization state and normalization state of the tumor, as suggested by Bohndiek and colleagues.

Conclusion

We show that hyperpolarized MRS using ^{13}C-fumarate is an early in vivo marker of response to sorafenib in MDA-MB-231 tumors and is positively correlated with DW-MRI, with a higher sensitivity for MA/FA ratio with respect to DW-MRI (dynamic ranges of 2.8 vs. 1.3, respectively, at day 5). Results are in accordance with ex vivo H&E and CC3 analysis. The lactate-to-pyruvate ratio does not seem to be an in vivo marker of tumor response to sorafenib in MDA-MB-231 tumors, likely due to vessel normalization.

Disclosure of Potential Conflicts of Interest

No potential conflicts of interest were disclosed.

Authors' Contributions

Conception and design: L. Mignion, P. Dutta, R.J. Gillies, B.F. Jordan
Development of methodology: L. Mignion, P. Dutta, P. Foroutan, R.J. Gillies, B.F. Jordan
Acquisition of data (provided animals, acquired and managed patients, provided facilities, etc.): L. Mignion, P. Dutta, G.V. Martinez, P. Foroutan, B.F. Jordan
Analysis and interpretation of data (e.g., statistical analysis, biostatistics, computational analysis): L. Mignion, P. Dutta, G.V. Martinez, R.J. Gillies, B.F. Jordan
Writing, review, and/or revision of the manuscript: L. Mignion, P. Dutta, P. Foroutan, R.J. Gillies, B.F. Jordan
Administrative, technical, or material support (i.e., reporting or organizing data, constructing databases): L. Mignion, P. Dutta
Study supervision: G.V. Martinez, B.F. Jordan

Acknowledgments

The authors thank the Analytical Microscopy Core Facility at Moffitt Cancer Center for support.

Grant Support

This study was supported by grants from the Belgian National Fund for Scientific Research (FNRS), the "Actions de Recherches Concertees-Communaute Française de Belgique-ARC 09/14-020." L. Mignion is "Televie" Researcher and B.F. Jordan is Research Associate for the Belgian National Fund for Scientific Research (FNRS).The authors acknowledge the financial support of the Wayne Huizinga Trust at Moffitt Cancer Center and R01 CA077575-14 (R.J. Gillies).

The costs of publication of this article were defrayed in part by the payment of page charges. This article must therefore be hereby marked advertisement in accordance with 18 U.S.C. Section 1734 solely to indicate this fact.

Received July 10, 2013; revised November 5, 2013; accepted November 21, 2013; published OnlineFirst November 27, 2013.

References

1. Pratilas CA, Solit DB. Targeting the mitogen-activated protein kinase pathway: physiological feedback and drug response. Clin Cancer Res 2010;16:3329–34.
2. Wilhelm SM, Carter C, Tang L, Wilkie D, McNabola A, Rong H, et al. BAY 43-9006 exhibits broad spectrum oral antitumor activity and targets the RAF/MEK/ERK pathway and receptor tyrosine kinases involved in tumor progression and angiogenesis. Cancer Res 2004; 64:7099–7109.
3. Wilhelm SM, Carter C, Lynch M, Lowinger T, Dumas J, Smith RA, et al. Discovery and development of sorafenib: a multikinase inhibitor for treating cancer. Nature Rev Cancer 2006;5:835–44.
4. Nabors LB, Supko JG, Rosenfeld M, Chamberlain M, Phuphanich S, Batchelor T, et al. Phase I trial of sorafenib in patients with recurrent or progressive malignant glioma. Neuro Oncol 2011;13:1324–30.
5. Kloos RT, Ringel MD, Knopp MV, Hall NC, King M, Stevens R, et al. Phase II trial of sorafenib in metastatic thyroid cancer. J Clin Oncol 2009;27:1675–84.
6. Lam ET, Ringel MD, Kloos RT, Prior TW, Knopp MV, Liang J, et al. Phase II clinical trial of sorafenib in metastatic medullary thyroid cancer. J Clin Oncol 2010;28:2323–30.
7. Brose MS, Nutting CM, Sherman SI, Shong YK, Smit JWA, Reike G, et al. Rationale and design of decision: a double-blind, randomized, placebo-controlled phase III trial evaluating the efficacy and safety of sorafenib in patients with locally advanced or metastatic radioactive iodine (RAI)-refractory, differentiated thyroid cancer. BMC Cancer 2011;11:349.
8. Ott PA, Hamilton A, Min C, Safarzadeh-Amiri S, Goldberg L, Yoon J, et al. A phase II trial of sorafenib in metastatic melanoma with tissue correlates. PLoS ONE 2010;5:e15588.
9. Margolin KA, Moon J, Flaherty LE, Lao CD, Akerley WL III, Othus M, et al. Randomized phase II trial of sorafenib with temsirolimus or Tipifarnib in untreated metastatic melanoma (S0438). Clin Cancer Res 2012;18:1129–37.
10. Ray-Coquard I, Italiano A, Bompas E, Le Cesne A, Robin Y-M, Chevreau C, et al. Sorafenib for patients with advanced angiosarcoma: a phase II trial from the French Sarcoma Group (GSF/GETO). Oncologist 2012;17:260–6.
11. Williamson SK, Moon J, Huang CH, Guaglianone PP, LeBlanc M, Wolf GT, et al. Phase II evaluation of sorafenib in advanced and metastatic squamous cell carcinoma of the head and neck: Southwest Oncology Group Study S0420. J Clin Oncol 2010;28:3330–35.
12. Borthakur G, Kantarjian H, Ravandi F, Zhang W, Konopleva M, Wright JJ, et al. Phase I study of sorafenib in patients with refractory or relapsed acute leukemias. Haematologica 2011;96:62–68.
13. von Mehren M, Rankin C, Goldblum JR, Demetri GD, Bramwell V, Ryan CW, et al. Phase II SWOG-directed intergroup trial (S0505) of sorafenib in advanced soft tissue sarcomas. Cancer 2012;118:770–6.
14. Koh D-M, Collins DJ. Diffusion-weighted MRI in the body: applications and challenges in oncology. AJR Am J Roentgenol 2007;188:1622–35.
15. Morse DL, Galons J-P, Payne CM, Jennings DL, Day S, Xia G, et al. MRI-measured water mobility increases in response to chemotherapy via multiple cell-death mechanisms. NMR Biomed 2007;20:602–14.
16. Hamstra DA, Rehemtulla A, Ross BD. Diffusion magnetic resonance imaging: a biomarker for treatment response in oncology. J Clin Oncol 2007;25:4104–109.
17. Lyng H, Haraldseth O, Rofstad EK. Measurement of cell density and necrotic fraction in human melanoma xenografts by diffusion weighted magnetic resonance imaging. Magnetic Resonance in Medicine 2000; 43:828–36.
18. Lodi A, Woods SM, Ronen SM. Treatment with the MEK inhibitor U0126 induces decreased hyperpolarized pyruvate to lactate conversion in breast, but not prostate, cancer cells. NMR Biomed. 2013;26: 299–306
19. Beloueche-Babari M, Chung Y-L, Al-Saffar NMS, Falck-Miniotis M, Leach MO. Metabolic assessment of the action of targeted cancer therapeutics using magnetic resonance spectroscopy. Br J Cancer 2010;102:1–7.
20. Ardenkjaer-Larsen JH, Fridlund B, Gram A, Hansson G, Hansson L, Lerche MH. Increase in signal-to-noise ratio of >10,000 times in liquid-state NMR. Proc Natl Acad Sci U S A 2003;100:10158–10163.
21. Bohndiek SE, Kettunen MI, Hu D, Kennedy BWC, Boren J, Gallagher FA, et al. Hyperpolarized [1-13C]-ascorbic and dehydroascorbic acid: vitamin C as a probe for imaging redox status in vivo. J Am Chem Soc 2011;133:11795–801.
22. Nelson SJ, Vigneron D, Kurhanewicz J, Chen A, Bok R, Hurd R. DNP-hyperpolarized ^{13}C magnetic resonance metabolic imaging for cancer applications. Appl Magn Reson 2008;34:533–44.
23. Kurhanewicz J, Vigneron DB, Brindle K, Chekmenev EY, Comment A, Cunningham CH, et al. Analysis of cancer metabolism by imaging hyperpolarized nuclei: prospects for translation to clinical research. Neoplasia 2011;13:81–97.
24. Nelson SJ, Kurhanewicz J, Vigneron DB, Larson P, Harzstarck A, Ferrone M, et al. Metabolic imaging of patients with prostate cancer using hyperpolarized [1-^{13}C] pyruvate. Sci Tran Medi 2013;5: 198ra108.
25. Gallagher FA, Kettunen MI, Hu D-E, Jensen PR, Zandt RI, Karlsson M, et al. Production of hyperpolarized [1,4-13C2]malate from [1,4-13C2]fumarate is a marker of cell necrosis and treatment response in tumors. Proc Natl Acad Sci U S A 2009;106:19801–6.
26. Brindle KM, Bohndiek SE, Gallagher FA, Kettunen MI. Tumor imaging using hyperpolarized 13C magnetic resonance spectroscopy. Magn Reson Med 2011;66:505–19.
27. Witney TH, Kettunen MI, Hu D, Gallagher FA, Bohndiek SE, Napolitano R, et al. Detecting treatment response in a model of human breast adenocarcinoma using hyperpolarised [1-13C]pyruvate and [1,4-13C2]fumarate. Br J Cancer 2010;103:1400–6.
28. Bohndiek SE, Kettunen MI, Hu D, Witney TH, Kennedy BWC, Gallagher FA, et al. Detection of tumor response to a vascular disrupting agent by hyperpolarized 13C magnetic resonance spectroscopy. Mol Cancer Ther 2010;9:3278–88.
29. Mallet RT. Pyruvate: metabolic protector of cardiac performance. Proc Soc Exp Biol Med 2000;223:136–48.
30. Park I, Larson PEZ, Zierhut ML, Hu S, Bok R, Ozawa T, et al. Hyperpolarized 13C magnetic resonance metabolic imaging: application to brain tumors. Neuro Oncol 2010;12:133–44.
31. Golman K, Zandt RI, Lerche M, Pehrson R, Ardenkjaer-Larsen JH. Metabolic imaging by hyperpolarized 13C magnetic resonance imaging for in vivo tumor diagnosis. Cancer Res 2006;66:10855–60.
32. Day SE, Kettunen MI, Gallagher FA, Hu D-E, Lerche M, Wolber J, et al. Detecting tumor response to treatment using hyperpolarized 13C magnetic resonance imaging and spectroscopy. Nat Med 2007;13: 1382–7.
33. Dafni H, Larson PEZ, Hu S, Yoshihara HAI, Ward CS, Venkatesh HS, et al. Hyperpolarized 13C spectroscopic imaging informs on hypoxia-

inducible factor-1 and myc activity downstream of platelet-derived growth factor receptor. Cancer Res 2010;70:7400–10.
34. Ward CS, Venkatesh HS, Chaumeil MM, Brandes AH, Vancriekinge M, Dafni H, et al. Noninvasive detection of target modulation following phosphatidylinositol 3-kinase inhibition using hyperpolarized 13C magnetic resonance spectroscopy. Cancer Res 2010;70:1296–1305.
35. Day SE, Kettunen MI, Cherukuri MK, Mitchell JB, Lizak MJ, Morris HD, et al. Detecting response of rat C6 glioma tumors to radiotherapy using hyperpolarized [1- 13C]pyruvate and 13C magnetic resonance spectroscopic imaging. Magn Reson Med 2011;65:557–63.
36. Dutta P, Le A, Vander Jagt DL, Tsukamoto T, Martinez GV, Dang CV, et al. Evaluation of LDH-A and glutaminase inhibition in vivo by hyperpolarized ^{13}C-pyruvate magnetic resonance spectroscopy of tumors. Cancer Res 2013;73:4190–5.
37. Mulrane L, Rexhepaj E, Penney S, Callanan JJ, Gallagher WM. Automated image analyses in histopathology: a valuable toll in medical diagnostics. Expert Rev Mol Diagn 2008;8:707–25
38. Brindle K. New approaches for imaging tumour responses to treatment. Nat. Rev. Cancer 2008;8:94–107.
39. Milano A, Perri F, Ciarmiello A, Caponigro F. Targeted-therapy and imaging response: a new paradigm for clinical evaluation? Rev Recent Clin Trials 2011;6:259–65.
40. Abou-Alfa GK, Schwartz L, Ricci S, Amadori D, Santoro A, Figer A, et al. Phase II study of sorafenib in patients with advanced hepatocellular carcinoma. J Clin Oncol 2006;24:4293–300.
41. Ahmad T, Eisen T. Kinase inhibition with BAY 43-9006 in renal cell carcinoma. Clin Cancer Res 2004;10:6388S–92S.
42. Flaherty KT, Brose M, Schuchter LM, Tuveson D, Lee R, Schwartz B, et al. Phase I/II trial of BAY 43-9006, carboplatin, and paclitaxel demonstrates preliminary antitumor activity in the expansion cohort of patients with metastatic melanoma. J Clin Oncol 2004;22:14S (abstr 7507).
43. Ratain MJ, Flaherty KT, Stadler WM, O'Dwyer P, Kaye S, Xiong H, et al. Preliminary antitumor activity of BAY 43-9006 in metastatic renal cell carcinoma and other advanced refractory solid tumors in a phase II randomized discontinuation trial (RDT). J Clin Oncol 2004;22:14S (abstr 4501).
44. Weber WA, Schwaiger M, Avril N. Quantitative assessment of tumor metabolism using FDG-PET imaging. Nucl Med Biol 2000;27:683–7.
45. Padhani AR. Dynamic contrast-enhanced MRI in clinical oncology: current status and future directions. J Magn Reson Imaging 2002;16: 407–22.
46. Chang J, Ormerod M, Powles TJ, Allred DC, Ashley SE, Dowsett M. Apoptosis and proliferation as predictors of chemotherapy response in patients with breast carcinoma. Cancer 2000;89:2145–52.
47. Bohndiek SE, Kettunen MI, Hu DE, Brindle KM. Hyperpolarized 13C spectroscopy detects early changes in tumor vasculature and metabolism after VEGF neutralization. Cancer Res 2012;72:854–64.
48. Galbraith SM, Lodge MA, Taylor NJ, Rustin GJS, Bentzen S, Stirling JJ, et al. Reproducibility of dynamic contrast-enhanced MRI in human muscle and tumours: comparison of quantitative and semiquantitative analysis. NMR Biomed 2002;15:132–42.
49. Harris T, Eliyahu G, Frydman L, Degani H. Kinetics of hyperpolarized 13C1-pyruvate transport and metabolism in living human breast cancer cells. Proc Natl Acad Sci U S A 2009;106:18131–6.
50. Wang Q, Morris ME. The role of monocarboxylate transporter 2 and 4 in the transport of gamma-hydroxybutyric acid in mammalian cells. Drug Metab Dispos 2007;35:1393–9.

Chapter IV : Discussions and perspectives

4.1 Discussion

This thesis involves the study of “classic” and “emerging” non-invasive MR biomarkers of response and their combinations to assess changes induced by modulators of the choline cycle. These in vivo techniques monitor changes in cellularity, membrane turnover, and cellular metabolism in a human breast cancer model. Tumor size measurement is not always adequate to monitor the tumor response to targeted treatments. Indeed, targeted therapies usually result in tumor size stabilization rather than in tumor size reduction, reducing the sensitivity of standard metrics of response, such as RECIST (Milano, 2011). Moreover, after chemotherapy, changes in tumor size can take several weeks before to be detectable. Therefore, the identification of more sensitively, non-invasive biomarkers are needed to guide diagnostic decisions, to predict response to therapy or to optimize the schedule and dosage of novels therapeutics. Breast MRS is used to distinguish benign and malignant lesions improving the accuracy of a MR scan by improving the selectivity. In human breast studies, the decrease of tCho suggests successful therapy (Bolan, 2013). Diffusion MR imaging provides information about the cell density and can have a major role in many clinical situations as: tumor detection and characterization; differentiation of abscess from necrotic tumors; follow-up of the patient with cancer to monitor and predict treatment response,… (Rajeshkannan, 2006 ; Koh, 2007). In clinical oncology, multimodality setting can permit to confirm diagnostic or to help to choose the right therapy.

4.11 Modulation of the choline pathway

In this work, the choline pathway or Kennedy pathway was studied as a predominant pathway for the cellular membrane anabolism and cells multiplication in cancer tissues. As stated in the introduction, the study of the choline pathway can be very complex with a lot of interactions at different levels. Many enzymes have a regulatory role in this pathway and can influence positively or negatively the cell membrane formation. All the mechanisms regulating the phosphatidylcholine synthesis may be more complex than what's immediately apparent. Also, reciprocal links between the major oncogenic pathways and the choline cycle have been established (i.e. with MAPK and PI3K pathways).

In a first study, we measured the total choline from in vivo volume localized inside a breast tumor and evaluated the response to targeted therapies using proton MR spectroscopy and DW-MRI. tCho levels can be determined non-invasively in tumors with ^{1}H-MRS. In vivo "total choline" is composed of several different choline metabolites that overlap and contribute to this peak. The variations of the total choline value are due to a lot of enzymes and it reflects the global tumoral activity, cellular proliferation and possibly, malignancy. In our work, this pharmacodynamic parameter was suitable to demonstrate if the inhibition of the choline pathway was active or not, it was even confirmed with ex vivo mass spectroscopy analysis that confirmed reduction in intratumoral phosphocholine levels. In line with these findings, inhibition of MAPK signaling with the U0126 MEK inhibitor has been reported to cause a drop in intratumoral tCho and phosphocholine levels in tumors (Beloueche-Babari, 2005). However, choline MRS was not suited to predict the actual response of a tumor to a choline-targeted treatment since

reductions in choline levels did not systematically mean a tumor growth retardation. Indeed, when targeting ChoK with a direct inhibitor (H89), a significant decrease of tCho was observed that was not associated with a drop of cellularity and a stabilization of tumor growth. Comparatively, the multi-kinase inhibitor sorafenib decreased the tumor content of tCho, which preceded decreased cellularity (measured with DW-MRI), necrosis and, ultimately, a reduction of tumor size (which became significant only 5 days post-treatment). As a conclusion of the first part of this work, we can state that tCho level quantification in vivo with ^{1}H-MRS is a sensitive pharmacodynamic marker of response for choline signaling targeted therapies. However, this measurement is not per se predictive of the tumor response to a treatment as tumors were responsive to sorafenib and not to H89. Longitudinal pre- and post-treatment measurements of ADCw values were more consistent in terms of response as there was a close agreement between ADCw values, tumor growth and tumor necrosis for both H89 and sorafenib treatments. Thus, DW-MRI combined with choline spectroscopy may provide a useful non-invasive marker of response for choline signaling-targeted therapies.

MRS and DW-MRI methods can present some technical limitations in the tumoral context. These limitations constitute a supplementary reason to combine methods to obtain a performing marker of response for choline signaling-targeted therapies.

- The tumoral tissue is generally very heterogeneous and ^{1}H-MRS measures the mean of the tCho in a determined voxel. For this reason the position of the voxel inside the tumor can influence the mean global value of tCho. Multi voxel imaging allows to have a better evaluation of the intra-tumoral heterogeneity of choline, yet with a

lower signal to noise ratio in each voxel under study. Using this method, responses in various areas can be observed after targeted therapy.

- The measurement of tCho peak using MRS can be very difficult if the lipid peak is large, this problem is relatively frequent in breast cancer.

- There is a large inter-subject variability in the level of metabolites detected using ^{1}H-MRS and in the ADCw measured using DW-MRI. For this reason, the two methods are adapted to a longitudinal follow up of individual tumors before and after treatment.

- Using DW-MRI some artifacts can arise from motion, Eddy currents, ghosting and susceptibility effects (Padhani, 2009). Water motion is also very sensitive to the local temperature. To reduce a part of these artifacts, the tissue of interest is placed in the centrum of the magnet, the movements of mice are restricted, the respiration is controlled using anesthesia and the temperature of the subject is regulated. For translational purposes, standardization procedures and multi-centric reproducibility studies still need to be implemented, although the technique is widely used in the clinical setting.

a. Choline pathway: alternative multi-modal approach

During the process of this thesis we accumulated some non-published data that are being discussed here in the context of the monitoring of the inhibition of the choline pathway.

The initial objective of the thesis was to combine PET (^{18}F choline) and choline-MRS data to obtain a complete overview of the choline cycle in-vivo before and after modulations of the choline pathway (Fig.27). Indeed, ^{18}F-choline is described to probe the uptake of choline into the cell whereas ^{1}H-MRS is assessing the whole total choline tumor pool, with a possibility to assess more specifically PCho using ^{31}P-MRS.

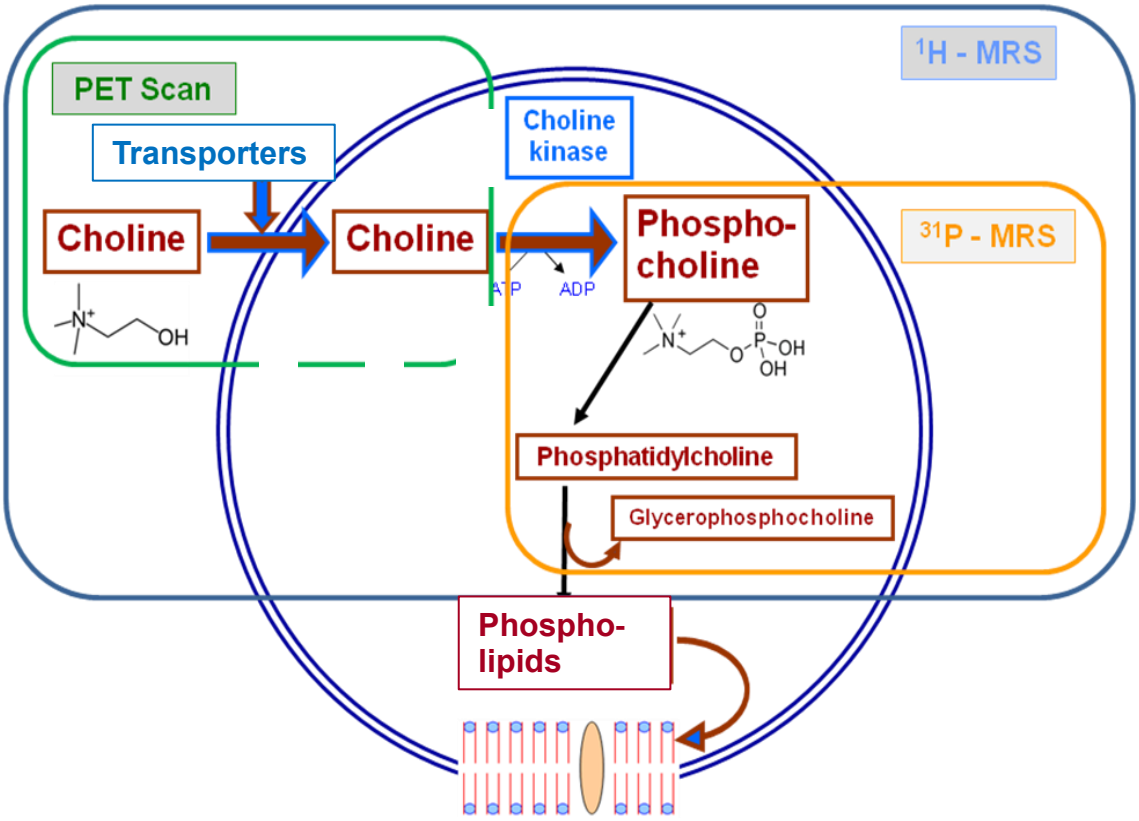

Fig.26. Choline pathway and corresponding multi-modal approach.

In a multi-modal approach, a complementary method to evaluate modulations in the free choline pool or on choline transport and intracellular choline is indeed Positron Emission Tomography (PET) after administration of one of the tracer ^{18}F or ^{11}C-choline. In our work, we used ^{18}F-choline to evaluate the choline uptake before and after treatment. Indeed, ^{18}F-choline (half-life 110min) has great structural similarity with natural choline. The

pathophysiological basis for the use of choline and its derivates for cancer imaging are the elevation of choline levels and the up-regulation of choline kinase activity in malignant cells (Kohlfurst, 2009). The first tests were performed on breast cancer mice xenografts, but the spatial resolution along with the relatively low signal to noise ratio obtained with ^{18}F-choline prevented the quantitative analysis of the data. ^{18}F-choline studies were therefore not pursued in this work.

In addition to ^{1}H-MRS, the measurement of PCho via ^{31}P-MRS can be performed using single voxel spectroscopy on a double tuned ^{1}H-^{31}P surface coil. If the measurement of PCho would be very interesting to evaluate the choline kinase activity, our in vivo ^{31}P-MRS data obtained from 7 mm breast cancer xenografts presented a limited signal-noise ratio that was too low for spectral editing and robust quantification, despite the major interest for this technique. Alternatively, ex vivo quantification of PCho was performed using mass spectrometry and confirmed in vivo results obtained in terms of tCho using ^{1}H-MRS.

b. Choline pathway: alternative targets

Besides choline kinase, alternative targets can be considered in the choline pathway, including inhibition of choline transport or of choline 'recycling' (fig.28).

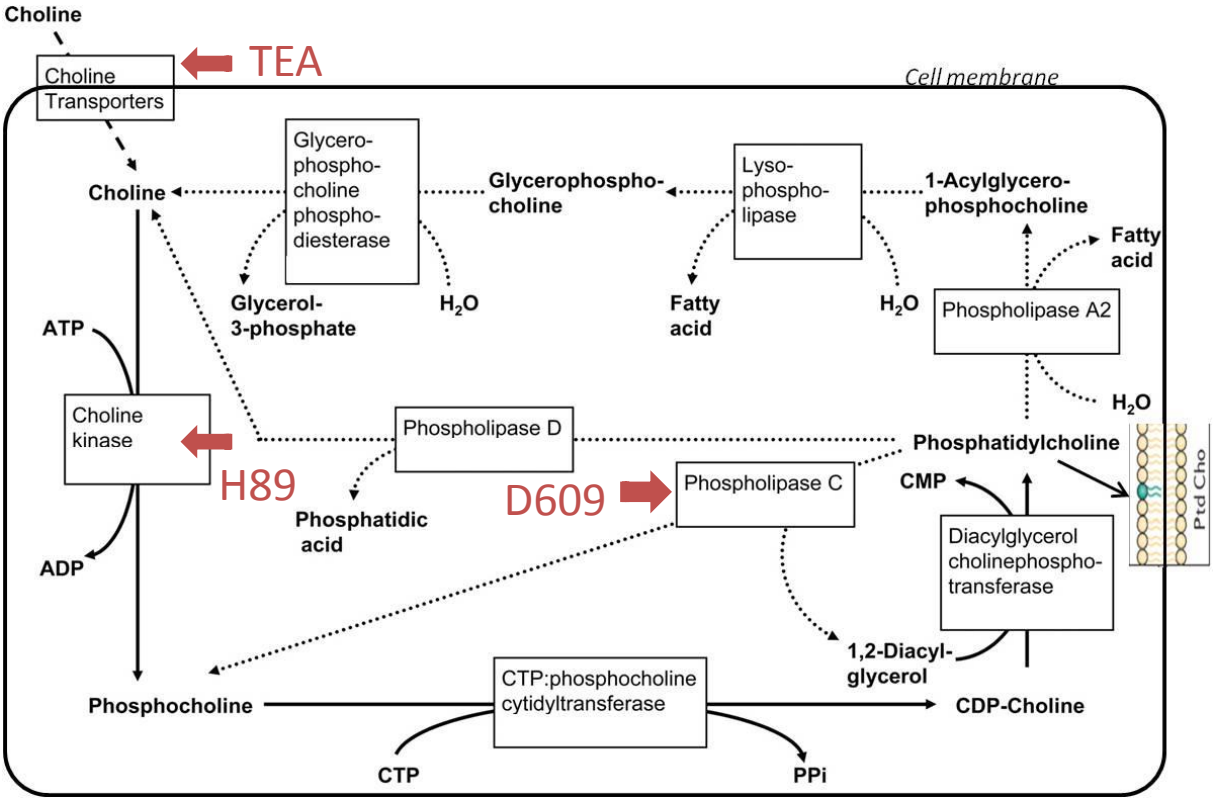

Fig.27. Choline pathway and specific inhibitors of the cycle. Adapted from Glunde, 2004.

Pilot experiments involving inhibition of the choline transport as well as of choline recycling were performed in the same xenograft tumor model. We could conclude from these preliminary tests that tetra-ethyl ammonium (TEA), an inhibitor of the organic cation transporters (OCT) was not able to significantly decrease ^{1}H-MRS tCho peak, contrarily to H89. This result can be explained by the complexity and the different systems of choline transport. The inhibition of OCT is probably not sufficient to impact the tCho level and there are probably some phenomena of bypass to compensate the inhibition of a specific type of choline transporter. An overall prominence of the transporters on kinases in the increase of tCho peak is present in specific models as rhabdomyosarcoma (Rommel, 2012). However, on MDA-MB-231 breast cancer cells, ChoK has the most important role in the increase of the tCho level

(Glunde, 2004). This can explain a part of the lack of response after TEA treatment.

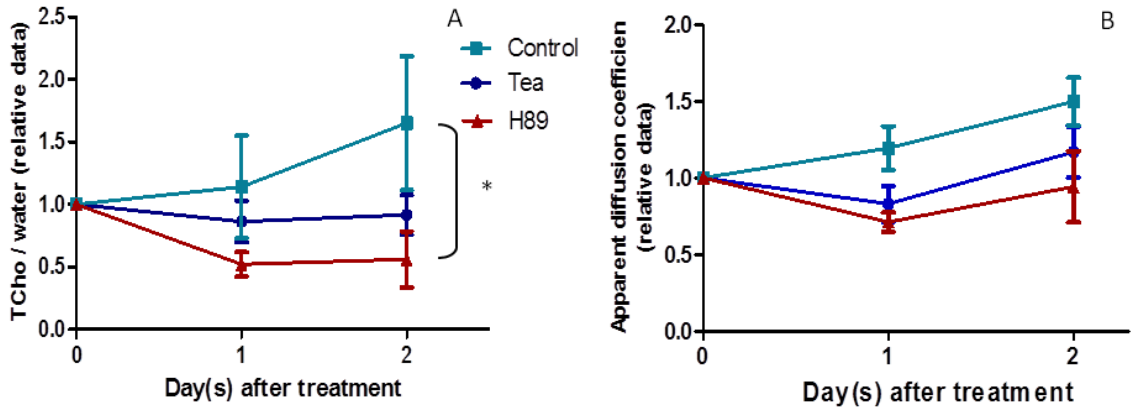

Fig.28. : (A) Evolution of total choline to water ratio before and after H89 treatment inhibiting choline kinase and TEA treatment inhibiting choline transport. A significant decrease in the choline to water ratio is observed after 48 hours of treatment with H89 (*). (B) Tumor ADCw following administration of H89 and TEA.

In an effort to identify a choline cycle inhibitor that would have a direct impact on tumor progression in vivo, the more recent inhibitor of choline 'recycling', D609, was tested in vivo. Actions of this inhibitor are attributed to the inhibition of phosphatidylcholine-specific phospholipase C (PC-PLC). This competitive PC-PLC inhibitor (D609) blocks cell proliferation in vitro and prevents these cells from entering in the S phase under growth factor stimulation (Ioro,2010). In our hands, this inhibitor had no significant effects in vivo on the tumor volume after 10 days of treatment in the breast cancer xenografts. These results were unpredictable because proliferation arrest, changes in cell morphology and formation of cytosolic lipid bodies typical of cell differentiation were induced by D609 in breast cancer cells (Abalsamo, 2012). However, another study indicated that inhibition of PC-PLC by D609 enhances

phospholipase D (PLD) activity in UMR-106 osteoblastic cells either due to a compensatory effect or that D609 directly increased PLD activity (Singh, 2000). It is also possible that this targeted treatment has no direct effect on the tumor size, as it is the case with the choline kinase inhibitor H89.

4.12 Emerging imaging markers of response based on the dynamic monitoring of metabolism

In a second part of the work, the combination of DNP and MRI was considered since it can image non-invasively the carbon metabolism in living system (Golman, 2006). There is a need for non-invasive imaging technique to develop imaging method that can detect metabolic transformations and treatment response before there is any change in tumor size. The transformation of ^{13}C-Fumarate to ^{13}C-Malate provides positive contrast and is suggested as a marker of cell death (Gallagher, 2009). The rate of labelled malate production showed good correlation with the level of tumor cell necrosis (Gallagher, 2009). In this study we showed an increase (2.8 folds) of the malate/fumarate ratio after Sorafenib treatment; these results are confirmed with the increase of necrosis measured by DW-MRI and H&E analysis. The net change in ^{13}C-fumarate conversion into malate marker was even more sensitive than DW-MRI. These results confirm the data of Bohndiek et al who showed that the changes in fumarate conversion were earlier and more sensitive than the change in ADCw in lymphoma tumors treated with combrestatin-A4-phosphate (Bohndiek, 2010).

The monitoring of pyruvate to lactate ratio did not show any sensitivity to treatment with sorafenib in this study on MDA-MB-231 xenografts. The ^{13}C isotope exchange flux between pyruvate and lactate is under equilibrium.

However lactate can be used as a biomarker of cancer aggressiveness, metastatic potential and treatment response (Sriram, 2015). A factor that could be involved in this lack of response to treatment is the potential normalization effect of sorafenib. Indeed, daily oral administration of this drug for 5 days strongly decreased the number and area of microvessels in the sorafenib-treated tumors, showing significant inhibition of angiogenesis (Wilhelm, 2004). Potential vessel normalization could contribute to an increase in delivery of pyruvate at day 2 of 5, which could in turn compensate for a potential decrease in the pyruvate-to-lactate ratio.

Co-hyperpolarised pyruvate and fumarate preparations could not be used in vivo as malate production was masked by overlapping signals from lactate and pyruvate hydrate formed from labelled pyruvate (Witney, 2010). However simultaneous evaluation of enzymatic pathways using multi-compound polarization would be a powerful method of probing multiple metabolic pathways in a single MR scan lasting only seconds (Wilson, 2010). Using this technique, information on metabolism, pH, necrosis and perfusion can be assessed simultaneously using ^{13}C-pyruvic acid, ^{13}C-sodium bicarbonate, ^{13}C-fumaric acid, and ^{13}C-urea with high levels of solution polarization (Wilson, 2010). Multi-compound polarization is a powerful method of probing multiple metabolic pathways.

DNP technique has been successfully used in pilot clinical studies at the University of California in San Francisco in prostate cancer. This recent first in man clinical trial utilized hyperpolarized ^{13}C-MR imaging. The goal of this study was to confirm the clinical potential and the feasibility of the technique in humans. No adverse effect or dose limiting toxicities have been reported. The results were extremely promising not only to confirm the safety of the agent

but also to show elevated ^{13}C-lactate/^{13}C-pyruvate ratio in cancerous regions (Nelson, 2013). This success opens a new perspective for hyperpolarized ^{13}C-imaging (Yen, 2011).

In pre-clinical disease models, several of the key metabolic shifts found in cancer, among which accelerated glycolysis, can be highlighted using hyperpolarized ^{13}C enriched substrates. Indeed, several cancers have a preference for aerobic glycolysis, whereby the pyruvate produced by glycolysis is converted to lactate, rather than entering in the Krebs cycle (Warburg effect) (Wilson, 2014). The hyperpolarization has the potential to revolutionize the way we use MR imaging. In particular, hyperpolarization addresses some of the intrinsic limitations of ^{1}H-MRS, including low sensitivity, overlap of key resonances, and lack of information about metabolism (Wilson, 2014). The use of ^{1}H and hyperpolarized ^{13}C-spectroscopy can help in the early diagnosis of cancer or to highlight an early treatment response. Future efforts in humans will be driven by new hyperpolarized biomarker probes identification and validation, improved methods for polarization and delivery of ^{13}C-substrates.

a. Place of hyperpolarized ^{13}C-spectroscopy vs PET imaging

FDG-PET is a reference method to predict pathological response in patients with breast cancer following chemotherapy (Biersack, 2004). However, with this method, the presence of infected or inflamed tissue can mask changes in tumor FDG uptake (Strauss, 1996) and patient received radiation doses. Recently, a combination of hyperpolarized ^{13}C-pyruvate magnetic resonance spectroscopic imaging and FDG-PET imaging was performed on a canine cancer patient using a clinical PET-MRI scanner. This study showed the co-localization of increased ^{13}C-lactate production and high ^{18}F-FDG uptake on PET (Gutte, 2015). This is in agreement with the fact that glycolysis and production of

lactate are increased in tumor cells compared to normal cells. PET alone is sometimes unable to localize small tumors or confirm whether FDG uptake in unusual sites reflects tumor or nontumor (Griffeth 2005).The combination of hyperpolarized ^{13}C-pyruvate MRS imaging and ^{18}F-FDG PET imaging may be valuable to discriminate high ^{18}F-FDG uptake due to activity in a muscle than high ^{18}F-FDG uptake due to Warburg effect in a tumor which will be accompanied by hight ^{13}C-lactate production. The hyperpolarized ^{13}C-pyruvate technique can be valuable with specific cancer localization where the ^{18}F-FDG uptake is not sufficient as in low-grade lymphoma.

4.2 General conclusion

The aim of the thesis was to assess response to modulations of the choline pathway in the context of the cholinic tumor phenotype. Conventional measurements like anatomically based endpoints may be inadequate to monitor the tumor response to targeted agents that usually do not result in tumor shrinkage while used in monotherapy. Therefore, the identification of more sensitively, non-invasive biomarkers are needed to optimize the schedule and dosage of novels therapeutics. The results illustrate that the assessment of total choline with ^{1}H-MRS is able to confirm the inhibition of the target but is not sufficient to predict tumor response to the targeted treatment. Adding DW-MRI as a marker of tumor response to choline inhibition improves specificity of the monitoring. In addition, ^{13}C-magnetic resonance spectroscopy and the detection of hyperpolarized ^{13}C-fumarate to ^{13}C-malate conversion has been suggested as a marker of cell death and treatment response in tumors. We showed here that hyperpolarized ^{13}C-fumarate, detected by ^{13}C-MRS, could constitute a new early in vivo marker of response to Sorafenib (MAPK inhibitor). The Sorafenib treatment targets a lot of kinases and its multi kinase action is closer to a non specific chemotherapeutic agent than to a very specific targeted treatment. It would be interesting to monitor the use of a more specific ChK inhibitor as MN-58b using ^{13}C fumarate. However, using Sorafenib treatment, the level of tumor cell necrosis after treatment has been described as a good prognostic indicator for treatment outcome in the absence of any change in tumor size. Our results show that the net change in ^{13}C-fumarate conversion into malate marker was even more sensitive than DW-MRI.

In conclusion, our studies illustrate that: (i) the total choline ^{1}H-MRS marker can constitute a pharmacodynamic marker of choline targeted

therapies, but does not presume the actual response to therapy, (ii) the combination of diffusion MRI and choline spectroscopy can be considered as a marker of response to choline targeted therapies, and (iii) the follow up of the metabolic ratio of ^{13}C-fumurate into ^{13}C-malate can be considered as an emerging marker of response to targeted therapies, with an improved sensitivity while compared with Diffusion-MRI.

4.3 Perspectives

4.31 In terms of inhibition of the choline pathway

The use of more specific and more efficient inhibitors of the choline pathway should be considered, including a specific and very efficient inhibitor of ChoK such as MN58b, as described in the introduction, but that is not commercially available. In the purpose, using in silico screening for small molecules that may interact with the choline kinase-α substrate binding domain, Clem et al. in 2011 identified a novel competitive inhibitor, N-(3,5-dimethylphenyl)-2-[[5-(4-ethylphenyl)-1H-1,2,4-triazol-3-yl]sulfanyl] acetamide (termed CK37) that inhibits purified recombinant human choline kinase-α activity, reduced the steady-state concentration of phosphocholine in transformed cells, and selectively suppressed the growth of neoplastic cells relative to normal epithelial cells. Interestingly, CK37 suppresses mitogen-activated protein kinase and phosphatidylinositol 3-kinase/AKT signaling and significantly decreased tumor growth in a lung tumor xenograft mouse model, suppressed tumor phosphocholine, and diminished activating phosphorylations of extracellular signal-regulated kinase and AKT in vivo. Also, more recently, in a T-lymphoma xenograft murine model, Chokα inhibitor CK37 remarkably retarded tumor growth, suppressed Ras-AKT/ERK signaling, increased lysophosphatidylcholine levels and induced in situ cell apoptosis/necropotosis (Xiong, 2015). It seems particularly relevant to monitor the effects of this choline kinase inhibitor in our breast cancer xenograft model using choline MRS, DW-MRI and ^{13}C-MRS hyperpolarized markers, since it is also inhibiting important signaling pathways in oncology, ie. MAPK and PI3K, that have been

described to be dependent on the choline cycle and more specifically on phosphatidic acid (Yalcin, 2010).

Other enzymes and steps of the choline pathway could be targeted, including using potent PC-PLC and PC-PLD inhibitors. There are some evidence that PC-PLC is implicated in metabolism, proliferation, and differentiation in mammalian cells (Spadaro, 2008). Moreover, increased PC-PLC activity was reported in breast tumor cells (Glunde, 2004). These data suggest the possible use of PC-PLC as a target for anti-cancer therapy. D609, a putatively selective antagonist of PC-PLC, increases PLD activity when PLC is inhibited in osteoblastic cells. This side effect might influence the downstream response to treatment (Singh, 2000). A combination of treatments should be used to inhibit PC-PLC and PC-PLD in the same time. Simultaneous use of a specific PLD inhibitor (Halopemide for example) with D-609 can be interesting for further studies. This combination of inhibitors is very interesting in theory; however the use of this combination of treatment can produce some neurologics side effects and mental disorders because halopemide a psychotropic agent, a analogue of neuroleptics (Loonen, 1985). For this reason a total inhibition of phospholipase C and D using this combination of treatments is not recommended, unless less toxic agents can be found.

Finally, recent studies strongly suggest the interest of combining choline kinase inhibition along with PLD1 inhibition. Indeed, the group of Z. Buhjwalla (Gadiya, 2014) reported a strong correlation between expression of Chokα and PLD1 with breast cancer malignancy. Data from patient samples established an association between estrogen receptor status and Chokα and PLD1 expression. In addition, these two enzymes were found to be interactive. Downregulation of Chokα with siRNA increased PLD1 expression, and downregulation of PLD1

increased Chokα expression. Simultaneous silencing of PLD1 and Chokα in MDA-MB-231 cells increased apoptosis as detected by the TUNEL assay.

These data provide new insights into choline phospholipid metabolism of breast cancer, and support multiple targeting of enzymes in choline phospholipid metabolism as a strategy for treatment.

4.32 In terms of acquisitions quality

For ^{1}H localized single voxel spectroscopy the new software “paravision 6” of bruker offers the possibility to realize adjustments and spectrum on circular regions of interest, contrarily to the version used in this study that only allows to define cubic regions of interest that have to be placed properly inside the tumor. This improvement can facilitate the acquisition of a spectrum from a tumor, which is generally not cubic.

For ^{13}C-acquisitions, optimized sequences for localized ^{13}C-spectroscopy would be required. Until now, the placement of the subcutaneous tumor was performed in order to be able to delimit a large slice covering the whole tumor without any other tissue interaction. Many groups have implemented optimized localized sequences with improved acquisition times (Nelson, Ozhinsky, 2013).

In addition, the optimization of localized ^{31}P-spectroscopy, to get a higher signal to noise ratio would be useful tool to monitor the transformation of choline in phosphocholine.

A major limitation of hyperpolarized magnetization is its unrecoverable decay, due not only to T1 relaxation but also to radio-frequency excitation. Some improvements can be done by eliminating the loss of hyperpolarized ^{13}C-

pyruvate magnetization due to radio frequency excitation. In this excitation scheme, the use of a spectral selective radio frequency pulse is involved to specifically exclude the excitation of ^{13}C-pyruvate, while uniformly exciting the key metabolites of interest (^{13}C-lactate, ^{13}C-alanine and ^{13}C-pyruvate-hydrate). The signal from downstream metabolite pools will be increased in terms of signal to noise ratio and lifetime (Chen, 2015). In the hyperpolarized applications, the life time is a critical point especially at high field.

4.33 In terms of techniques or post-processing

There is now considerable interest in applying more sophisticated mathematical models to DW-MRI data to extract quantitative parameters that reflect tissue microcapillary perfusion. By acquiring DW-MRI images using multiple b values (typically 6 or more), the DW-MRI data may be fitted using a biexponential mathematical model. Using such an approach, quantitative parameters that reflect vascular flow and tissue diffusivity can be derived. It is still unclear today whether such an approach does improve the assessment of drug effects and further studies are warranted (Afaq, 2010).

The use of hyperpolarized ^{13}C or ^{15}N choline can be very interesting to follow the choline metabolism. This approach can be potentially used as an imaging biomarker of cancer similar to choline positron emission tomography tracers to image and stage a cancer (Shchepin, 2013). In this context, hyperpolarized choline imaging with MRI was recently shown to be feasible using a stable isotope labeled choline analog (CMP1 or 1,1,2,2-D4 , 1-(13) C]choline chloride) (Friesen-Waldner, 2015). In addition, an earlier study demonstrated the feasibility of detecting hyperpolarized ^{15}N labeled choline in vivo in a rat head at 9.4 T (Cudalbu, 2010).

Finally, spectroscopic imaging, both for 1H and 13C MRS could be used to probe tumor heterogeneity of response.

Nowadays, no single technique is completely able to highlight early treatment response with high sensitivity and specificity because each of these techniques has its limitations. The use of hyperpolarized ^{13}C spectroscopy in combination with ^{1}H spectroscopy and DW-MRI will furnish complementary informations to improve the monitoring of cancer response to treatment. In the future, multimodal non-invasive imaging will probably allow a more accurate diagnostic and treatment individualization by early prediction of optimal therapeutic response.

4.34 Future clinical applications

While considering future potential clinical applications of this work, several aspects have to be considered, including technical implementation of the technologies into the clinical setting, identification of the real added value of using early markers of response in order to improve individualized therapy, and consideration of toxic secondary effects of single treatments as well as added toxicities in treatment combinations. All three aspects must be addressed before any translational relevance can be established.

The recent development of sterile polarizer systems permits the translation of the use of the hyperpolarized technology to the clinical practices. A first in human study has been already performed at the University of California in San Francisco (Nelson, 2013b). In this study, the potential of hyperpolarized pyruvate to stage a prostate cancer and to differentiate malignant versus benign tissue has been successfully investigated. During this

study, no dose-limiting toxicities were observed for ^{13}C pyruvate confirming the safety of the agent. This first in human's success opens the doors for other developpements to more diverse populations of cancer patients and to other applications as the assessing of a treatment effect. Hyperpolarized ^{13}C metabolic imaging may be valuable to precise the initial diagnostic and to monitor the efficacy of a therapy. For this last goal, a comparison of the lactate/pyruvate or malate/fumarate ratio before and after a treatment could be considered to assess treatment efficacy. These imaging biomarkers could therefore aid in the diagnosis, prognosis, and monitoring of tumors. With respect to drug development, the choice of the best targeted therapy for each type of tumor type could be facilitated by the use of hyperpolarized 13C-MRS markers .

A more straightforward clinical application is proton spectroscopy in humans that has already shown a role in predicting prognostic indicators of tumor aggressiveness in patients, including in breast cancer patients (Shin, 2012). The choline concentration is associated with biologic aggressiveness; difference in choline detection between invasive and in situ cancers may reflect the distinct histopathologic and biologic subtypes of breast cancer (Yeung, 2002). Total choline content measured by MRS is a non-invasive biomarker of cell proliferation and is associated with tumor aggressiveness. Morover the spectroscopic imaging can furnish a map of the concentration of the total choline compounds inside the tumor. This "choline level" map can help to characterize different area in the tumor and to predict the response or non response of each area to a defined treatment. The use of spectroscopy in addition to the traditional breast MRI could provide a non-invasive accurate characterization of the tumor and could help to adapt the treatment.

In this thesis, differences in choline content and apparent diffusion coefficient before and after a phamacological treatment were recorded using single voxel magnetic resonance spectroscopy and diffusion weighted imaging respectively. These two methods can be directly used in the clinic using a similar protocol to assess treatment efficacy very early after the beginning of the therapy. Depending of the molecular characteristics and the agressiviness of the tumor, a targeted treatment can be chosen and its efficacy can be assessed quite early after the first administration (i.e. several days) using choline spectroscopy and diffusion. These data should be compared with data before any treatment to see the early evolution of tumor. Moreover, an elevated basal level of choline could be tested as a prognostic biomarker to differentiate sensitive and resistant tumor to a defined treatment. However, converting these results into a clinically usefull response indicator has a long way to go, it requires the identification and validation of reliable threshold values that may be able to distinguish between responders and non-responders (van Asten, 2015). It is necessary to validate these findings in further clinical studies to have an individual and optimal therapy for the right patient.

In order to clearly determine if early imaging markers of response could be an added value in treatment individualization, randomized studies using imaging and spectroscopic markers should be designed, involving a comparision of a group for which the treatment is shifted to a ‘rescue’ therapy when imaging markers do not show any early tumor change versus a group that keeps the initial treatment. This trial should therefore be performed on a tumor type that has more than one therapeutic option. In the purpose, breast cancer patients could be considered for this trial. This study design would help to determine if the use of imaging markers to switch therapy very early in the treatment course could have a real impact on patient outcome. Moreover,

sparing patients from futile cycles of therapy could also be an endpoint of such a study, while considering the numerous side effects of anti-cancer treatments, as well as the cost of such therapies. If successful, this trial would constitue the first objective finding showing that a proper use of early imaging biomarkers could be a step towards a better individualized therapy, and possibly meet critical clinical needs in oncology.

Considering the drugs used in the current study, the toxicity profile of Sorafenib does certainly not make it a good candidate for proof of concept imaging markers studies in the clinical setting. Due to its multiple targets, Sorafenib induces mostly cardiac, dermatological, and gastro-intestinal toxicities. Therefore, the choice of a more targeted agent would be judicious. Regarding specific ChoKα inhibitors, they have recently entered clinical trials as a novel antitumor strategy. If HC-3 is well known to induce neurotoxicity, second generation choline kinase inhibitors (Mn58B, TCD717) have been designed to decrease neurotoxicity (de la Cueva, 2013). In the purpose, TCD717 has been tested in a first Phase I multi-centric clinical trial in advanced cancer patients between 2010 and 2014 (clinical trial of Brahmer Julie R, Johns Hopkins University) with no published results at this stage.

Chapter V : Bibliography

Bibliography :

Abalsamo, L., Spadaro, F., Bozzuto, G., Paris, L., Cecchetti, S., Lugini, L., Iorio, E., Molinari, A., Ramoni, C., and Podo, F. (2012). Inhibition of phosphatidylcholine-specific phospholipase C results in loss of mesenchymal traits in metastatic breast cancer cells. Breast Cancer Res *14*, R50.

Aboagye, E.O., and Bhujwalla, Z.M. (1999). Malignant transformation alters membrane choline phospholipid metabolism of human mammary epithelial cells. Cancer Res. *59*, 80–84.

Afaq, A., Andreou, A., and Koh, D.M. (2010). Diffusion-weighted magnetic resonance imaging for tumour response assessment: why, when and how? Cancer Imaging *10 Spec no A*, S179–S188.

Al-Saffar, N.M.S., Troy, H., Ramírez de Molina, A., Jackson, L.E., Madhu, B., Griffiths, J.R., Leach, M.O., Workman, P., Lacal, J.C., Judson, I.R., et al. (2006). Noninvasive magnetic resonance spectroscopic pharmacodynamic markers of the choline kinase inhibitor MN58b in human carcinoma models. Cancer Res. *66*, 427–434.

Al-Saffar, N.M.S., Jackson, L.E., Raynaud, F.I., Clarke, P.A., Ramírez de Molina, A., Lacal, J.C., Workman, P., and Leach, M.O. (2010). The phosphoinositide 3-kinase inhibitor PI-103 downregulates choline kinase alpha leading to phosphocholine and total choline decrease detected by magnetic resonance spectroscopy. Cancer Res. *70*, 5507–5517.

Amtmann, E. (1996). The antiviral, antitumoural xanthate D609 is a competitive inhibitor of phosphatidylcholine-specific phospholipase C. Drugs Exp Clin Res *22*, 287–294.

Amtmann, E., and Sauer, G. (1987). Selective killing of tumor cells by xanthates. Cancer Lett. *35*, 237–244.

Aoyama, C., Liao, H., and Ishidate, K. (2004). Structure and function of choline kinase isoforms in mammalian cells. Prog. Lipid Res. *43*, 266–281.

Ardenkjaer-Larsen, J.H., Fridlund, B., Gram, A., Hansson, G., Hansson, L., Lerche, M.H., Servin, R., Thaning, M., and Golman, K. (2003). Increase in signal-to-noise ratio of > 10,000 times in liquid-state NMR. Proc. Natl. Acad. Sci. U.S.A. *100*, 10158–10163.

Asghar Butt, S., Søgaard, L.V., Ardenkjaer-Larsen, J.H., Lauritzen, M.H., Engelholm, L.H., Paulson, O.B., Mirza, O., Holck, S., Magnusson, P., and Akeson, P. (2014). Monitoring mammary tumor progression and effect of tamoxifen treatment in MMTV-PymT using MRI and magnetic resonance spectroscopy with hyperpolarized [1-(13) C]pyruvate. Magn Reson Med.

Bakovic, M., Waite, K., and Vance, D.E. (2003). Oncogenic Ha-Ras transformation modulates the transcription of the CTP:phosphocholine cytidylyltransferase alpha gene via p42/44MAPK and transcription factor Sp3. J. Biol. Chem. *278*, 14753–14761.

Bammer, R. (2003). Basic principles of diffusion-weighted imaging. Eur J Radiol *45*, 169–184.

Bansal, A., Harris, R.A., and DeGrado, T.R. (2012). Choline phosphorylation and regulation of transcription of choline kinase α in hypoxia. J. Lipid Res. *53*, 149–157.

Barnes, A.B., Paëpe, G.D., van der Wel, P.C.A., Hu, K.-N., Joo, C.-G., Bajaj, V.S., Mak-Jurkauskas, M.L., Sirigiri, J.R., Herzfeld, J., Temkin, R.J., et al. (2008). High-Field Dynamic Nuclear Polarization for Solid and Solution Biological NMR. Appl Magn Reson *34*, 237–263.

Bell, J.D., and Bhakoo, K.K. (1998). Metabolic changes underlying 31P MR spectral alterations in human hepatic tumours. NMR Biomed *11*, 354–359.

Beloueche-Babari, M., Jackson, L.E., Al-Saffar, N.M.S., Workman, P., Leach, M.O., and Ronen, S.M. (2005). Magnetic resonance spectroscopy monitoring of mitogen-activated protein kinase signaling inhibition. Cancer Res. *65*, 3356–3363.

Beloueche-Babari, M., Jackson, L.E., Al-Saffar, N.M.S., Eccles, S.A., Raynaud, F.I., Workman, P., Leach, M.O., and Ronen, S.M. (2006). Identification of magnetic resonance detectable metabolic changes associated with inhibition of

phosphoinositide 3-kinase signaling in human breast cancer cells. Mol. Cancer Ther. *5*, 187–196.

Beloueche-Babari, M., Chung, Y.-L., Al-Saffar, N.M.S., Falck-Miniotis, M., and Leach, M.O. (2010). Metabolic assessment of the action of targeted cancer therapeutics using magnetic resonance spectroscopy. Br. J. Cancer *102*, 1–7.

Biersack, H.-J., Bender, H., and Palmedo, H. (2004). FDG-PET in monitoring therapy of breast cancer. Eur. J. Nucl. Med. Mol. Imaging *31 Suppl 1*, S112–S117.

Bluff, J.E., Reynolds, S., Metcalf, S., Alizadeh, T., Kazan, S.M., Bucur, A., Wholey, E.G., Bibby, B.A.S., Williams, L., Paley, M.N., et al. (2015). Measurement of the acute metabolic response to hypoxia in rat tumours in vivo using magnetic resonance spectroscopy and hyperpolarised pyruvate. Radiother Oncol.

Blusztajn, J.K. (1998). Choline, a vital amine. Science *281*, 794–795.

Bohndiek, S.E., Kettunen, M.I., Hu, D., Witney, T.H., Kennedy, B.W.C., Gallagher, F.A., and Brindle, K.M. (2010). Detection of tumor response to a vascular disrupting agent by hyperpolarized 13C magnetic resonance spectroscopy. Mol. Cancer Ther. *9*, 3278–3288.

Bolan, P.J. (2013). Magnetic resonance spectroscopy of the breast: current status. Magn Reson Imaging Clin N Am *21*, 625–639.

Brahmer, J.R., LoRusso,P. (2010) Clinical trial : Study of Intravenous TCD-717 in Patients With Advanced Solid Tumors, https://clinicaltrials.gov/ct2/show/study/NCT01215864

Brindle, K. (2008). New approaches for imaging tumour responses to treatment. Nat. Rev. Cancer *8*, 94–107.

Brindle, K. (2012). Watching tumours gasp and die with MRI: the promise of hyperpolarised 13C MR spectroscopic imaging. Br J Radiol *85*, 697–708.

Brindle, K. (2015). Imaging Metabolism with Hyperpolarized 13C-Labeled Cell Substrates. J. Am. Chem. Soc, 137 (20), 6418-6427.

Brindle, K.M., Bohndiek, S.E., Gallagher, F.A., and Kettunen, M.I. (2011). Tumor imaging using hyperpolarized 13C magnetic resonance spectroscopy. Magn Reson Med *66*, 505–519.

Buchanan, F.G., McReynolds, M., Couvillon, A., Kam, Y., Holla, V.R., Dubois, R.N., and Exton, J.H. (2005). Requirement of phospholipase D1 activity in H-RasV12-induced transformation. Proc. Natl. Acad. Sci. U.S.A. *102*, 1638–1642.

Cabot, M.C., Zhang, Z., Cao, H., Lavie, Y., Giuliano, A.E., Han, T.Y., and Jones, R.C. (1997). Tamoxifen activates cellular phospholipase C and D and elicits protein kinase C translocation. Int. J. Cancer *70*, 567–574.

Cairns, R.A., Harris, I.S., and Mak, T.W. (2011). Regulation of cancer cell metabolism. Nat. Rev. Cancer *11*, 85–95.

Cantley, L.C. (2002). The phosphoinositide 3-kinase pathway. Science *296*, 1655–1657.

Carver, T.R., and Slichter, C.P. (1956). Experimental Verification of the Overhauser Nuclear Polarization Effect. Phys. Rev. *102*, 975–980.

Chen, W.C., Teo, X.Q., Lee, M.Y., Radda, G.K., and Lee, P. (2015). Robust hyperpolarized (13) C metabolic imaging with selective non-excitation of pyruvate (SNEP). NMR Biomed *28*, 1021–1030.

Choubey, V., Maity, P., Guha, M., Kumar, S., Srivastava, K., Puri, S.K., and Bandyopadhyay, U. (2007). Inhibition of Plasmodium falciparum choline kinase by hexadecyltrimethylammonium bromide: a possible antimalarial mechanism. Antimicrob. Agents Chemother. *51*, 696–706.

Choyke, P.L., Dwyer, A.J., and Knopp, M.V. (2003). Functional tumor imaging with dynamic contrast-enhanced magnetic resonance imaging. J Magn Reson Imaging *17*, 509–520.

Chua, B.T., Gallego-Ortega, D., Ramirez de Molina, A., Ullrich, A., Lacal, J.C., and Downward, J. (2009). Regulation of Akt(ser473) phosphorylation by choline kinase in breast carcinoma cells. Mol. Cancer *8*, 131.

Clem, B.F., Clem, A.L., Yalcin, A., Goswami, U., Arumugam, S., Telang, S., Trent, J.O., and Chesney, J. (2011). A novel small molecule antagonist of choline

kinase-α that simultaneously suppresses MAPK and PI3K/AKT signaling. Oncogene *30*, 3370–3380.

Clive, S., Gardiner, J., and Leonard, R.C. (1999). Miltefosine as a topical treatment for cutaneous metastases in breast carcinoma. Cancer Chemother. Pharmacol. *44 Suppl*, S29–S30.

Cudalbu, C., Comment, A., Kurdzesau, F., van Heeswijk, R.B., Uffmann, K., Jannin, S., Denisov, V., Kirik, D., and Gruetter, R. (2010). Feasibility of in vivo 15N MRS detection of hyperpolarized 15N labeled choline in rats. Phys Chem Chem Phys *12*, 5818–5823.

Culverwell, A.D., Scarsbrook, A.F., and Chowdhury, F.U. (2011). False-positive uptake on 2-[^{18}F]-fluoro-2-deoxy-D-glucose (FDG) positron-emission tomography/computed tomography (PET/CT) in oncological imaging. Clin Radiol *66*, 366–382.

Dafni, H., Larson, P.E.Z., Hu, S., Yoshihara, H.A.I., Ward, C.S., Venkatesh, H.S., Wang, C., Zhang, X., Vigneron, D.B., and Ronen, S.M. (2010). Hyperpolarized 13C spectroscopic imaging informs on hypoxia-inducible factor-1 and myc activity downstream of platelet-derived growth factor receptor. Cancer Res. *70*, 7400–7410.

Danishad, K.K.A., Sharma, U., Sah, R.G., Seenu, V., Parshad, R., and Jagannathan, N.R. (2010). Assessment of therapeutic response of locally advanced breast cancer (LABC) patients undergoing neoadjuvant chemotherapy (NACT) monitored using sequential magnetic resonance spectroscopic imaging (MRSI). NMR Biomed *23*, 233–241.

Davies, S.P., Reddy, H., Caivano, M., and Cohen, P. (2000). Specificity and mechanism of action of some commonly used protein kinase inhibitors. Biochem. J. *351*, 95–105.

Day, S.E., Kettunen, M.I., Gallagher, F.A., Hu, D.-E., Lerche, M., Wolber, J., Golman, K., Ardenkjaer-Larsen, J.H., and Brindle, K.M. (2007). Detecting tumor response to treatment using hyperpolarized 13C magnetic resonance imaging and spectroscopy. Nat. Med. *13*, 1382–1387.

Day, S.E., Kettunen, M.I., Cherukuri, M.K., Mitchell, J.B., Lizak, M.J., Morris, H.D., Matsumoto, S., Koretsky, A.P., and Brindle, K.M. (2011). Detecting response of rat C6 glioma tumors to radiotherapy using hyperpolarized [1-13C]pyruvate and 13C magnetic resonance spectroscopic imaging. Magn Reson Med *65*, 557–563.

De Boer, W., and Niinikoski, T.O. (1974). Dynamic proton polarization in propanediol below 0.5 K. Nuclear Instruments and Methods *114*, 495–498.

De Graaf, R.A. (2007). In Vivo NMR Spectroscopy: Principles and Techniques, 2nd Edition. Wiley**.**

De la Cueva, A., Ramírez de Molina, A., Alvarez-Ayerza, N., Ramos, M.A., Cebrián, A., Del Pulgar, T.G., and Lacal, J.C. (2013). Combined 5-FU and ChoKα inhibitors as a new alternative therapy of colorectal cancer: evidence in human tumor-derived cell lines and mouse xenografts. PLoS ONE *8*, e64961.

Direcks, W.G.E., Berndsen, S.C., Proost, N., Peters, G.J., Balzarini, J., Spreeuwenberg, M.D., Lammertsma, A.A., and Molthoff, C.F.M. (2008). [18F]FDG and [18F]FLT uptake in human breast cancer cells in relation to the effects of chemotherapy: an in vitro study. Br. J. Cancer *99*, 481–487.

Dueck, D.A., Chan, M., Tran, K., Wong, J.T., Jay, F.T., Littman, C., Stimpson, R., and Choy, P.C. (1996). The modulation of choline phosphoglyceride metabolism in human colon cancer. Mol. Cell. Biochem. *162*, 97–103.

Elbashir, S.M., Lendeckel, W., and Tuschl, T. (2001). RNA interference is mediated by 21- and 22-nucleotide RNAs. Genes Dev. *15*, 188–200.

Eliyahu, G., Kreizman, T., and Degani, H. (2007). Phosphocholine as a biomarker of breast cancer: molecular and biochemical studies. Int. J. Cancer *120*, 1721–1730.

Elshafey, R., Elattar, A., Mlees, M., and Esheba, N. (2014). Role of quantitative diffusion-weighted MRI and 1H MR spectroscopy in distinguishing between benign and malignant thyroid nodules. The Egyptian Journal of Radiology and Nuclear Medicine *45*, 89–96.

Evelhoch, J.L., Gillies, R.J., Karczmar, G.S., Koutcher, J.A., Maxwell, R.J., Nalcioglu, O., Raghunand, N., Ronen, S.M., Ross, B.D., and Swartz, H.M. (2000).

Applications of magnetic resonance in model systems: cancer therapeutics. Neoplasia *2*, 152–165.

Fayad, L.M., Salibi, N., Wang, X., Machado, A.J., Jacobs, M.A., Bluemke, D.A., and Barker, P.B. (2010). Quantification of muscle choline concentrations by proton MR spectroscopy at 3 T: technical feasibility. AJR Am J Roentgenol *194*, W73–W79.

Fire, A., Xu, S., Montgomery, M.K., Kostas, S.A., Driver, S.E., and Mello, C.C. (1998). Potent and specific genetic interference by double-stranded RNA in Caenorhabditis elegans. Nature *391*, 806–811.

Friesen-Waldner, L.J., Wade, T.P., Thind, K., Chen, A.P., Gomori, J.M., Sosna, J., McKenzie, C.A., and Katz-Brull, R. (2015). Hyperpolarized choline as an MR imaging molecular probe: feasibility of in vivo imaging in a rat model. J Magn Reson Imaging *41*, 917–923.

Gabellieri, C., Beloueche-Babari, M., Jamin, Y., Payne, G.S., Leach, M.O., and Eykyn, T.R. (2009). Modulation of choline kinase activity in human cancer cells observed by dynamic 31P NMR. NMR Biomed *22*, 456–461.

Gadiya, M., Mori, N., Cao, M.D., Mironchik, Y., Kakkad, S., Gribbestad, I.S., Glunde, K., Krishnamachary, B., and Bhujwalla, Z.M. (2014). Phospholipase D1 and choline kinase-α are interactive targets in breast cancer. Cancer Biol. Ther. *15*, 593–601.

Gallagher, F.A., Kettunen, M.I., Day, S.E., Hu, D.-E., Ardenkjaer-Larsen, J.H., Zandt, R. in ’t, Jensen, P.R., Karlsson, M., Golman, K., Lerche, M.H., et al. (2008). Magnetic resonance imaging of pH in vivo using hyperpolarized 13C-labelled bicarbonate. Nature *453*, 940–943.

Gallagher, F.A., Kettunen, M.I., Hu, D.-E., Jensen, P.R., Zandt, R.I. ’t, Karlsson, M., Gisselsson, A., Nelson, S.K., Witney, T.H., Bohndiek, S.E., et al. (2009). Production of hyperpolarized [1,4-13C2]malate from [1,4-13C2]fumarate is a marker of cell necrosis and treatment response in tumors. Proc. Natl. Acad. Sci. U.S.A. *106*, 19801–19806.

Gallagher, F.A., Kettunen, M.I., Day, S.E., Hu, D., Karlsson, M., Gisselsson, A., Lerche, M.H., and Brindle, K.M. (2011). Detection of tumor glutamate

metabolism in vivo using (13)C magnetic resonance spectroscopy and hyperpolarized [1-(13)C]glutamate. Magn Reson Med *66*, 18–23.

Gallego-Ortega, D., Ramirez de Molina, A., Ramos, M.A., Valdes-Mora, F., Barderas, M.G., Sarmentero-Estrada, J., and Lacal, J.C. (2009). Differential role of human choline kinase alpha and beta enzymes in lipid metabolism: implications in cancer onset and treatment. PLoS ONE *4*, e7819.

Gao, P., Tchernyshyov, I., Chang, T.-C., Lee, Y.-S., Kita, K., Ochi, T., Zeller, K.I., De Marzo, A.M., Van Eyk, J.E., Mendell, J.T., et al. (2009). c-Myc suppression of miR-23a/b enhances mitochondrial glutaminase expression and glutamine metabolism. Nature *458*, 762–765.

Geilen, C.C., Wieder, T., and Reutter, W. (1992). Hexadecylphosphocholine inhibits translocation of CTP:choline-phosphate cytidylyltransferase in Madin-Darby canine kidney cells. J. Biol. Chem. *267*, 6719–6724.

George, T.P., Morash, S.C., Cook, H.W., Byers, D.M., Palmer, F.B., and Spence, M.W. (1989). Phosphatidylcholine biosynthesis in cultured glioma cells: evidence for channeling of intermediates. Biochim. Biophys. Acta *1004*, 283–291.

Gillies, R.J., and Morse, D.L. (2005). In vivo magnetic resonance spectroscopy in cancer. Annu Rev Biomed Eng *7*, 287–326.

Glunde, K., and Bhujwalla, Z.M. (2011). Metabolic tumor imaging using magnetic resonance spectroscopy. Semin. Oncol. *38*, 26–41.

Glunde, K., Jie, C., and Bhujwalla, Z.M. (2004). Molecular causes of the aberrant choline phospholipid metabolism in breast cancer. Cancer Res. *64*, 4270–4276.

Glunde, K., Raman, V., Mori, N., and Bhujwalla, Z.M. (2005). RNA interference-mediated choline kinase suppression in breast cancer cells induces differentiation and reduces proliferation. Cancer Res. *65*, 11034–11043.

Glunde, K., Shah, T., Winnard, P.T., Raman, V., Takagi, T., Vesuna, F., Artemov, D., and Bhujwalla, Z.M. (2008). Hypoxia regulates choline kinase expression through hypoxia-inducible factor-1 alpha signaling in a human prostate cancer model. Cancer Res. *68*, 172–180.

Glunde, K., Bhujwalla, Z.M., and Ronen, S.M. (2011). Choline metabolism in malignant transformation. Nat. Rev. Cancer *11*, 835–848.

Golman, K., Zandt, R.I., Lerche, M., Pehrson, R., and Ardenkjaer-Larsen, J.H. (2006). Metabolic imaging by hyperpolarized 13C magnetic resonance imaging for in vivo tumor diagnosis. Cancer Res. *66*, 10855–10860.

Griffeth, L.K. (2005). Use of PET/CT scanning in cancer patients: technical and practical considerations. Proc (Bayl Univ Med Cent) *18*, 321–330.

Guimaraes, M.D., Schuch, A., Hochhegger, B., Gross, J.L., Chojniak, R., and Marchiori, E. (2014). Functional magnetic resonance imaging in oncology: state of the art. Radiol Bras *47*, 101–111.

Gutte, H., Hansen, A.E., Henriksen, S.T., Johannesen, H.H., Ardenkjaer-Larsen, J., Vignaud, A., Hansen, A.E., Børresen, B., Klausen, T.L., Wittekind, A.-M.N., et al. (2015). Simultaneous hyperpolarized (13)C-pyruvate MRI and (18)F-FDG-PET in cancer (hyperPET): feasibility of a new imaging concept using a clinical PET/MRI scanner. Am J Nucl Med Mol Imaging *5*, 38–45.

Hanahan, D., and Weinberg, R.A. (2011). Hallmarks of cancer: the next generation. Cell *144*, 646–674.

Hernández-Alcoceba, R., Saniger, L., Campos, J., Núñez, M.C., Khaless, F., Gallo, M.A., Espinosa, A., and Lacal, J.C. (1997). Choline kinase inhibitors as a novel approach for antiproliferative drug design. Oncogene *15*, 2289–2301.

Hernández-Alcoceba, R., Fernández, F., and Lacal, J.C. (1999). In vivo antitumor activity of choline kinase inhibitors: a novel target for anticancer drug discovery. Cancer Res. *59*, 3112–3118.

Hsu, P.P., and Sabatini, D.M. (2008). Cancer cell metabolism: Warburg and beyond. Cell *134*, 703–707.

Imamura, F., Horai, T., Mukai, M., Shinkai, K., Sawada, M., and Akedo, H. (1993). Induction of in vitro tumor cell invasion of cellular monolayers by lysophosphatidic acid or phospholipase D. Biochem. Biophys. Res. Commun. *193*, 497–503.

Iorio, E., Mezzanzanica, D., Alberti, P., Spadaro, F., Ramoni, C., D'Ascenzo, S., Millimaggi, D., Pavan, A., Dolo, V., Canevari, S., et al. (2005). Alterations of choline phospholipid metabolism in ovarian tumor progression. Cancer Res. *65*, 9369–9376.

Iorio, E., Ricci, A., Bagnoli, M., Pisanu, M.E., Castellano, G., Di Vito, M., Venturini, E., Glunde, K., Bhujwalla, Z.M., Mezzanzanica, D., et al. (2010). Activation of phosphatidylcholine cycle enzymes in human epithelial ovarian cancer cells. Cancer Res. *70*, 2126–2135.

Jacobs, M.A., Barker, P.B., Bottomley, P.A., Bhujwalla, Z., and Bluemke, D.A. (2004). Proton magnetic resonance spectroscopic imaging of human breast cancer: a preliminary study. J Magn Reson Imaging *19*, 68–75.

Jeffrey, F.M., Rajagopal, A., Malloy, C.R., and Sherry, A.D. (1991). 13C-NMR: a simple yet comprehensive method for analysis of intermediary metabolism. Trends Biochem. Sci. *16*, 5–10.

Jennings, D., Raghunand, N., and Gillies, R.J. (2008). Imaging hemodynamics. Cancer Metastasis Rev. *27*, 589–613.

Jiménez-López, J.M., Carrasco, M.P., Segovia, J.L., and Marco, C. (2002). Hexadecylphosphocholine inhibits phosphatidylcholine biosynthesis and the proliferation of HepG2 cells. Eur. J. Biochem. *269*, 4649–4655.

Jones, D. K. (2010). Diffusion MRI: Theory, Methods, and Applications, First Edition. Oxford university press**.**

Jordan, B.F., Black, K., Robey, I.F., Runquist, M., Powis, G., and Gillies, R.J. (2005a). Metabolite changes in HT-29 xenograft tumors following HIF-1alpha inhibition with PX-478 as studied by MR spectroscopy in vivo and ex vivo. NMR Biomed *18*, 430–439.

Jordan, B.F., Runquist, M., Raghunand, N., Baker, A., Williams, R., Kirkpatrick, L., Powis, G., and Gillies, R.J. (2005b). Dynamic contrast-enhanced and diffusion MRI show rapid and dramatic changes in tumor microenvironment in response to inhibition of HIF-1alpha using PX-478. Neoplasia *7*, 475–485.

Karroum, O., Mignion, L., Kengen, J., Karmani, L., Levêque, P., Danhier, P., Magat, J., Bol, A., Labar, D., Grégoire, V., et al. (2013). Multimodal imaging of

tumor response to sorafenib combined with radiation therapy: comparison between diffusion-weighted MRI, choline spectroscopy and 18F-FLT PET imaging. Contrast Media Mol Imaging *8*, 274–280.

Katz-Brull, R., and Degani, H. (1996). Kinetics of choline transport and phosphorylation in human breast cancer cells; NMR application of the zero trans method. Anticancer Res. *16*, 1375–1380.

Kauppinen, R.A. (2002). Monitoring cytotoxic tumour treatment response by diffusion magnetic resonance imaging and proton spectroscopy. NMR Biomed *15*, 6–17.

Kent, C. (1997). CTP:phosphocholine cytidylyltransferase. Biochim. Biophys. Acta *1348*, 79–90.

Khegai, O., Schulte, R.F., Janich, M.A., Menzel, M.I., Farrell, E., Otto, A.M., Ardenkjaer-Larsen, J.H., Glaser, S.J., Haase, A., Schwaiger, M., et al. (2014). Apparent rate constant mapping using hyperpolarized [1-(13)C]pyruvate. NMR Biomed *27*, 1256–1265.

Koh, D.-M., and Collins, D.J. (2007). Diffusion-weighted MRI in the body: applications and challenges in oncology. AJR Am J Roentgenol *188*, 1622–1635.

Kohlfürst, S., Malle, P., Igerc, I., Gallowitsch, H.J., and Lind, P. (2009). The Role of F-18 Choline PET and PET/CT in Prostate Cancer. Imaging Decisions MRI *13*, 97–103.

Krishnamachary, B., Glunde, K., Wildes, F., Mori, N., Takagi, T., Raman, V., and Bhujwalla, Z.M. (2009). Noninvasive detection of lentiviral-mediated choline kinase targeting in a human breast cancer xenograft. Cancer Res. *69*, 3464–3471.

Kumar, V., and Sahal, D. (2000). Genetic Engineering. In Ullmann's Encyclopedia of Industrial Chemistry, (Wiley-VCH Verlag GmbH & Co. KGaA),.

Kumar, R., Shandal, V., Jana, S., Shamim, S.A., and Malhotra, A. (2010). Role of PET and PET/CT in Anticancer Drug Therapy Response Evaluation. The Open Conference Proceedings Journal *1*, 91–97.

Kurhanewicz, J., Vigneron, D.B., Brindle, K., Chekmenev, E.Y., Comment, A., Cunningham, C.H., Deberardinis, R.J., Green, G.G., Leach, M.O., Rajan, S.S., et al. (2011). Analysis of cancer metabolism by imaging hyperpolarized nuclei: prospects for translation to clinical research. Neoplasia *13*, 81–97.

Li, Y., Park, I., and Nelson, S.J. (2015). Imaging tumor metabolism using in vivo magnetic resonance spectroscopy. Cancer J *21*, 123–128.

Lin, G., Andrejeva, G., Wong Te Fong, A.-C., Hill, D.K., Orton, M.R., Parkes, H.G., Koh, D.-M., Robinson, S.P., Leach, M.O., Eykyn, T.R., et al. (2014). Reduced Warburg effect in cancer cells undergoing autophagy: steady- state 1H-MRS and real-time hyperpolarized 13C-MRS studies. PLoS ONE *9*, e92645.

Liu, D., Hutchinson, O.C., Osman, S., Price, P., Workman, P., and Aboagye, E.O. (2002). Use of radiolabelled choline as a pharmacodynamic marker for the signal transduction inhibitor geldanamycin. Br. J. Cancer *87*, 783–789.

Lochner, A., and Moolman, J.A. (2006). The many faces of H89: a review. Cardiovasc Drug Rev *24*, 261–274.

Lockman, P.R., and Allen, D.D. (2002). The transport of choline. Drug Dev Ind Pharm *28*, 749–771.

Lodi, A., Woods, S.M., and Ronen, S.M. (2013). Treatment with the MEK inhibitor U0126 induces decreased hyperpolarized pyruvate to lactate conversion in breast, but not prostate, cancer cells. NMR Biomed *26*, 299–306.

Loonen A.J.M., Soudijn W. (1985). Halopemide, a new psychotropic agent: Cerebral distribution and receptor interactions. Pharmaceutisch Weekblad 7 (1), 1-9.

McKinley, E.T., Ayers, G.D., Smith, R.A., Saleh, S.A., Zhao, P., Washington, M.K., Coffey, R.J., and Manning, H.C. (2013). Limits of [18F]-FLT PET as a biomarker of proliferation in oncology. PLoS ONE *8*, e58938.

Menendez, J.A., and Lupu, R. (2007). Fatty acid synthase and the lipogenic phenotype in cancer pathogenesis. Nat. Rev. Cancer *7*, 763–777.

Michel, V., Yuan, Z., Ramsubir, S., and Bakovic, M. (2006). Choline transport for phospholipid synthesis. Exp. Biol. Med. (Maywood) *231*, 490–504.

Milano, A., Perri, F., Ciarmiello, A., and Caponigro, F. (2011). Targeted-therapy and imaging response: a new paradigm for clinical evaluation? Rev Recent Clin Trials *6*, 259–265.

Moffat, B.A., Hall, D.E., Stojanovska, J., McConville, P.J., Moody, J.B., Chenevert, T.L., Rehemtulla, A., and Ross, B.D. (2004). Diffusion imaging for evaluation of tumor therapies in preclinical animal models. MAGMA *17*, 249–259.

Moore, C.B., Guthrie, E.H., Huang, M.T.-H., and Taxman, D.J. (2010). Short hairpin RNA (shRNA): design, delivery, and assessment of gene knockdown. Methods Mol. Biol. *629*, 141–158.

Morse, D.L., Galons, J.-P., Payne, C.M., Jennings, D.L., Day, S., Xia, G., and Gillies, R.J. (2007). MRI-measured water mobility increases in response to chemotherapy via multiple cell-death mechanisms. NMR Biomed *20*, 602–614.

Müller, S.A., Holzapfel, K., Seidl, C., Treiber, U., Krause, B.J., and Senekowitsch-Schmidtke, R. (2009). Characterization of choline uptake in prostate cancer cells following bicalutamide and docetaxel treatment. Eur. J. Nucl. Med. Mol. Imaging *36*, 1434–1442.

Munir, E., Yoon, J.J., Tokimatsu, T., Hattori, T., and Shimada, M. (2001). A physiological role for oxalic acid biosynthesis in the wood-rotting basidiomycete Fomitopsis palustris. Proc. Natl. Acad. Sci. U.S.A. *98*, 11126–11130.

Muzi, M., Mankoff, D.A., Grierson, J.R., Wells, J.M., Vesselle, H., and Krohn, K.A. (2005). Kinetic Modeling of 3'-Deoxy-3'-Fluorothymidine in Somatic Tumors: Mathematical Studies. J Nucl Med *46*, 371–380.

Negendank, W. (1992). Studies of human tumors by MRS: a review. NMR Biomed *5*, 303–324.

Nelson, S.J., Kurhanewicz, J., Vigneron, D.B., Larson, P.E.Z., Harzstark, A.L., Ferrone, M., van Criekinge, M., Chang, J.W., Bok, R., Park, I., et al. (2013a). Metabolic imaging of patients with prostate cancer using hyperpolarized [1-^{13}C]pyruvate. Sci Transl Med *5*, 198ra108.

Nelson, S.J., Ozhinsky, E., Li, Y., Park, I. woo, and Crane, J. (2013b). Strategies for rapid in vivo 1H and hyperpolarized 13C MR spectroscopic imaging. J. Magn. Reson. *229*, 187–197.

Nimmagadda, S., Glunde, K., Pomper, M.G., and Bhujwalla, Z.M. (2009). Pharmacodynamic markers for choline kinase down-regulation in breast cancer cells. Neoplasia *11*, 477–484.

Norris, D.G. (2001). The effects of microscopic tissue parameters on the diffusion weighted magnetic resonance imaging experiment. NMR Biomed *14*, 77–93.

O'Regan, S., Traiffort, E., Ruat, M., Cha, N., Compaore, D., and Meunier, F.M. (2000). An electric lobe suppressor for a yeast choline transport mutation belongs to a new family of transporter-like proteins. Proc. Natl. Acad. Sci. U.S.A. *97*, 1835–1840.

Osorio-Garcia, M.I. (2011). Advances signal processing for magnetic resonance spectroscopy. Final thesis manuscript from Katholieke Universiteit Leuven.

Overhauser, A.W. (1953). Polarization of Nuclei in Metals. Phys. Rev. *92*, 411–415.

Padhani, A.R., and Leach, M.O. (2005). Antivascular cancer treatments: functional assessments by dynamic contrast-enhanced magnetic resonance imaging. Abdom Imaging *30*, 324–341.

Padhani, A.R., Liu, G., Mu-Koh, D., Chenevert, T.L., Thoeny, H.C., Takahara, T., Dzik-Jurasz, A., Ross, B.D., Van Cauteren, M., Collins, D., et al. (2009). Diffusion-Weighted Magnetic Resonance Imaging as a Cancer Biomarker: Consensus and Recommendations. Neoplasia *11*, 102–125.

Plevin, R., Cook, S.J., Palmer, S., and Wakelam, M.J. (1991). Multiple sources of sn-1,2-diacylglycerol in platelet-derived-growth-factor-stimulated Swiss 3T3 fibroblasts. Evidence for activation of phosphoinositidase C and phosphatidylcholine-specific phospholipase D. Biochem. J. *279 (Pt 2)*, 559–565.

Podo, F. (1999). Tumour phospholipid metabolism. NMR Biomed *12*, 413–439.

Podo, F., Canevari, S., Canese, R., Pisanu, M.E., Ricci, A., and Iorio, E. (2011). MR evaluation of response to targeted treatment in cancer cells. NMR Biomed *24*, 648–672.

Porporato, P.E., Payen, V.L., Pérez-Escuredo, J., De Saedeleer, C.J., Danhier, P., Copetti, T., Dhup, S., Tardy, M., Vazeille, T., Bouzin, C., et al. (2014). A mitochondrial switch promotes tumor metastasis. Cell Rep *8*, 754–766.

Pratilas, C.A., and Solit, D.B. (2010). Targeting the mitogen-activated protein kinase pathway: physiological feedback and drug response. Clin. Cancer Res. *16*, 3329–3334.

Radda, G.K. (1986). The use of NMR spectroscopy for the understanding of disease. Science *233*, 640–645.

Rajeshkannan, R., Moorthy, S., Sreekumar, K., Rupa, R., and Prabhu, N. (2006). Clinical applications of diffusion weighted MR imaging: A review. Indian Journal of Radiology and Imaging *16*, 705.

Rajeshkumar, N.V., Dutta, P., Yabuuchi, S., de Wilde, R.F., Martinez, G.V., Le, A., Kamphorst, J.J., Rabinowitz, J.D., Jain, S.K., Hidalgo, M., et al. (2015). Therapeutic Targeting of the Warburg Effect in Pancreatic Cancer Relies on an Absence of p53 Function. Cancer Res. *75*, 3355–3364.

Ramírez de Molina, A., Gutiérrez, R., Ramos, M.A., Silva, J.M., Silva, J., Bonilla, F., Sánchez, J.J., and Lacal, J.C. (2002a). Increased choline kinase activity in human breast carcinomas: clinical evidence for a potential novel antitumor strategy. Oncogene *21*, 4317–4322.

Ramírez de Molina, A., Penalva, V., Lucas, L., and Lacal, J.C. (2002b). Regulation of choline kinase activity by Ras proteins involves Ral-GDS and PI3K. Oncogene *21*, 937–946.

Ramírez de Molina, A., Rodríguez-González, A., Gutiérrez, R., Martínez-Piñeiro, L., Sánchez, J., Bonilla, F., Rosell, R., and Lacal, J. (2002c). Overexpression of choline kinase is a frequent feature in human tumor-derived cell lines and in lung, prostate, and colorectal human cancers. Biochem. Biophys. Res. Commun. *296*, 580–583.

Ramírez de Molina, A., Báñez-Coronel, M., Gutiérrez, R., Rodríguez-González, A., Olmeda, D., Megías, D., and Lacal, J.C. (2004). Choline kinase activation is a critical requirement for the proliferation of primary human mammary epithelial cells and breast tumor progression. Cancer Res. *64*, 6732–6739.

Ramírez de Molina, A., Gallego-Ortega, D., Sarmentero, J., Bañez-Coronel, M., Martín-Cantalejo, Y., and Lacal, J.C. (2005). Choline kinase is a novel oncogene that potentiates RhoA-induced carcinogenesis. Cancer Res. *65*, 5647–5653.

Ramírez de Molina, A., Sarmentero-Estrada, J., Belda-Iniesta, C., Tarón, M., Ramírez de Molina, V., Cejas, P., Skrzypski, M., Gallego-Ortega, D., de Castro, J., Casado, E., et al. (2007). Expression of choline kinase alpha to predict outcome in patients with early-stage non-small-cell lung cancer: a retrospective study. Lancet Oncol. *8*, 889–897.

Ridgway, J.P. (2010). Cardiovascular magnetic resonance physics for clinicians: part I. J Cardiovasc Magn Reson *12*, 71.

Rodríguez-González, A., Ramírez de Molina, A., Fernández, F., Ramos, M.A., del Carmen Núñez, M., Campos, J., and Lacal, J.C. (2003). Inhibition of choline kinase as a specific cytotoxic strategy in oncogene-transformed cells. Oncogene *22*, 8803–8812.

Rodríguez-González, A., Ramirez de Molina, A., Fernández, F., and Lacal, J.C. (2004). Choline kinase inhibition induces the increase in ceramides resulting in a highly specific and selective cytotoxic antitumoral strategy as a potential mechanism of action. Oncogene *23*, 8247–8259.

Rodríguez-González, A., Ramírez de Molina, A., Bañez-Coronel, M., Megias, D., and Lacal, J.C. (2005). Inhibition of choline kinase renders a highly selective cytotoxic effect in tumour cells through a mitochondrial independent mechanism. Int. J. Oncol. *26*, 999–1008.

Rommel, D., Abarca-Quinones, J., De Saeger, C., Peeters, F., Leclercq, I., and Duprez, T. (2012). Enhanced choline metabolism in a rodent rhabdomyosarcoma model: correlation between RT-PCR and translational 3 T H-MRS. Magn Reson Imaging *30*, 1010–1016.

Ross, B.D., Moffat, B.A., Lawrence, T.S., Mukherji, S.K., Gebarski, S.S., Quint, D.J., Johnson, T.D., Junck, L., Robertson, P.L., Muraszko, K.M., et al. (2003). Evaluation of cancer therapy using diffusion magnetic resonance imaging. Mol. Cancer Ther. *2*, 581–587.

Saito, K., Matsumoto, S., Takakusagi, Y., Matsuo, M., Morris, H.D., Lizak, M.J., Munasinghe, J.P., Devasahayam, N., Subramanian, S., Mitchell, J.B., et al. (2015). 13C-MR spectroscopic imaging with hyperpolarized [1-13C]pyruvate detects early response to radiotherapy in SCC tumors and HT-29 tumors. Clin. Cancer Res.

Salibi, N., Brown, M.A. (1998). Clinical MR spectroscopy, first principles. Wiley .

Schick, H.D., Danhauser-Riedl, S., Amtmann, E., Busch, R., Reichert, A., Steinhauser, G., Rastetter, J., Sauer, G., and Berdel, W.E. (1989). Antitumoral activity of a xanthate compound. II. Therapeutic studies in murine leukemia and tumor models in vivo. Cancer Lett. *46*, 149–152.

Semenza, G.L. (2013). HIF-1 mediates metabolic responses to intratumoral hypoxia and oncogenic mutations. J. Clin. Invest. *123*, 3664–3671.

Shaw, G.M., Carmichael, S.L., Yang, W., Selvin, S., and Schaffer, D.M. (2004). Periconceptional dietary intake of choline and betaine and neural tube defects in offspring. Am. J. Epidemiol. *160*, 102–109.

Shchepin, R.V., and Chekmenev, E.Y. (2013). Synthetic approach for unsaturated precursors for parahydrogen induced polarization of choline and its analogs. J Labelled Comp Radiopharm *56*, 655–662.

Shields, A.F. (2006). Positron emission tomography measurement of tumor metabolism and growth: its expanding role in oncology. Mol Imaging Biol *8*, 141–150.

Shin H.J., Baek H.M., Cha J.H., Kim H.H. (2012) Evaluation of breast cancer using proton MR spectroscopy: total choline peak integral and signal-to-noise ratio as prognostic indicators. AJR Am J Roentgenol 198 (5), w488-497

Simon, J.R., and Kuhar, M.J. (1976). High affinity choline uptake: ionic and energy requirements. J. Neurochem. *27*, 93–99.

Singh, A.T., Radeff, J.M., Kunnel, J.G., and Stern, P.H. (2000). Phosphatidylcholine-specific phospholipase C inhibitor, tricyclodecan-9-yl xanthogenate (D609), increases phospholipase D-mediated phosphatidylcholine hydrolysis in UMR-106 osteoblastic osteosarcoma cells. Biochim. Biophys. Acta *1487*, 201–208.

Spadaro, F., Ramoni, C., Mezzanzanica, D., Miotti, S., Alberti, P., Cecchetti, S., Iorio, E., Dolo, V., Canevari, S., and Podo, F. (2008). Phosphatidylcholine-specific phospholipase C activation in epithelial ovarian cancer cells. Cancer Res. *68*, 6541–6549.

Sriram, R., Van Criekinge, M., Hansen, A., Wang, Z.J., Vigneron, D.B., Wilson, D.M., Keshari, K.R., and Kurhanewicz, J. (2015). Real-time measurement of hyperpolarized lactate production and efflux as a biomarker of tumor aggressiveness in an MR compatible 3D cell culture bioreactor. NMR Biomed *28*, 1141–1149.

Strauss, L.G. (1996). Fluorine-18 deoxyglucose and false-positive results: a major problem in the diagnostics of oncological patients. Eur J Nucl Med *23*, 1409–1415.

Swinnen, J.V., Brusselmans, K., and Verhoeven, G. (2006). Increased lipogenesis in cancer cells: new players, novel targets. Curr Opin Clin Nutr Metab Care *9*, 358–365.

Tehrani, O.S., and Shields, A.F. (2013). PET imaging of proliferation with pyrimidines. J. Nucl. Med. *54*, 903–912.

Thoeny, H.C., and Ross, B.D. (2010). Predicting and monitoring cancer treatment response with diffusion-weighted MRI. J Magn Reson Imaging *32*, 2–16.

Valk, P.E., Bailey, D.L., Townsend, D.W., Maisey, M.N. (2003). Positron emission tomography: Basic Science and Clinical Practice. Springer-Verlag.

Vance, J.E., and Vance, D.E. (2004). Phospholipid biosynthesis in mammalian cells. Biochem. Cell Biol. *82*, 113–128.

Van Asten J.J., Vettukattil R., Buckle T., Rottenberg S., van Leeuwen F., Bathen T.F., Heerschap A. (2015) Increased levels of choline metabolites are an early

marker of docetaxel treatment response in BRCA1-mutated mouse mammary tumors: an assessment by ex vivo proton magnetic resonance spectroscopy. J Transl Med 13, 114.

Vigneaud, V. du, Chandler, J.P., Cohn, M., and Brown, G.B. (1940). The Transfer of the Methyl Group from Methionine to Choline and Creatine. J. Biol. Chem. *134*, 787–788.

Vivanco, I., and Sawyers, C.L. (2002). The phosphatidylinositol 3-Kinase AKT pathway in human cancer. Nat. Rev. Cancer *2*, 489–501.

Wald, L.L., Nelson, S.J., Day, M.R., Noworolski, S.E., Henry, R.G., Huhn, S.L., Chang, S., Prados, M.D., Sneed, P.K., Larson, D.A., et al. (1997). Serial proton magnetic resonance spectroscopy imaging of glioblastoma multiforme after brachytherapy. J. Neurosurg. *87*, 525–534.

Wang, T., Li, J., Chen, F., Zhao, Y., He, X., Wan, D., and Gu, J. (2007). Choline transporters in human lung adenocarcinoma: expression and functional implications. Acta Biochim. Biophys. Sin. (Shanghai) *39*, 668–674.

Warburg, O., Wind, F., and Negelein, E. (1927). THE METABOLISM OF TUMORS IN THE BODY. J. Gen. Physiol. *8*, 519–530.

Ward C.S., Eriksson P., Izquierdo-Garcia J.L., Brandes A.H., Ronen S.M. (2013) HDAC inhibition induces increased choline uptake and elevated phosphocholine levels in MCF7 breast cancer cells. Plos One 8(4), e62610.

Ward, C.S., Venkatesh, H.S., Chaumeil, M.M., Brandes, A.H., Vancriekinge, M., Dafni, H., Sukumar, S., Nelson, S.J., Vigneron, D.B., Kurhanewicz, J., et al. (2010). Noninvasive detection of target modulation following phosphatidylinositol 3-kinase inhibition using hyperpolarized 13C magnetic resonance spectroscopy. Cancer Res. *70*, 1296–1305.

Wieprecht, M., Wieder, T., and Geilen, C.C. (1994). N-[2-bromocinnamyl(amino)ethyl]-5-isoquinolinesulphonamide (H-89) inhibits incorporation of choline into phosphatidylcholine via inhibition of choline kinase and has no effect on the phosphorylation of CTP:phosphocholine cytidylyltransferase. Biochem. J. *297 (Pt 1)*, 241–247.

Wilhelm, S., Carter, C., Lynch, M., Lowinger, T., Dumas, J., Smith, R.A., Schwartz, B., Simantov, R., and Kelley, S. (2006). Discovery and development of sorafenib: a multikinase inhibitor for treating cancer. Nat Rev Drug Discov *5*, 835–844.

Wilhelm, S.M., Carter, C., Tang, L., Wilkie, D., McNabola, A., Rong, H., Chen, C., Zhang, X., Vincent, P., McHugh, M., et al. (2004). BAY 43-9006 exhibits broad spectrum oral antitumor activity and targets the RAF/MEK/ERK pathway and receptor tyrosine kinases involved in tumor progression and angiogenesis. Cancer Res. *64*, 7099–7109.

Wilson, D.M., and Kurhanewicz, J. (2014). Hyperpolarized 13C MR for molecular imaging of prostate cancer. J. Nucl. Med. *55*, 1567–1572.

Wilson, D.M., Keshari, K.R., Larson, P.E.Z., Chen, A.P., Hu, S., Van Criekinge, M., Bok, R., Nelson, S.J., Macdonald, J.M., Vigneron, D.B., et al. (2010). Multi-compound polarization by DNP allows simultaneous assessment of multiple enzymatic activities in vivo. J. Magn. Reson. *205*, 141–147.

Witney, T.H., Kettunen, M.I., Day, S.E., Hu, D., Neves, A.A., Gallagher, F.A., Fulton, S.M., and Brindle, K.M. (2009). A comparison between radiolabeled fluorodeoxyglucose uptake and hyperpolarized (13)C-labeled pyruvate utilization as methods for detecting tumor response to treatment. Neoplasia *11*, 574–582, 1 p following 582.

Witney, T.H., Kettunen, M.I., Hu, D.–., Gallagher, F.A., Bohndiek, S.E., Napolitano, R., and Brindle, K.M. (2010). Detecting treatment response in a model of human breast adenocarcinoma using hyperpolarised [1-13C]pyruvate and [1,4-13C2]fumarate. Br. J. Cancer *103*, 1400–1406.

Wu, C.-L., Jordan, K.W., Ratai, E.M., Sheng, J., Adkins, C.B., DeFeo, E.M., Jenkins, B.G., Ying, L., McDougal, W.S., and Cheng, L.L. (2010). Metabolomic Imaging for Human Prostate Cancer Detection. Sci Transl Med *2*, 16ra8.

Xiong, J., Bian, J., Wang, L., Zhou, J.-Y., Wang, Y., Zhao, Y., Wu, L.-L., Hu, J.-J., Li, B., Chen, S.-J., et al. (2015). Dysregulated choline metabolism in T-cell lymphoma: role of choline kinase-α and therapeutic targeting. Blood Cancer J *5*, 287.

Yalcin, A., Clem, B., Makoni, S., Clem, A., Nelson, K., Thornburg, J., Siow, D., Lane, A.N., Brock, S.E., Goswami, U., et al. (2010). Selective inhibition of choline kinase simultaneously attenuates MAPK and PI3K/AKT signaling. Oncogene *29*, 139–149.

Yen, Y.-F., Nagasawa, K., and Nakada, T. (2011). Promising application of dynamic nuclear polarization for in vivo (13)C MR imaging. Magn Reson Med Sci *10*, 211–217.

Yeung, D.K.W., Yang, W.T., Tse, G.M.K. (2002). Breast Cancer: In Vivo Proton MR Spectroscopy in the Characterization of Histopathologic Subtypes and Preliminary Observations in Axillary Node Metastases. Radiology 225, 190-197.

Yuan, Z., Tie, A., Tarnopolsky, M., and Bakovic, M. (2006). Genomic organization, promoter activity, and expression of the human choline transporter-like protein 1. Physiol. Genomics *26*, 76–90.

Zeisel, S.H. (2012). A brief history of choline. Ann. Nutr. Metab. *61*, 254–258.

Zeisel, S.H., and Blusztajn, J.K. (1994). Choline and human nutrition. Annu. Rev. Nutr. *14*, 269–296.

Zhao, D., Jiang, L., and Mason, R.P. (2004). Measuring changes in tumor oxygenation. Meth. Enzymol. *386*, 378–418.

Zhao, S., Lin, Y., Xu, W., Jiang, W., Zha, Z., Wang, P., Yu, W., Li, Z., Gong, L., Peng, Y., et al. (2009). Glioma-derived mutations in IDH1 dominantly inhibit IDH1 catalytic activity and induce HIF-1alpha. Science *324*, 261–265.